POLITECNICO DI MILANO

Facoltà di Ingegneria
Corso di Laurea in Ingegneria Nucleare
Dipartimento di Ingegneria Nucleare C.E.S.N.E.F.

Electromagnetic waves in non periodic media.

Relatore:
Prof. Marco G. Beghi

Tesi di Laurea di:
Alessandro Brolis
Matricola: 739973

III Sessione - Aprile
Anno Accademico 2010 - 2011

Index

Introduction

In the last few years a great deal of effort has been put in studying periodic dielectric structures that can offer complete control over the propagation of light, called photonic crystals. Photonic crystals are composed of periodic dielectric or metallo-dielectric nanostructures that affect the propagation of electromagnetic waves in the same way as the periodic potential in a semiconductor crystal affects the electron motion by defining allowed and forbidden electronic energy bands. Essentially, photonic crystals contain regularly repeating internal regions of high and low dielectric constant. Photons (behaving as waves) propagate through this structure - or not - depending on their wavelength. Wavelengths of light that are allowed to travel are known as modes, and groups of allowed modes form bands. Disallowed bands of wavelengths are called photonic band gaps. This gives rise to distinct optical phenomena such as inhibition of spontaneous emission, high-reflecting omni-directional mirrors and low-loss-waveguiding.

In my work I payed particular attention to omni-directional mirrors to be used in photovoltaic cells. The underlying idea aims to integrate a Gretzel photovoltaic cell with a highly reflective mirror used as the substrate of the cell itself, in order to improve total efficiency. Designing such a mirror is crucial and that's why I developed a new software that can simulate the behavior of monodimensional photonic crystals. For the sake of generality and flexibility I wanted to create a program able to handle completely non-periodic structures. Even though it's possible to find other software which can perform similar calculations, those software are BLACK-BOX, i.e. non editable by the user. In most cases commercial software ignore complete non-periodicity or the presence of conducting and magnetic materials, making the BLACK-BOX structure even more limiting for non-standard applications. The full accessibility to the source code was therefore required by the experimenters. With this in mind I configured the software as a core simulator which can be expended by other users with ease.

This presentation has been divided into 8 chapters:

***Chapter 1** is an introduction of the different numerical methods used to solve photonic problems.*

***Chapter 2** describes the main features of dielectric mirrors and the process used to produce them.*

***Chapter 3** summarizes the theoretical knowledge needed to understand the physical behavior of electromagnetic waves in matter.*

Chapter 4 *deals with the specific case of electromagnetic waves in multilayered structures and describes the mathematical approach used to develop the software.*

Chapter 5 *is an in-depth discussion of the software designed to solve isotropic multilayered structures.*

Chapter 6 *is dedicated to the design of an omni-directional mirror to be used with photovoltaic cells using the software described in chapter 5.*

Chapter 7 *explains in detail the mathematical approach used to develop the software which solves propagation problems for anisotropic media. A brief overview of the difference between isotropic and anisotropic mirrors is also given in this chapter.*

Chapter 8 *considers the propagation of electromagnetic waves by the photonic band approach and presents a possible evolution of the software for multidimensional analysis through the plane wave method and Fourier transform.*

Source codes of all realized software are available in ***appendix****.*

Chapter 1

Computational Photonics

Even as recently as twenty years ago, it would have been unusual to present solutions to the Maxwell equations without first describing the computational method in great detail. Since then, photonics research has undergone the same profound change that has swept through all areas of science and engineering in the last half century, catalyzed by the availability of powerful computers.
The situation in photonics is especially favorable for computation because the Maxwell equations are practically exact, the relevant material properties are well known, and the length scales are not too small. Therefore, an aspect of this field is that quantitative theoretical predictions can be made ***ab-initio*** *(from first principles), without any questionable assumptions or simplifications. The results of such computations have consistently agreed with experiments. This makes it possible and preferable to optimize the design of photonic crystals on a computer, and then manufacture them. The computer becomes the pre-laboratory.*
Broadly speaking there are three different categories of problems in computational photonics:

1. ***Frequency-domain responses***
2. ***Frequency-domain eigenproblems***
3. ***Time-domain simulations***

1.1 Frequency-domain responses

We often want to know how electromagnetic waves emitted from a given source at a given frequency are transmitted and reflected by a photonic [1]. Computational approach for such problems, called frequency-domain responses, consists in finding the values of the electric fields by solving a linear matrix equation of the form:

$$Ax = B$$

We obtains an *N*×*N matrix equation* for the unknown fields (column vector) *x* in terms of the known terms B. Solving such a set of equations directly requires $O(N^2)$ storage and $O(N^3)$ time. Transmission and scattering calculations typically require “open” boundaries. This means that the scattered fields must radiate to infinity instead of reflecting when they hit the edge of the (finite)

computational region. This problem is typically handled by adding a **perfectly matched layer**[1] (**PML**) around the edges of the computational region. A PML is an artificial absorbing material designed so that there are (theoretically) no reflections from the edge of the material.

1.2 Frequency-domain eigensolver

A frequency-domain eigensolver solves the Maxwell eigenproblem for the frequencies of a periodic system (or nonperiodic), as given by equation:

$$(\mathrm{i}\mathbf{k} + \nabla) \times \left(\frac{1}{\varepsilon(\boldsymbol{r})} (\mathrm{i}\mathbf{k} + \nabla) \times H(r) \right) = \left(\frac{\omega}{c} \right)^2 H(r) \qquad (1.1)$$

The solution to the previous equation as a function of **k** yields the band structure of the system representing which frequencies are free to propagate and which are filtered by the crystal[2].

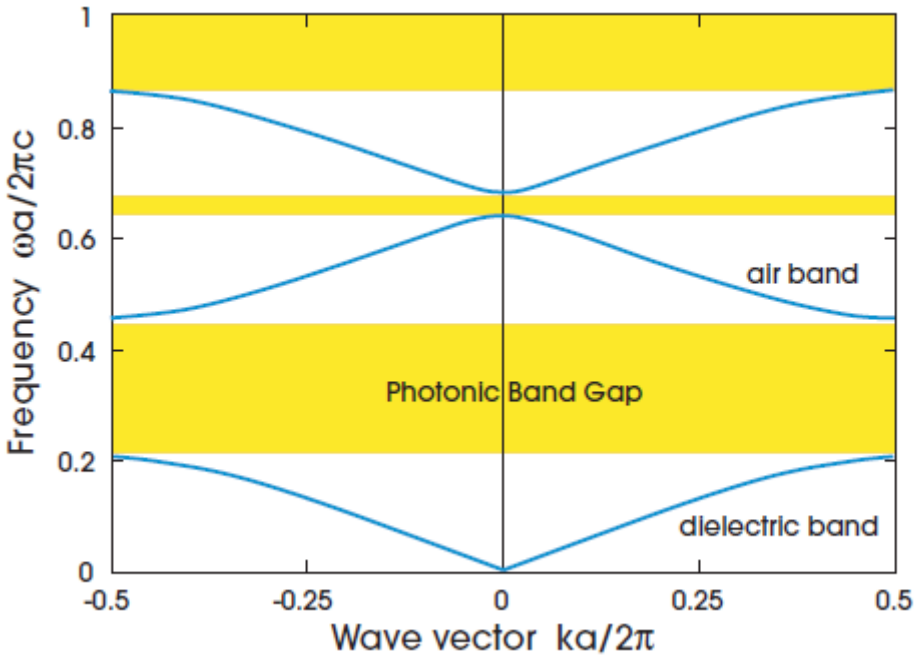

Figure 1 photonic bands structure in a multilayer, from [4].

On a computer, the eigenequation must be discretized into *N* degrees of freedom using numerical methods such as :

[1] **PML** was initially designed for time-domain methods (see, e.g., Taflove and Hagness, 2000 [2]; Chewet al., 2001 [3]), but in frequency domain the same idea applies (and, in fact, is even simpler becauseonly a single frequency ω need be handled).

[2] Instead of looking for eigenvalues ω^2 at a fixed **k**, it is possible to formulate the eigenproblem at a fixed ω for the wave vector *k* at along a single periodic (or uniform) direction as a generalized Hermitian eigenproblem with eigenvalue *k* (Johnson et al., 2001*b*; Johnson et al., 2002*b*).

- **Finite differences**: represent unknown functions $f\ (x)$ by their values $fn\ \approx\ f\ (n\Delta x)$ at discrete points on a grid, and derivatives by differences on the grid. The most straightforward case is a uniform Cartesian grid, e.g. $\frac{df}{dx}\ \approx \frac{fn+1-fn-1}{2\Delta x}$.
- **Finite Elements**: divide space into a set of finite geometric elements (e.g., irregular triangles or tetrahedra), and represent unknown functions by simple approximations defined on each element (typically, low-degree polynomials). In a sense, this method is a generalization of finite differences.
- **Spectral methods**: represent unknown functions as a series expansion ina complete basis set of smooth functions, truncating the series to have a finite number of terms. Usually, a Fourier series is used; this is also called a **planewave method** in two or three dimensions (where the terms in the Fourier series are plane waves).

such a discretization yields a finite **generalized eigenproblem** $Ax = \omega^2 Bx$, where *A* and *B* are *N*×*N* matrices and *x* is the eigenvector.
One difficulty is the transversality constraint, which we must somehow impose in addition to the eigenequation[3]. The simplest way to impose transversality is to choose a basis that is automatically transverse, such as the planewave basis. An efficient way to solve the eigenequation is by **iterative methods**, which compute a small number *p* of the eigenvalues and eigenvectors, such as the *p* smallest eigenvalues. They work by taking a starting guess for *x* (e.g., random numbers) and applying some process to iteratively improve the guess, converging quickly to the true eigenvector. In this way, any desired accuracy can be obtained in a small number of steps. Direct resolution of the eigenequation requires storage memory proportional to O(N^2) and O(N^3) time to be computed. Iterative methods require O(N*p*) memory and O($N^2 p$) time, which make them preferable if *p*<<N.

1.3 Time-domain simulations

Arguably the most general numerical methods for electromagnetism are those that simulate the full time-dependent Maxwell equations, propagating the fields in both space and time. Such *time-domain* methods can easily support strongly nonlinear or active (time-varying) media. Frequency-domain methods have more difficulty with those cases because frequency is no longer conserved. Software exists that solves Maxwell's equations with this method, mostly based on finite differences, and I decided not to used it for my programs.

[3] This fact can be derived by taking the divergence of both sides of the eigenequation (1.1). Since the divergence of the curl is zero, one is left with an expression $\omega^2(i\boldsymbol{k} + \nabla) \cdot H(\boldsymbol{r}) = 0$. That is, the eigenequation itself implies that transversality is satisfied if $\omega \neq 0$.

Chapter 2

Bragg's Mirror and PLD

This chapter investigates the properties and the physical phenomena involved with Bragg's mirror and offers an overview on pulsed laser deposition (PLD), a molecular deposition technique used to produce highly precise multilayered structures with thicknesses on nanometric scale.

2.1 Bragg's Mirror

A **dielectric mirror**, also known as a **Bragg mirror**, is a type of a mirror composed of multiple thin layers of dielectric material, typically deposited on a substrate of glass or some other optical material. By careful choice of the type and thickness of the dielectric layers, one can design an optical coating with specified reflectivity at different wavelengths of light. Dielectric mirrors are also used to produce ultra-high reflectivity mirrors: values of 99.999% or better over a narrow range of wavelengths can be produced using special techniques. One of the most used techniques used to produce Bragg mirrors is molecular deposition via PLD (Pulsed Laser Deposition). Dielectric mirrors function based on the interference of light reflected from the different layers of dielectric stack. Simple dielectric mirrors function like one-dimensional photonic crystals, consisting of a stack of layers with a high refractive index interleaved with layers of a low refractive index (see figure 1). The thicknesses of the layers are chosen such that the path-length differences for reflections from different high-index layers are integer multiples of the wavelength for which the mirror is designed. The reflections from the low-index layers have exactly half a wavelength in path length difference, but there is a 180-degree difference in phase shift at a low-to-high index boundary, compared to a high-to-low index boundary, which means that these reflections are also in phase. In the case of a mirror at normal incidence, the layers have a thickness of a quarter wavelength

.

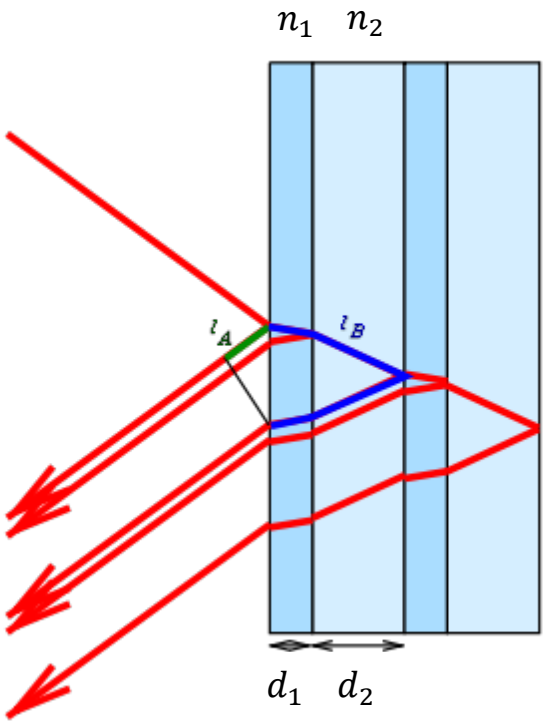

Figure 1: Diagram of a dielectric mirror. Thin layers with a high refractive index n_1 are interleaved with thicker layers with a lower refractive index n_2. The path lengths l_A and l_B differ by exactly one wavelength, which leads to constructive interference.

2.2 Bragg's Diffraction and Bragg's Law

Bragg diffraction occurs when electromagnetic radiation or subatomic particle waves with wavelength comparable to atomic spacings are incident upon a crystalline sample, are scattered in a specular fashion by the atoms in the system, and undergo constructive interference in accordance to Bragg's law. For a crystalline solid, the waves are scattered from lattice planes separated by the interplanar distance *d (see figure 2)*. Where the scattered waves interfere constructively, they remain in phase since the path length of each wave is equal to an integer multiple of the wavelength. The path difference between two waves undergoing constructive interference is given by $2dsin\theta$, where θ is the scattering angle. This leads to **Bragg's law**, which describes the condition for constructive interference from successive crystallographic planes of the crystalline lattice:

$$2d \sin\theta = n\lambda$$

where *n* is an integer determined by the order given, and λ is the wavelength.

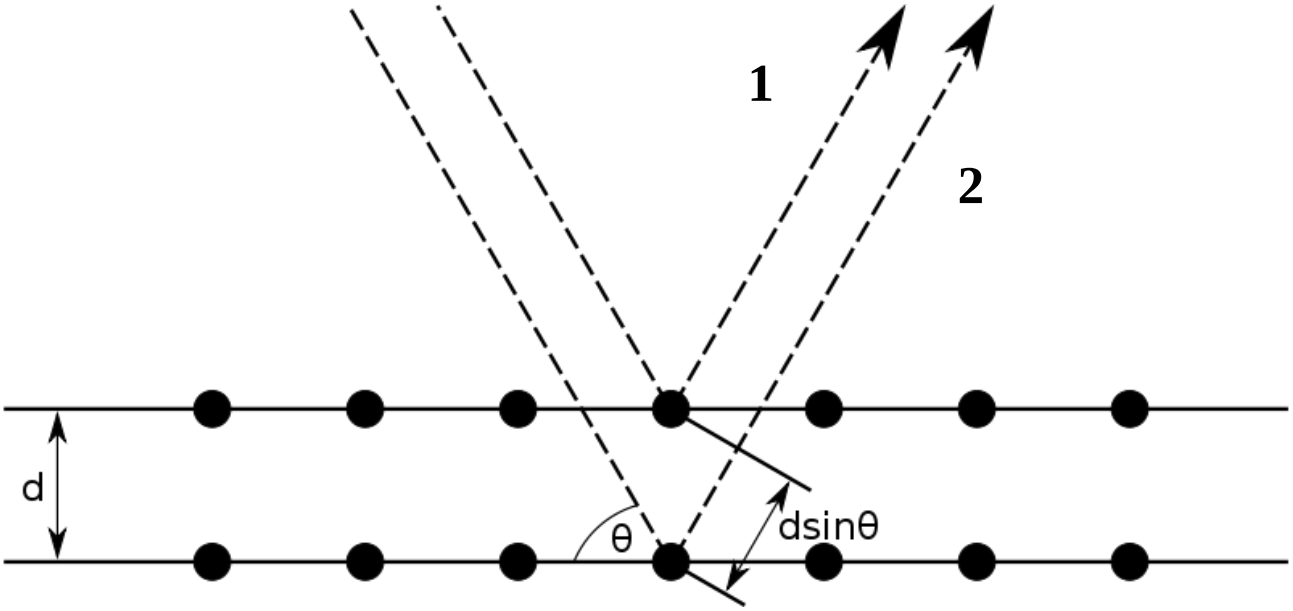

Figure 2: Bragg diffraction. Two beams with identical wavelength and phase approach a crystalline solid and are scattered off two different atoms within it. The lower beam traverses an extra length of $2dsin\theta$. Constructive interference occurs when this length is equal to an integer multiple of the wavelength of the radiation.

2.3 Pulsed Laser Deposition

Pulsed laser deposition (PLD) is a thin film deposition (specifically a physical vapor deposition, PVD) technique where a high power pulsed laser beam is focused inside a vacuum chamber to strike a target of the material that is to be deposited. This material is vaporized from the target (in a plasma plume) which deposits it as a thin film on a substrate. This process can occur in vacuum or in the presence of a background gas, such as oxygen which is commonly used when depositing oxides to fully oxygenate the deposited films, i.e TiO_2, titanium oxide, widely used).

While the basic-setup is simple relative to many other deposition techniques, the physical phenomena of laser-target interaction and film growth are quite complex. When the laser pulse is absorbed by the target, energy is first converted to electronic excitation and then into thermal, chemical and mechanical energy resulting in evaporation, ablation, plasma formation and even exfoliation[1].

[1] Further information can be found in [5]

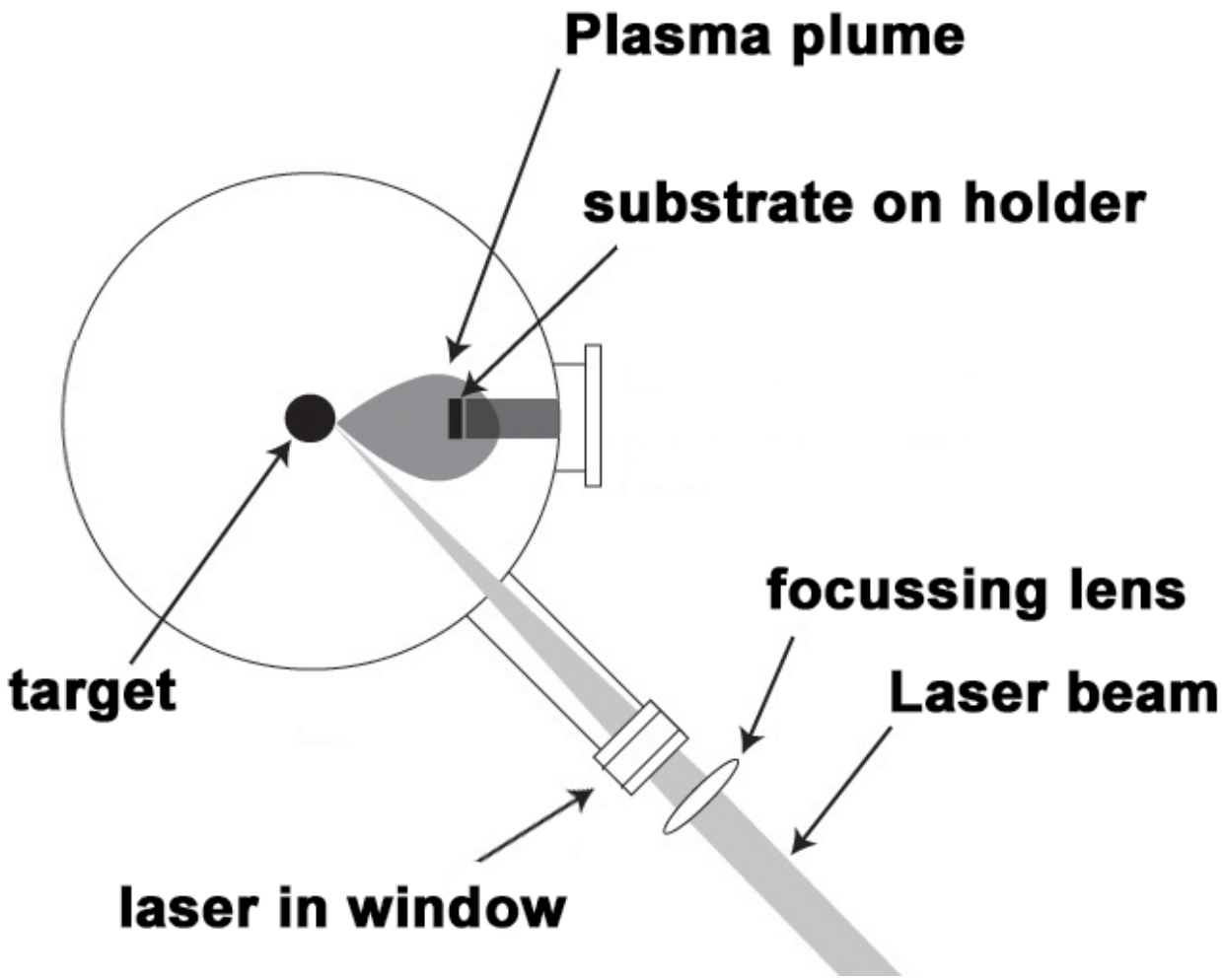

Figure 3: One possible configuration of a PLD deposition chamber.

The detailed mechanisms of PLD are very complex including the ablation process of the target material by the laser irradiation, the development of a plasma plume with high energetic ions, electrons as well as neutrals and the crystalline growth of the film itself on the heated substrate. The process of PLD can generally be divided into four stages:

- Laser ablation of the target material and creation of a plasma
- Dynamic of the plasma
- Deposition of the ablation material on the substrate
- Nucleation and growth of the film on the substrate surface

Each of these steps is crucial for the crystallinity and uniformity of the resulting film.

Laser ablation of the target material and creation of a plasma

The ablation of the target material upon laser irradiation and the creation of plasma are very complex processes. The removal of atoms from the bulk material is done by vaporization of the bulk at the surface region in a state of non-equilibrium. In this the incident laser pulse penetrates into the surface of the material within the penetration depth. This dimension is dependent on the laser wavelength and the index of refraction of the target material at the applied laser wavelength and is typically in the region of 10 nm for most materials. The strong electrical field generated by the laser light is sufficiently strong to remove the electrons from the bulk material of the penetrated volume. This process occurs within 10 ps of a ns laser pulse and is caused by non-linear processes such as multiphoton ionization which are enhanced by microscopic cracks at the surface, voids, and nodules, which increase the electric field. The free electrons oscillate within the electromagnetic field of the laser light and can collide with the atoms of the bulk material thus transferring some of their energy to the lattice of the target material within the surface region. The surface of the target is then heated up and the material is vaporized.

Dynamic of the plasma

In the second stage the material expands in a plasma parallel to the normal vector of the target surface towards the substrate due to Coulomb repulsion and recoil from the target surface. The spatial distribution of the plume is dependent on the background pressure inside the PLD chamber. The density of the plume can be described by a law with a shape similar to a Gaussian curve. The dependency of the plume shape on the pressure can be described in three stages:

- **The vacuum stage**, where the plume is very narrow and forward directed; almost no scattering occurs with the background gases.
- **The intermediate region** where a splitting of the high energetic ions from the less energetic species can be observed. The time-of-flight (TOF) data can be fitted to a shock wave model; however, other models could also be possible.
- **High pressure region** where we find a more diffusion-like expansion of the ablated material. Naturally this scattering is also dependent on the mass of the background gas and can influence the stoichiometry of the deposited film.

The most important consequence of increasing the background pressure is the slowing down of the high energetic species in the expanding plasma plume. It has been shown that particles with kinetic energies around 50 eV can sputter the film already deposited on the substrate. This results in a lower deposition rate and can furthermore result in a change in the properties of the film.

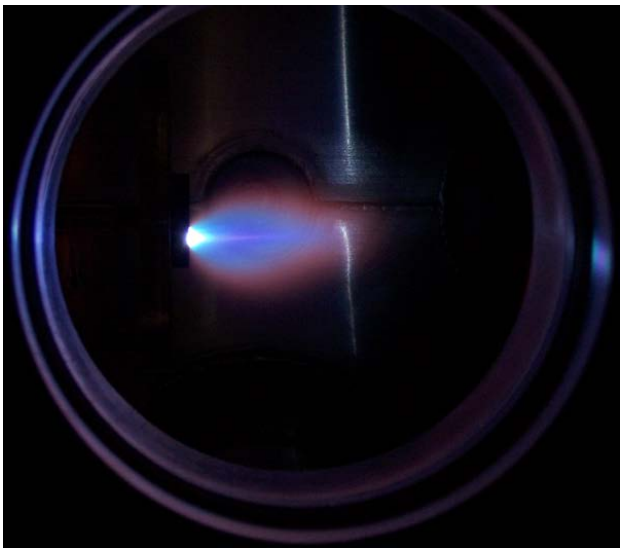

Figure 3 A plume ejected from a $SrRuO_3$ target during pulsed laser deposition.

Deposition of the ablation material on the substrate

The third stage is important to determine the quality of the deposited films. The high energetic species ablated from the target are bombarding the substrate surface and may cause damage to the surface by sputtering off atoms from the surface but also by causing defect formation in the deposited film. The sputtered species from the substrate and the particles emitted from the target form a collision region, which serves as a source for condensation of particles. When the condensation rate is high enough, a thermal equilibrium can be reached and the film grows on the substrate surface at the expense of the direct flow of ablation particles and the thermal equilibrium obtained.

Nucleation and growth of the film on the substrate surface

The nucleation process and growth kinetics, i.e. the aggregation of new atoms that reach specific position on the substrate, called nucleation sites where favorable conditions randomly arise (ablated atomic clusters are typical nucleation sites) of the film depend on several growth parameters including:

- ***Laser parameters*** – several factors such as the laser fluence [Joule/cm^2], laser energy, and ionization degree of the ablated material will affect the film quality, the stoichiometry, and the deposition flux. Generally, the nucleation density increases when the deposition flux is increased.
- ***Surface temperature*** – The surface temperature has a large effect on the nucleation density. Generally, the nucleation density decreases as the temperature is increased.

- ***Substrate surface*** – The nucleation and growth can be affected by the surface preparation, the miscut of the substrate, as well as the roughness of the substrate.
- ***Background pressure*** – Common in oxide deposition, an oxygen background is needed to ensure stoichiometric transfer from the target to the film. If, for example, the oxygen background is too low, the film will grow off stoichiometry which will affect the nucleation density and film quality.

.

Chapter 3

Electromagnetic waves in matter

This chapter is an introduction to electrodynamics in isotropic dielectric and conducting media with particular attention to the laws ruling the propagation of electromagnetic waves[1]*. Propagation in anisotropic media is considered in its general traits at the end of the chapter.*

3.1 Maxwell's Equations in matter

Maxwell's equations in terms of free charge and current are:

$$\nabla \cdot D = \rho_f \qquad \nabla \cdot B = 0$$

$$\nabla \times E = -\frac{\partial B}{\partial t} \qquad \nabla \times H = \frac{\partial D}{\partial t} + J_f$$

Where D is the electric displacement and H is the magnetic field, defined as:

$$D = \varepsilon E \qquad H = \frac{1}{\mu} B$$

ε and μ are called electrical susceptibility and magnetic permeability, respectively, and depends on the medium. This formulation of Maxwell's equations is particularly useful because divides the charge and the current in bound and free. The free charge and current are those we can control directly, the bound charge and current, on the contrary, always arise inside polarized matter, but we don't have any control over them.

3.2 Uniform plane waves in nonconducting media

A basic feature of Maxwell's equations for the electromagnetic fields is the existence of travelling wave solutions which represent the transport of energy from one point to another. The simplest,

[1] For an in-depth discussion on electromagnetic waves in matter see [6] and [7].

most foundamental electromagnetic waves are transverse, plane waves. Plane waves depend only on the direction of propagation. This imply the fields are uniform over every plane perpendicular to the direction of propagation.

In the absence of source Maxwell's equations in a medium are:

$$\nabla \cdot E = 0 \qquad \nabla \cdot B = 0$$

$$\nabla \times E = -\frac{1}{c}\frac{\partial B}{\partial t} \qquad \nabla \times B = \frac{\mu\varepsilon}{c}\frac{\partial E}{\partial t}$$

Where the medium is characterized by the constant parameters μ and ε, the permeability and the susceptibility. By combining the curl equation and making use of the vanishing divergences we find that E and B satisfy the following partial second order differential equation for each cartesian component:

$$\nabla^2 u - \frac{1}{v^2}\frac{\partial^2 u}{\partial t^2} = 0 \quad \text{(wave equation)}$$

Where v is the phase velocity of the wave in the medium, which is given by:

$$v = \frac{\omega}{k}$$

The relation between phase speed, and speed of light, c, is known as **refractive index**, $n = \frac{c}{v} = \frac{ck}{\omega}$. Taking the derivative of $\omega = \frac{ck}{n}$, we get the group speed:

$$\frac{d\omega}{dk} = \frac{c}{n} - \frac{ck}{n^2} \cdot \frac{dn}{dk}$$

Noting that $\frac{c}{n} = v$, this shows that group speed is equal to phase speed only when the refractive index is a constant: $\frac{dn}{dk} = 0$. Otherwise, when the phase velocity varies with frequency, velocities differ and the medium is called **dispersive**[2].

The wave equation has the well known solution:

$$\tilde{u} = \tilde{A} e^{i\boldsymbol{kx} - i\omega t}$$

[2] Phase velocity can exceed the speed of light. Even group velocity in same special cases can exceed the speed of light. This happens for example in the vicinity of a region of anomalous dispersion, where $\frac{d\omega}{dk}$ varies rapidly. Relativity isn't violated because in this region group velocity is no longer a meaningful concept, as can be seen in [10] and [11].

Which represent a sinusoidal wave. $\tilde{A}$ represent the complex amplitude which incorporates the phase constant $e^{i\delta}$. The actual wave function is the real part of $\tilde{u}$. We know that every function can be described by a linear combination of armonic functions using the Fourier Transformation. This is true if the principle of superposition holds, but the principle is always true for linear systems, such as those described by Maxwell's equations. The frequency ω and the wave vector **k** are releted by:

$$\boldsymbol{k} = \sqrt{\mu\varepsilon}\,\frac{\omega}{c}$$

The requirments $\nabla \cdot E = 0$, $\nabla \cdot B = 0$ imply that **E** and **B** are both perpendicular to the direction of propagation **k.** Such a wave is called ***transverse****.*

3.3 Polarization

A plane wave of the form $\boldsymbol{E_1}(x,t) = \boldsymbol{\epsilon_1} E_1 e^{ikx - i\omega t}$ represent a wave with its electric field always in the direction $\boldsymbol{\epsilon_1}$**.** Such a wave is said to be linearly polarized with polarization vector $\boldsymbol{\epsilon_1}$. To describe a general state of polarization we need another linearly polarized wave which is independent of the first. A general solution for a plane wave propagating in the direction **k** is then obtained by linear superposition of the 2 waves:

$$\boldsymbol{E}(x,t) = (\boldsymbol{\epsilon_1} E_1 + \boldsymbol{\epsilon_2} E_2) e^{ikx - i\omega t}$$

If $E_1$and E_2 have the same phase, $\boldsymbol{E}(x,t)$, representig the sum, will be linearly polarized, otherwise $\boldsymbol{E}(x,t)$ will be elliptically polarized.

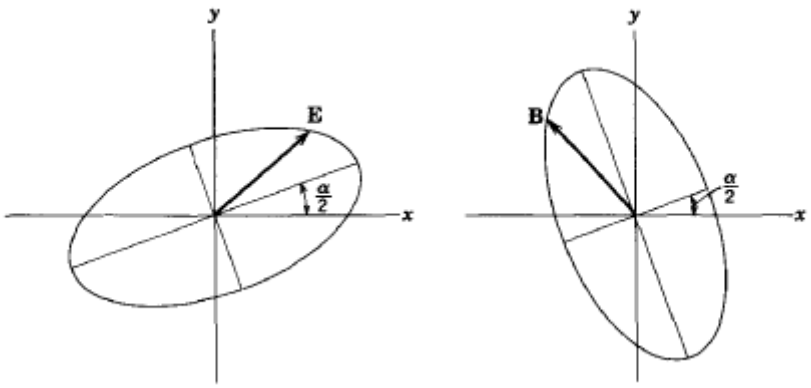

Figure 1 Electric and Magnetic fields for an elliptically polarized wave

3.4 Energy and momentum in electromagnetic waves

The Energy per unit volume stored in electromagnetic fiels is:

$$u = \frac{1}{2}\left(\epsilon E^2 + \frac{1}{\mu}B^2\right)$$

For a plane wave with a well defined wave vector **k** and a definite frequency ω, also called a monochromatic wave, the electric and magnetic contribution to the energy are equal. In fact:

$$B^2 = \mu\epsilon E^2$$

And the the energy density becomes:

$$u = \epsilon E^2$$

The energy flux density transported by the fields is given by the Poynting vector:

$$\boldsymbol{S} = \frac{1}{\mu}(E \times B)$$

For monochromatic plane waves propagating in the $\hat{z}$ direction:

$$\boldsymbol{S} = vu\hat{\boldsymbol{z}}$$

Electromagnetic waves not only carry energy, but also carry momentum. The momentum density stored in the fields is:

$$\wp = \frac{1}{v}u\hat{\boldsymbol{z}}$$

Momentum and energy oscillate as a cosine squared. Tipically we're interested in the average of those quantities, which means:

$$\langle u \rangle = \frac{1}{2}\epsilon E^2$$

$$\langle S \rangle = \frac{1}{2}v\langle u \rangle\hat{\boldsymbol{z}}$$

$$\langle \wp \rangle = \frac{1}{2v}\langle u \rangle\hat{\boldsymbol{z}}$$

The $\frac{1}{2}$ term is exactly the average of a cosine squared over a cycle. The quantity $\langle S \rangle$ represent the average power trasported per unit area by an EM wave, and it's called Intensity.

3.5 Reflection and refraction of EM waves at a plane interface between dielectrics

A monochromatic wave

$$\tilde{E}_i(r,t) = E_0 e^{ikx - i\omega t}$$

$$\tilde{B}_i(r,t) = \sqrt{\mu\epsilon}\,\frac{\boldsymbol{k}\times\boldsymbol{E}}{k}$$

Incident on a plane interface between dielectrics, gives rise to a reflected and a transmitted wave of equations:

$$\tilde{E}_r = E_{0r} e^{ik_r x - i\omega t} \quad \tilde{B}_r(r,t) = \sqrt{\mu_r\epsilon_r}\,\frac{\boldsymbol{k_r}\times\boldsymbol{E_r}}{k_r}$$

$$\tilde{E}_t = E_{0t} e^{ik_t x - i\omega t} \quad \tilde{B}_t(r,t) = \sqrt{\mu_t\epsilon_t}\,\frac{\boldsymbol{k_t}\times\boldsymbol{E_t}}{k_t}$$

At the interface between two different media the time and space variation of all fields must be the same, consequently we must have all phase factor equal, and all frequencies equal as well. This implies:

$$\boldsymbol{k_i}\cdot\boldsymbol{x} = \boldsymbol{k_r}\cdot\boldsymbol{x} = \boldsymbol{k_t}\cdot\boldsymbol{x}$$

Which means all three vectors must lie in a plane, called plane of incidence. Furthermore we have, considering fig.2:

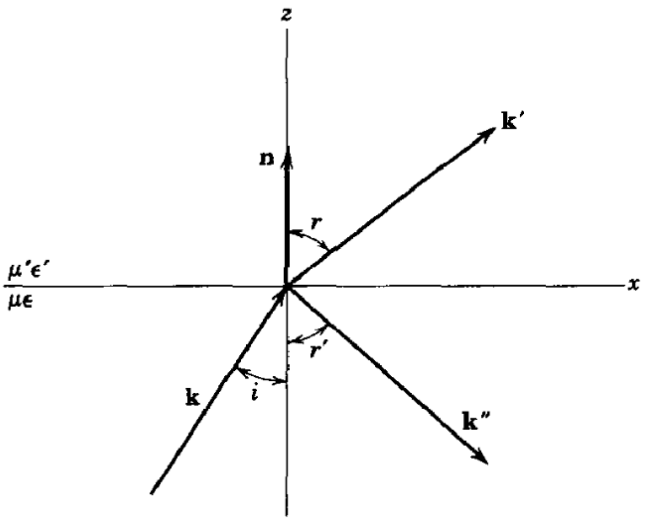

Figure 2: incident wave $\boldsymbol{k} = \boldsymbol{k_i}$ strikes plane interface between different media, giving rise to refracted wave $\boldsymbol{k}' = \boldsymbol{k_t}$ and reflected wave $\boldsymbol{k}'' = \boldsymbol{k_r}$

$$k_i \sin i = k_r \sin r = k_t \sin t$$

$$k_i = k_r = \frac{\omega}{c}\sqrt{\mu\epsilon}$$

The reflection angle equals the incidence angle, while the transmission angle is give by Snell's law:

$$\frac{\sin i}{\sin t} = \frac{n_t}{n_i}$$

Where n is the index of refraction, defined as $\sqrt{\frac{\mu\epsilon}{\mu_0\epsilon_0}}$, with μ_0 is the vacuum permeability and $\epsilon_0$is the vacuum susceptibility.

The boundary conditions at the interface are:

$$[\epsilon(\boldsymbol{E_i} - \boldsymbol{E_r}) - \epsilon_t \boldsymbol{E_t}] \cdot \boldsymbol{n} = 0$$

$$(\boldsymbol{k_i} \times \boldsymbol{E_i} + \boldsymbol{k_r} \times \boldsymbol{E_r} - \boldsymbol{k_t} \times \boldsymbol{E_t}) \cdot \boldsymbol{n} = 0$$

$$(\boldsymbol{E}_i + E_r - E_t) \times \boldsymbol{n} = \boldsymbol{0}$$

$$\left[\frac{1}{\mu}(\boldsymbol{k}_i \times \boldsymbol{E_i} + \boldsymbol{k_r} \times \boldsymbol{E_r}) - \frac{1}{\mu_t}(\boldsymbol{k_t} \times \boldsymbol{E_t})\right] \times \boldsymbol{n} = 0$$

Those conditions means that normal components of fields **D** and **B**, and tangential components of **E** and **H** are continuous across the interface. In applying those boundary conditions it is convenient to consider two separate situations, one in which the incident plane wave is linearly polarized with its polarization vector perpendicular to the plane of incidence, and the other in which the polarization vector is parallel to the plane of incidence. The boundary conditions simplify as follows:

For perpendicular polarization

$$E_i + E_r - E_t = 0$$

$$\sqrt{\frac{\epsilon}{\mu}}(E_i - E_r)\cos i - \sqrt{\frac{\epsilon_t}{\mu_t}} E_t \cos t = 0$$

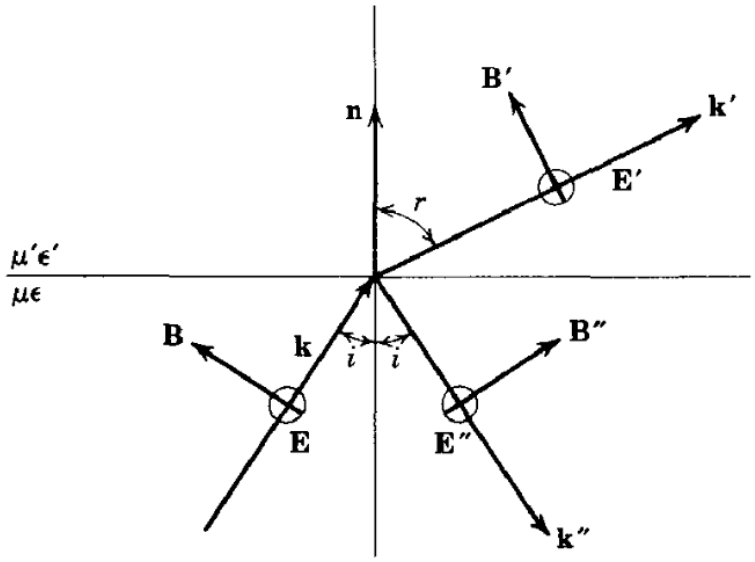

Figure 3: Perpendicularly polarized (TE-transverse electric) wave

And for parallel polarization

$$\cos i\,(E_i - E_r) - \cos t\,E_t = 0$$

$$\sqrt{\frac{\epsilon}{\mu}}(E_i + E_r) - \sqrt{\frac{\epsilon_t}{\mu_t}}E_t = 0$$

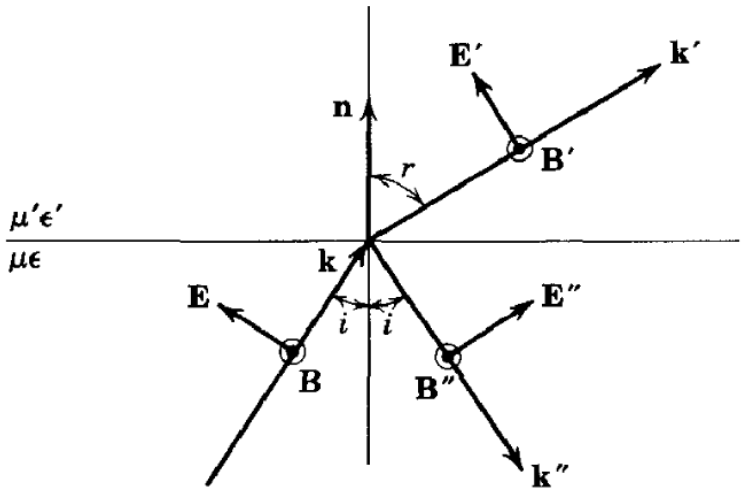

Figure 4: Parallel polarized (TM-transverse magnetic) wave

3.6 Brewster's angle and total internal reflection

For polarization parallel to the plane of incidence there is an angle of incidence, called Brewster's angle, at which there is no reflection. This angle is :

$$i_B = \tan^{-1}\left(\frac{n_t}{n}\right)$$

The total internal reflection arise when the incident and reflected waves are in a medium of higher index of refraction then the refracted wave $(n_t > n)$. If $(n_t > n)$, then the angle of refraction is larger then the angle of incidence. When the angle of refraction in equal to $\frac{\pi}{2}$ the refracted wave is propagated parallel to the surface and there is no energy flow across the interface. The angle of refraction is $\frac{\pi}{2}$ when the angle of incidence is equal to:

$$i_l = \sin^{-1}\left(\frac{n_t}{n}\right)$$

For the value i_l of the angle of incidence we have total internal reflection. For bigger values of i_l the refracted wave is still propageted parallel to the surface, but is also attenuated exponentially beyond the surface. The attenuation occurs within a very few wavelenghts from the surface.

3.7 Electromagnetic waves in conductors[3]

Maxwell's equations for conductors are

$$\nabla \cdot E = \frac{1}{\epsilon}\rho_f \qquad \nabla \cdot B = 0$$

$$\nabla \times E = -\frac{\partial B}{\partial t} \qquad \nabla \times B = \mu\sigma E + \mu\epsilon\frac{\partial E}{\partial t}$$

In a conductor the free current density J_f is generally not zero and proportional to the electric field through the relation

$$J_f = \sigma E$$

where σ is the conductivity. Maxwell's equations can further be simplified is we consider that free charge dissipates(flows out from the conductor) in a characteristic time[4] $\tau = \frac{\epsilon}{\sigma}$, which could be

[3] Incidentally, conductors are dispersive.

[4] N.Ashby [8] points out that for good conductors τ is absurdly short (10^{-19}s for copper whereas the time between collision is $\tau_c = 10^{-14}$s). The problem is Ohm's law breaks down on time scale shorter than τ_c; actually the time it takes free charge to dissipate in a good conductor is τ_c. [9] shows that fields and currents take even longer to equilibrate.

considered as a mesure of how good a conductor is. "Perfect" conductor have $\tau = 0$, "good" conductors have very little values for τ while "poor" conductors have nonnegligible values for τ.

Simplified Maxwel's equations are:

$$\nabla \cdot E = 0 \qquad \nabla \cdot B = 0$$

$$\nabla \times E = -\frac{\partial B}{\partial t} \qquad \nabla \times B = \mu\sigma E + \mu\epsilon \frac{\partial E}{\partial t}$$

This equations still admit plane wave solution of the form

$$\widetilde{\boldsymbol{E}} = \tilde{E} e^{i\boldsymbol{kx} - i\omega t} \qquad \widetilde{\boldsymbol{B}} = \tilde{B} e^{i\boldsymbol{kx} - i\omega t}$$

But this time the wave vector *k* is complex. The real and imaginary part of *k* can be expressed by:

$$k_r = \omega \sqrt{\frac{\mu\epsilon}{2}} \left[\sqrt{1 + \left(\frac{\sigma}{\omega\epsilon}\right)^2} + 1 \right]^{\frac{1}{2}} \qquad k_i = \omega \sqrt{\frac{\mu\epsilon}{2}} \left[\sqrt{1 + \left(\frac{\sigma}{\omega\epsilon}\right)^2} - 1 \right]^{\frac{1}{2}}$$

So that $k = k_r + ik_i$. The imaginary part results in an attenuation of the wave. The distance it takes to reduce the amplitude by a factor $\frac{1}{e}$ is called skin depth:

$$d = \frac{1}{k_i}$$

The imaginary part is responsable for another interesting feature: the electric and magnetic fields are no longer in phase, the magnetic field lag behind the electric. In good conductors the energy field is almost entirely magnetic in nature.

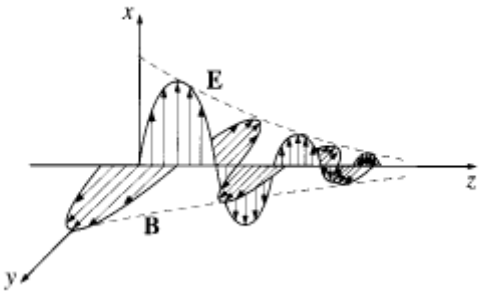

Figure 5: Electric and Magnetic fields in a conductor

3.7 Reflection at a conducting surface

The boundary conditions we used to analyze reflection and refraction at an interface between two dielectrics do not hold in the presence of free charges and current. We have the more general relations:

$$\epsilon_1 E_1^{\perp} - \epsilon_2 E_2^{\perp} = \sigma_f \qquad E_1^{\parallel} - E_2^{\parallel} = 0$$

$$B_1^{\perp} - B_2^{\perp} = 0 \qquad \frac{1}{\mu_1} B_1^{\parallel} - \frac{1}{\mu_2} B_2^{\parallel} = K_f \times \hat{\boldsymbol{n}}$$

Where K_f is the free surface current, σ_f the free surface charge and $\hat{\boldsymbol{n}}$ is a unit vector perpendicular to the surface, pointing from medium (2) to medium (1). If we suppose medium (1) to be a dielectric and medium (2) to be a good conductor we obtain results that are formally identical to those we discovered for nonconductors. The relations between incident, reflected and refracted fields for waves polarized parallel to the plane of incidence are:

$$\tilde{E}_R = \left(\frac{\alpha - \tilde{\beta}}{\alpha + \tilde{\beta}}\right) \tilde{E}_I \quad \tilde{E}_T = \left(\frac{2}{\alpha + \tilde{\beta}}\right) \tilde{E}_I$$

α and β are called Fresnel coefficients and are equal to:

$$\alpha = \frac{\cos\theta_T}{\cos\theta_I} \quad \tilde{\beta} = \frac{\mu_1 v_1}{\mu_2 \omega} \tilde{k}_2$$

The resemblance is only formal with dielectric case, because now $\tilde{\beta}$ is complex.

3.8 Electromagnetic waves in anisotropic media

The properties of an anisotropic medium with respect to electromagnetic waves are defined by the tensors $\boldsymbol{\epsilon}$, $\boldsymbol{\mu}$, and by the relations

$$\boldsymbol{D} = \boldsymbol{\epsilon E} \quad \boldsymbol{B} = \boldsymbol{\mu H}$$

$\boldsymbol{\epsilon}$ and $\boldsymbol{\mu}$ are second-order tensor completely determined by three mutually perpendicular vectors $\boldsymbol{\epsilon_i}$and $\boldsymbol{\mu_i}$ whose directions are called **principal axis.**

$$\boldsymbol{\epsilon} = \begin{bmatrix} \epsilon_{11} & \epsilon_{12} & \epsilon_{13} \\ \epsilon_{21} & \epsilon_{22} & \epsilon_{23} \\ \epsilon_{31} & \epsilon_{32} & \epsilon_{33} \end{bmatrix} \quad \boldsymbol{\mu} = \begin{bmatrix} \mu_{11} & \mu_{12} & \mu_{13} \\ \mu_{21} & \mu_{22} & \mu_{23} \\ \mu_{31} & \mu_{32} & \mu_{33} \end{bmatrix}$$

Using the generalized principle of the symmetry of the kinetic coefficients it is easy to demonstrate that $\epsilon_{ik} = \epsilon_{ki}$ and $\mu_{ik} = \mu_{ki}$. The tensor are therefore symmetric.

In anisotropic media the wave vector k, the fields D and H are all mutually perpendicular, and so are the fields H and E. The vectors D, k and E, being all perpendicular to H, are coplanar. With respect to k, D and H are always transverse, but E is not, in general. Similarly the Poynting vector, which describes the energy flux, has not, in general, the same direction of k as well. As a consequence the index of refraction n depends on the direction as well as on the frequency of incident waves.

A detailed explanation on how the electromagnetic waves propagate and are reflected and refracted at the interface between two anisotropic media will be given in chapter 5, in relation with the program written to simulate them.

3.9 Optical properties of Crystals

Crystals cannot be considered isotropic, they must be analyzed using the theory for anisotropic media. The optical properties of crystals depends primarily upon the symmetry of their dielectric tensor ϵ_{ik}. All crystals fall under 3 types: cubic, uniaxial and biaxial. In a crystal of the cubic system $\epsilon_{ik} = \epsilon\delta_{ik}$, i.e the three principal values of the tensor are equal, and the direction of the principal axis are arbitrary. As regards their optical properties, cubic crystal are no different from isotropic bodies. The uniaxial crystal include those of the rhombohedral, tetragonal and hexagonal systems. The hexagonal system is particularly important because it can be demonstrated that any structures that has in-plane isotropy and out-of-plane anisotropy posses hexagonal symmetry. In uniaxial crystals one of the principal axes of the tensor $\boldsymbol{\epsilon}$ is chosen to coincide with the threefold, fourfold or sixfold axis of symmetry of the crystal; this axis is called the ***optical axis*** of the crystal, and we shall take it as the z-axis in a Cartesian representation, denoting the corresponding principal value of $\boldsymbol{\epsilon}$ by $\boldsymbol{\epsilon_{\parallel}}$**.** The direction of the other two principal axes, in a plane perpendicular to the optical axis, are arbitrary, and the corresponding principal values are equal and denote by $\boldsymbol{\epsilon_{\perp}}$.

In a uniaxial crystal two types of waves can propagate. With respect to one type, called ***ordinary waves***, the crystal behaves like an isotropic medium with refractive index $n = \sqrt{\frac{\epsilon_{\perp}\mu}{\epsilon_0\mu_0}}$. The magnitude of the wave vector is $\omega\frac{n}{c}$ whatever its direction, and the direction of the ray vector is that of the wave vector.

The ray vector is a quantity that characterizes the propagation of light in anisotropic medium (and in geometrical optics, of course). The direction of light rays is given by the group velocity $\frac{\partial\omega}{\partial k}\widehat{\boldsymbol{k}}$. In isotropic medium the direction of the wave vector is always the same as the direction of the ray vector, but in anisotropic medium the two in general do not coincide. The magnitude is given by $\boldsymbol{n}\cdot\boldsymbol{s} = \mathbf{1}$ where $\boldsymbol{n}$ is the refractive index vector, and $\boldsymbol{s}$ the ray vector.

The waves of the second type, called ***extraordinary waves***, the index of refraction *n* depends upon the angle θ between the wave vector and the optical axis through the relation

$$\frac{1}{n^2} = \frac{(\sin\theta)^2}{\epsilon_{\parallel}} + \frac{(\cos\theta)^2}{\epsilon_{\perp}}$$

For the wave vector and the ray vector are not on the same direction but lies in the same plane, along with the optical axis. In uniaxial crystals two refracted waves are formed, a phenomenon known as ***double refraction*** or ***birefringence.*** The ordinary refracted waves is entirely analogous to the refracted waves in isotropic bodies and lies in the plane of incidence with the incident and the reflected wave. The extraordinary wave still has its wave vector lying in the plane of incidence, but its ray vector generally does not.

Biaxial crystals have the three principal values of the tensor $\boldsymbol{\epsilon}$ all different. Crystals of the triclinic, monoclinic and orthorhombic systems are of this type. This type of crystals aren't of interest in the simulation of multilayer produced by molecular deposition because it can occur only for layers which are not in-plane isotropic.

Chapter 4

Electromagnetic waves in multilayered structures

This chapter is a detail explanation of the mathematical model used to simulate the propagation and the interaction of electromagnetic waves at the interface between two different isotropic media.

4.1 Propagation and superposition of waves in a multilayer

First we consider a plane, monochromatic electromagnetic wave P, incident with an angle θ with the surface of a multilayered structure made of n layers, separated by plane and parallel interfaces. At every interface two waves are generated, the transmitted wave, which travels to the next layer and the reflected wave which travels back, with direction given by Snell's law. We also consider two different polarizations, parallel and perpendicular to the plane of incidence.

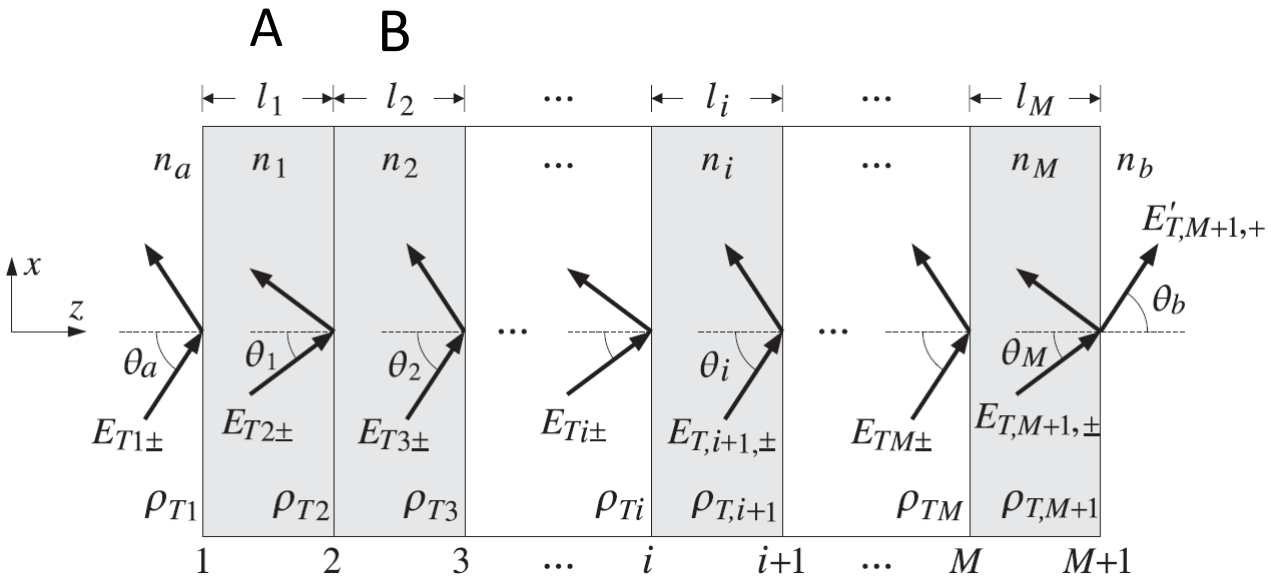

Figure 1: Electromagnetic waves propagating in a multilayer

The fields in a generic layer n are:

$$\tilde{E}_n(r,t) = \tilde{E}_{Tn}e^{i\omega t + ik_n \boldsymbol{r}} + \tilde{E}_{Rn}e^{i\omega t - ik_n \boldsymbol{r}}$$

$\tilde{E}_{nT}$ and $\tilde{E}_{nR}$ are the complex amplitudes of the waves propagating in direction $+\boldsymbol{k_x} + \boldsymbol{k_z}$ and $+\boldsymbol{k_x} - \boldsymbol{k_z}$, where **r** is the position vector. We can express the position vector **r** in terms of the Cartesian components **x, y** and **z** represented in the figure; **z** points in the direction perpendicular to the interface of two layers while **x** and **y** points in the parallel direction. Depending on polarization the previous equation become

$$\tilde{E}_n(r,t) = \tilde{E}_{nT}e^{i\omega t + i(\boldsymbol{k_{xn}x} + \boldsymbol{k_{zn}z})} + \tilde{E}_{nR}e^{i\omega t + i(\boldsymbol{k_{xn}x} - \boldsymbol{k_{zn}z})}$$

for parallel polarization and

$$\tilde{E}_n(r,t) = \tilde{E}_{nT}e^{i\omega t + i(\boldsymbol{k_{xn}y} + \boldsymbol{k_{zn}z})} + \tilde{E}_{nR}e^{i\omega t + i(\boldsymbol{k_{xn}y} - \boldsymbol{k_{zn}z})}$$

For perpendicular.

We have M layers, plus 2 semi infinite layers representing the air and the substrate called respectively material A and material B in figure 1. This means we have M+1 interfaces to which we impose the boundary conditions expressed in the previous chapter:

$$\epsilon_1 E_1^{\perp} = \epsilon_2 E_2^{\perp} \qquad E_1^{\parallel} = E_2^{\parallel}$$

$$B_1^{\perp} = B_2^{\perp} \quad \frac{1}{\mu_1} B_1^{\parallel} = \frac{1}{\mu_2} B_2^{\parallel}$$

Using the relation $B = \frac{E}{v_n}$, with *v* speed of light in medium *n,* we can express the boundary conditions in terms of electric fields only.

We want to find the amplitudes $\tilde{E}_{ik}$ of the fields in every layer in order to derive meaningful physical quantities like reflectivity and transmissivity. To do so we observe that the unknown waves are two for each layer, except for the last one where we don't have any reflected wave because the layer is assumed to be infinite. The amplitude of the incident wave $\tilde{E}_{T1}$ is given and therefore we have to calculate $(2M + 1 + 1) = (2M + 2)$ unknowns. If we consider the waves as linearly polarized in direction perpendicular and parallel to the plane of incidence, as described before, the independent boundary conditions reduce to 2, instead of 4. This is no problem, considered we have M+1 interfaces to where the conditions apply, $2(M + 1) = 2M + 2$, and the number of unknown equal the number of equations.

In the case of perpendicular polarization the meaningful conditions are, since the electric fields have no components perpendicular to the interface, $E_1^{\parallel} = E_2^{\parallel}$, $B_1^{\perp} = B_2^{\perp}$, $\frac{1}{\mu_1} B_1^{\parallel} = \frac{1}{\mu_2} B_2^{\parallel}$, but using Snell's law the second replicates the third and the system becomes:

$$e^{i\omega t}[\tilde{E}_{1R}e^{+i(\boldsymbol{k_{x1}y_1-k_{z1}z_1})}-\tilde{E}_{2T}e^{i(\boldsymbol{k_{x2}y_1+k_{z2}z_1})}-\tilde{E}_{2R}e^{+i(\boldsymbol{k_{x2}y-k_{z2}z_1})}]=-e^{i\omega t}\tilde{E}_{1T}e^{i(\boldsymbol{k_{x1}y+k_{z1}z_1})}$$

$$e^{i\omega t}[-\frac{1}{\mu_1 v_1}\tilde{E}_{1R}e^{+i(\boldsymbol{k_{x1}y_1-k_{z1}z_1})}\cos i_1-\frac{1}{\mu_2 v_2}(\tilde{E}_{2T}e^{i(\boldsymbol{k_{x2}y_1+k_{z2}z_1})}-\tilde{E}_{2R}e^{+i(\boldsymbol{k_{x2}y_1-k_{z2}z_1})})\cos t_2]=$$
$$-\frac{1}{\mu_1 v_1}e^{i\omega t}\tilde{E}_{1T}e^{i(\boldsymbol{k_{x1}y_1+k_{z1}z_1})}\cos i_1$$

$$e^{i\omega t}[\tilde{E}_{2T}e^{i(\boldsymbol{k_{x2}y+k_{z2}z_2})}+\tilde{E}_{2R}e^{+i(\boldsymbol{k_{x2}y_2-k_{z2}z_2})}-\tilde{E}_{3T}e^{i(\boldsymbol{k_{x3}y_2+k_{z3}z_2})}-\tilde{E}_{3R}e^{+i(\boldsymbol{k_{x3}y_2-k_{z3}z_2})}]=0$$

$$e^{i\omega t}[\frac{1}{\mu_2 v_2}(\tilde{E}_{2T}e^{i(\boldsymbol{k_{x2}y_2+k_{z2}z_2})}-\tilde{E}_{2R}e^{+i(\boldsymbol{k_{x2}y_2-k_{z2}z_2})})\cos i_2-\frac{1}{\mu_2 v_2}(\tilde{E}_{3T}e^{i(\boldsymbol{k_{x3}y_2+k_{z2}z_2})}-\tilde{E}_{3R}e^{+i(\boldsymbol{k_{x3}y_2-k_{z3}z_2})})\cos t_3]=0$$

$$\vdots \qquad\qquad \vdots \qquad\qquad \vdots$$

$$e^{i\omega t}[(\tilde{E}_{MT}e^{+i(\boldsymbol{k_{xM}y-k_{zM}z_{M+1}})}+\tilde{E}_{MT}e^{i(\boldsymbol{k_{xM}y_{M+1}+k_{zM}z_{M+1}})})-\tilde{E}_{M+1T}e^{+i(\boldsymbol{k_{xM+1}y_{M+1}-k_{zM+1}z_{M+1}})}]=0$$

$$e^{i\omega t}[\frac{1}{\mu_M v_M}(\tilde{E}_{MT}e^{+i(\boldsymbol{k_{xM}y_{M+1}-k_{zM}z_{M+1}})}-\tilde{E}_{MT}e^{i(\boldsymbol{k_{xM}y_{M+1}+k_{zM}z_{M+1}})})\cos i_M-\frac{1}{\mu_{M+1}v_{M+1}}\tilde{E}_{M+1T}e^{+i(\boldsymbol{k_{xM+1}y_{M+1}-k_{zM+1}z_{M+1}})}\cos t_{M+1}]$$
$$=0$$

While for parallel polarization the meaningful conditions are $\epsilon_1 E_1^{\perp}=\epsilon_2 E_2^{\perp}$, $B_1^{\perp}=B_2^{\perp}$ $\frac{1}{\mu_1}B_1^{\parallel}=\frac{1}{\mu_2}B_2^{\parallel}$ because now the fields are all perpendicular to the interface. Once again thanks to Snell' law the second condition replicates the third and the system is:

$$e^{i\omega t}[-\tilde{E}_{1R}e^{+i(\boldsymbol{k_{x1}x_1-k_{z1}z_1})}\cos i_1-(\tilde{E}_{2T}e^{i(\boldsymbol{k_{x2}x_1+k_{z2}z_1})}-\tilde{E}_{2R}e^{+i(\boldsymbol{k_{x2}x_1-k_{z2}z_1})})\cos t_2]=-e^{i\omega t}\tilde{E}_{1T}e^{i(\boldsymbol{k_{x1}x_1+k_{z1}z_1})}\cos i_1$$
$$e^{i\omega t}[\frac{1}{\mu_1 v_1}\tilde{E}_{1R}e^{+i(\boldsymbol{k_{x1}x_1-k_{z1}z_1})}-\frac{1}{\mu_2 v_2}(\tilde{E}_{2T}e^{i(\boldsymbol{k_{x2}x_1+k_{z2}z_1})}-\tilde{E}_{2R}e^{+i(\boldsymbol{k_{x2}x_1-k_{z2}z_1})})]=-\frac{1}{\mu_1 v_1}e^{i\omega t}\tilde{E}_{1T}e^{i(\boldsymbol{k_{x1}x_1+k_{z1}z_1})}\cos i_1$$
$$e^{i\omega t}[(\tilde{E}_{2T}e^{i(\boldsymbol{k_{x2}x_2+k_{z2}z_2})}-\tilde{E}_{2R}e^{+i(\boldsymbol{k_{x2}x_2-k_{z2}z_2})})\cos i_2-(\tilde{E}_{3T}e^{i(\boldsymbol{k_{x3}x_2+k_{z3}z_2})}-\tilde{E}_{3R}e^{+i(\boldsymbol{k_{x3}x_2-k_{z3}z_2})})\cos t_3]=0$$
$$e^{i\omega t}[\frac{1}{\mu_2 v_2}(\tilde{E}_{2T}e^{i(\boldsymbol{k_{x2}x_2+k_{z2}z_2})}+\tilde{E}_{2R}e^{-i(\boldsymbol{k_{x2}x_2+k_{z2}z_2})})-\frac{1}{\mu_2 v_2}(\tilde{E}_{3T}e^{i(\boldsymbol{k_{x3}x_2+k_{z2}z_2})}+\tilde{E}_{3R}e^{-i(\boldsymbol{k_{x3}x_2+k_{z3}z_2})})]=0$$
$$\vdots \qquad\qquad \vdots \qquad\qquad \vdots$$
$$e^{i\omega t}[(\tilde{E}_{MT}e^{+i(\boldsymbol{k_{xM}x_{M+1}-k_{zM}z_{M+1}})}-\tilde{E}_{MT}e^{i(\boldsymbol{k_{xM}x_{M+1}+k_{zM}z_{M+1}})})\cos i_M-\tilde{E}_{M+1T}e^{+i(\boldsymbol{k_{xM+1}x_{M+1}-k_{zM+1}z_{M+1}})}\cos t_{M+1}]=0$$
$$e^{i\omega t}[\frac{1}{\mu_M v_M}(\tilde{E}_{MT}e^{+i(\boldsymbol{k_{xM}x_{M+1}-k_{zM}z_{M+1}})}+\tilde{E}_{MT}e^{i(\boldsymbol{k_{xM}x_{M+1}+k_{zM}z_{M+1}})})-\frac{1}{\mu_{M+1}v_{M+1}}\tilde{E}_{M+1T}e^{+i(\boldsymbol{k_{xM+1}x_{M+1}-k_{zM+1}z_{M+1}})}]=0$$

The system could be rewritten using matrix representation in the form

$$\boldsymbol{C\cdot A=T}$$

Where **C** is the matrix holding the coefficients, **A** is the unknown vector and **T** is the vector holding the known values of the fields.

It's possible to simplify the notation by considering that $e^{i\omega t}$ appears on both sides of every equation and by remembering that the parallel components of electric fields must be conserved at the interface, thus simplifying the exponential terms dependent on **x**:

$$e^{i\boldsymbol{k}_{y,n-1}\boldsymbol{y}_n} = e^{i\boldsymbol{k}_{y,n}\boldsymbol{y}_n}$$

In the case of perpendicular polarization **C** becomes:

$$\boldsymbol{C} =$$

$$\begin{pmatrix}
e^{-ik_{z1}z_1} & -e^{ik_{z2}z_1} & -e^{-ik_{z2}z_1} & 0 & \dots \\
-\frac{1}{\mu_1 v_1}e^{-ik_{z1}z_1}\cos i_1 & -\frac{1}{\mu_2 v_2}e^{ik_{z2}z_1}\cos t_2 & \frac{1}{\mu_2 v_2}e^{-ik_{z2}z_1}\cos t_2 & 0 & \cdots \\
0 & e^{ik_{z2}z_2} & e^{-ik_{z2}z_2} & -e^{ik_{z3}z_2} & -e^{-ik_{z3}z_2} & 0 & \dots \\
0 & \frac{1}{\mu_2 v_2}e^{ik_{z2}z_2}\cos i_2 & -\frac{1}{\mu_2 v_2}e^{-ik_{z2}z_2}\cos i_2 & \frac{1}{\mu_3 v_3}e^{ik_{z3}z_2}\cos t_3 & \frac{1}{\mu_3 v_3}e^{-ik_{z3}z_2}\cos t_3 & 0 & \dots \\
 & & & \vdots & & & \\
0 & \dots & e^{ik_{zM}z_{M+1}} & e^{ik_{zM}z_{M+1}} & -e^{-ik_{zM+1}z_{M+1}} & & \\
0 & \dots & \frac{1}{\mu_M v_M}e^{-ik_{zM}z_{M+1}}\cos i_M & -\frac{1}{\mu_M v_M}e^{-ik_{zM}z_{M+1}}\cos i_M & -\frac{1}{\mu_{M+1} v_{M+1}}e^{-ik_{zM+1}z_{M+1}}\cos t_{M+1} & &
\end{pmatrix}$$

$$\boldsymbol{A} = \begin{pmatrix} \tilde{E}_{R1} \\ \tilde{E}_{T2} \\ \tilde{E}_{R2} \\ \tilde{E}_{T3} \\ \vdots \\ \tilde{E}_{TM+1} \end{pmatrix}$$

$$\boldsymbol{T} = \begin{pmatrix} -\frac{1}{\mu_1 v_1}e^{-ik_{z1}z_1} \\ -\frac{1}{\mu_1 v_1}e^{-ik_{z1}z_1}\cos i_1 \\ 0 \\ \vdots \\ 0 \\ 0 \end{pmatrix}$$

The same can be done with parallel polarization, leading to similar results.

The easiest way to find solutions consists in multiply both sides of $\boldsymbol{C}\cdot\boldsymbol{A} = \boldsymbol{T}$ by the inverse matrix $\boldsymbol{C}^{-1}$ ($\boldsymbol{C}^{-1}\cdot\boldsymbol{C} = \boldsymbol{I}$) and solving for ***A:***

$$\boldsymbol{A} = \boldsymbol{C}^{-1}\cdot\boldsymbol{T}$$

Chapter 5

The isotropic programs

This chapter shows in detail the structure of the software specifically designed to simulate the propagation of electromagnetic waves in isotropic multilayered media. The software has been designed using Matlab environment, a widespread mathematical software.

5.1 Matlab programs multidiel.m and multidielPar.m

Matlab programs MultistratoPer.m and MultistratoPar.m are designed to solve the problem of reflection and transmission of electromagnetic waves in a multilayer structure using the procedure illustrated in chapter 3. Basically those programs solve the problem $\boldsymbol{A} = \boldsymbol{C}^{-1}\boldsymbol{T}$ for the two possible linear polarization of the incident wave. Matrix **C** has $(2M + 2) \times (2M + 2)$ elements (M is the numbers of layers) which grow quadratically with the numbers of layers.

It is important to understand that the programs do not simulate the propagations of waves as they move from one layer to the other and go through reflection or transmission, but gives the superposition of all the transmitted and all the reflected waves at a particular interface which satisfy the boundary conditions explained previously. That being said it is obvious the output for, let's say, the first interface, which represent the boundary between air, chosen as the first layer by default, and the second layers, which is arbitrary, is the global reflectivity of the whole multilayer structure.

The default streamline of the programs computes the response for a multilayer structure made by two different media, called medium A and medium B. Medium A and medium B periodically repeat in the structure, with material A coming on top of ,material B. Those media can be of any type: dielectrics, conductors, magnetic; they are defined by the index of refraction, the permeability and the conductivity and the programs will handle the different user defined configurations. There are no limitation to the nature of the media involved. In order to account for not perfectly transparent media the programs work with complex values of the properties, as explained in chapter 2. The number of layers is arbitrary and the thicknesses are given by their ratio to the wavelength of the incident wave, which represent the only intrinsic length scale of the problem. The problems are solved for a particular wavelength and this allows us to solve the equations for fixed values the dependence of the index of refraction, the conductivity and the permeability upon the frequency. If results are needed for different wavelengths the computations are simply repeated for the appropriate frequency dependent values of the material properties. The programs are designed to calculate the variation of the fields in the structure for an arbitrary angle of incidence, chosen by the user, thus dramatically increasing the generality of the simulation.

The amplitude of the incident wave is required as input from the user, but of course changing it changes nothing for the reflectivity and represent a mere constant shift in the amplitudes of the waves obtained by superposition in every layer. It's set by default to 1.

In the programs I added a feature which let the user set any number of what in literature are called "defects". A defect is an anomaly in the multilayer periodical structure which can manifest itself in a localized difference in thickness or material type or both. By means of this feature is possible to analyze the response of virtually endless configuration of multilayer and analyze also structures which don't posses any periodical structure at all.

5.2 Data acquisition

The default structure of the multilayer is implemented in Matlab programs and need rewriting in the source code to be changed. The user have to manually replace important parameters as:

- Thickness
- Index of refraction
- Conductivity
- Relative Permeability
- Angle of Incidence
- Wavelength

This approach cannot be used for the implementation of defects data, because the defects can be so numerous to deem as infeasible such a design. For maximum portability and efficiency a C++ program has been created which acquire defects data and feed them directly to the main MatLab program. C++ acquire critical parameters such as:

- Number of Layers
- Number of Defects in the multilayered structure, which can even by equal to the number of layers itself, thus bypassing the default structure in MatLab
- Position of the defects, because even position matters in the overall response
- Index of refraction of defects
- Conductivity
- Relative Permeability (set by default to 1 is not explicitly requested by the user)
- Thicknesses

5.3 The generic matrix element

I will point out in more detail how every element in the resolving matrix is obtained. The generic matrix element can be written as:

$$\{a_{rc}\} = \mathcal{A} \cdot \mathcal{B} \cdot \mathcal{C}^{\mathcal{D}} e^{\mathcal{E} \cdot k_{\mathcal{F}} x_{\mathcal{G}}} \cdot \mathcal{H}$$

Where $\mathcal{A}\ \mathcal{B}\ \mathcal{C}\ \mathcal{D}\ \mathcal{E}\ \mathcal{F}\ \mathcal{G}\ \mathcal{H}$ are coefficient chosen to give in the generic position (r, c) , where r represents the rows in the solving matrix and c represents the columns, the right result.

- $\mathcal{A}$ indicates if the element is different from zero
- $\mathcal{B}$ deontes the sign of the element
- $\mathcal{C}$ is the coefficient for the magnetic field
- $\mathcal{D}$ can be zero, if we're considering rows where we compute electric fields, or one, if we're considering rows where the magnetic field is involved.
- $\mathcal{E}$ gives the sign of the exponential
- $\mathcal{F}$ is the index of k
- $\mathcal{G}$ is the index of x
- $\mathcal{H}$ gives the angular dependence

$\mathcal{A}$

This parameter tells us which element are different from zero in our matrix. Let's focus on a 20×20 matrix and let's see in detail which elements are nonzero.

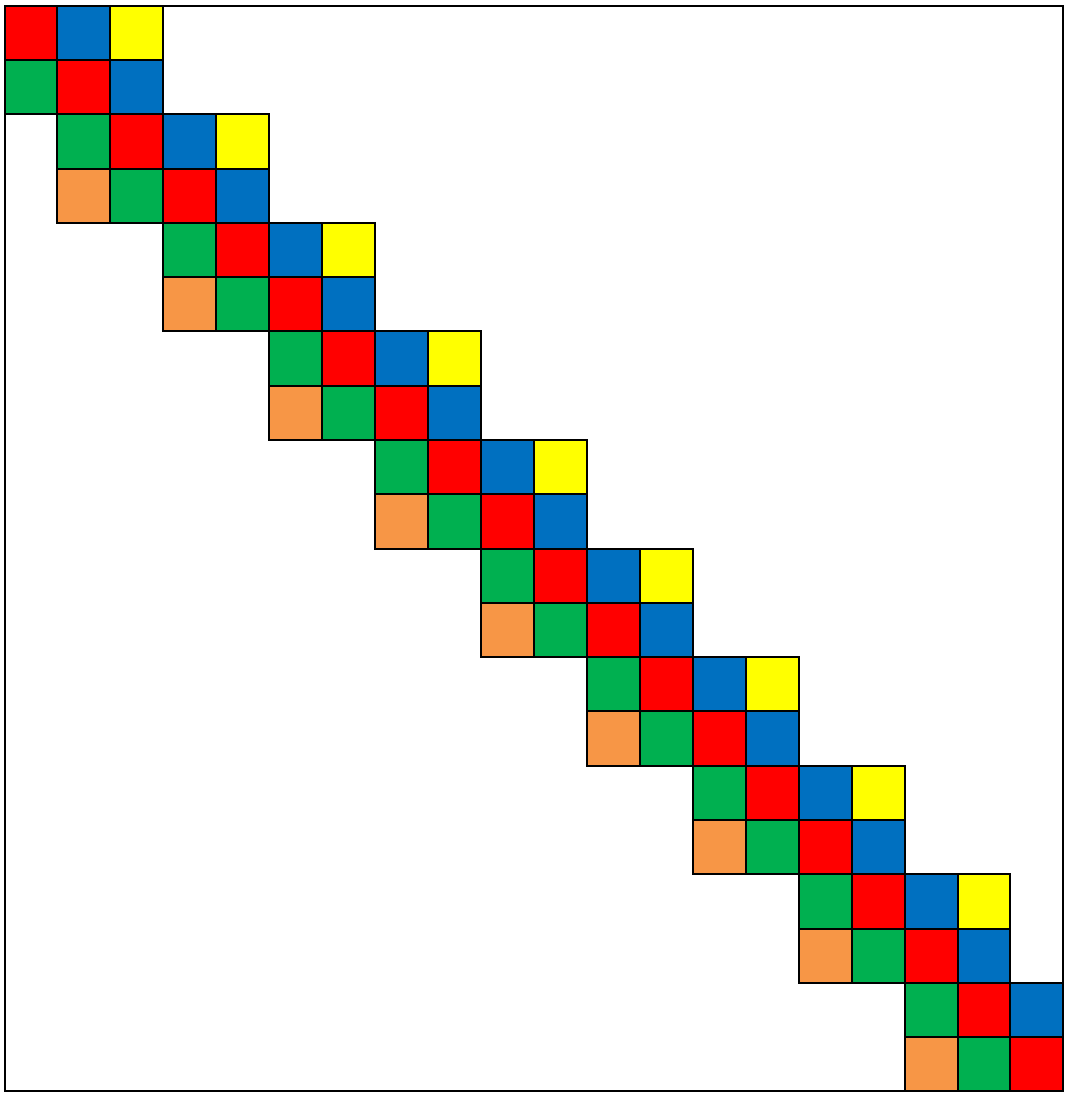

Tab.1: Elements that differ from zero are highlighted with different colours

- Elements on the principal diagonal, in red, occupy positions (r, c)
- Elements in blue occupy positions $(r, c+1)$
- Elements in green occupy positions $(r+1, c)$
- Elements in yellow occupy positions $(r, c+2)$, with odd r
- Elements in orange occupy positions $(r+2, c)$, with even c

To tell Matlab which elements is different from zero has been designed the program delta.m, which behaves like the Kronecker Delta:

$$\delta_{ij} = \begin{cases} 0 & when \quad i \neq j \\ 1 & when \quad i = j \end{cases}$$

$\boldsymbol{\mathcal{A}_{red}} = \boldsymbol{\delta_{r,c}}$ and similarly for the other colors. In order to be nonzero only the elements on the "orange" diagonal (and same for the yellow) I've used the relation:

$$\boldsymbol{\mathcal{A}_{orange}} = \frac{1-(-1)^r}{2}\boldsymbol{\delta_{orange}}$$

In the end $\boldsymbol{\mathcal{A}} = \boldsymbol{\mathcal{A}_{red}} + \boldsymbol{\mathcal{A}_{green}} + \boldsymbol{\mathcal{A}_{blue}} + \boldsymbol{\mathcal{A}_{yellow}} + \boldsymbol{\mathcal{A}_{orange}}$

$\mathcal{B}$

$\mathcal{B}$ identifies the sign of the element in the matrix. Signs are distributed as follows:

For Perpendicular polarization

+	+	-	-
+	-	-	+

Tab.2: Signs of the element in the matrix for perpendicular polarization

For parallel polarization

+	-	-	+
+	+	-	+

Tab.3: Signs of the element in the matrix for parallel polarization

This sign pattern, which is a 2×4 matrix, repeats periodically for every nonzero element. MatLab programs automatically assign every sign to the corresponding delta.

$\mathcal{E}$

$\mathcal{E}$ identifies the sign of the exponential term. I've used the same function as $\mathcal{B}$ to track down the sign for the corresponding matrix element, with the slight difference that the sign has been reversed for blue and red diagonals. Signs are equal for parallel and perpendicular polarizations.

+	-	+	-
+	-	+	-

Tab.4: Signs of the exponentials

$\mathcal{D}$ and $\mathcal{H}$

$\mathcal{D}$ and $\mathcal{H}$ are responsible for the magnetic field coefficient and for the angular coefficient respectively. For parallel polarization those coefficients appear only in odd rows, thus $\mathcal{D}$ and $\mathcal{H}$ have the form:

$$\mathcal{D} = \mathcal{H} = \frac{1-(-1)^r}{2}$$

For perpendicular polarization, on the other side, they appear only for even rows:

$$\mathcal{D} = \mathcal{H} = \frac{1+(-1)^r}{2}$$

$\mathcal{C}, \mathcal{F}, \mathcal{G}$

Those coefficients are assigned through nested **for** cycles. The idea behind the algorithm which assigns them their value is the following:

For the $\mathcal{F}$ and $\mathcal{C}$ coefficients:

- Starting from column 2 $(c = 2)$ $\mathcal{F}$ and $\mathcal{C}$ must be the same for the column we're considering and for the next (in this case column 2 and 3). This can be generalized for column n and column n+1.
- The first and the last column have their $\mathcal{F}$ and $\mathcal{C}$ values assigned outside the nested for.

The first **for** cycles through every layer except the first and the last, while another **for** cycles through the columns. The first column have the default air values assigned, while the second and third are recognized by the matching counters of **for** cycles as belonging to material A, and consequently fourth and fifth are assigned to Material B and so on. The last layer is assigned by default to the material chosen to be the substrate, called Final material in the program. If defects are assigned for counters cycle through defect position and match them with the corresponding layer, overwriting default data with defect data acquired via C++.

For $\boldsymbol{\mathcal{G}}$ coefficients the algorithm is very similar, except now we consider the rows and not the columns.

- Starting from row 2 $(r = 2)$ $\boldsymbol{\mathcal{G}}$ must be the same for the row we're considering and for the next (in this case row 2 and 3). This can be generalized for row m and row m+1.
- The first and the last row have their $\boldsymbol{\mathcal{G}}$ values assigned outside the nested for

The way the for act upon the rows and the layers is analogous to what explained before.

5.3 Target: efficiency

Let's take a close look at matrix **C**: it's squared $n \times n$. Let's divide it in 4 squared sub matrix $\frac{n}{2} \times \frac{n}{2}$. Let's call the matrix we obtain A_{11}, A_{12}, A_{21} and A_{22}. The determinant of matrix **C** can be calculated using Laplace's formula: $\det(\boldsymbol{C}) = \det(A_{11}) \times \det(A_{22}) - \det(A_{12}) \times \det(A_{21})$. For what we've seen before about the structure of matrix **C,** $\det(A_{12})$ and $\det(A_{21})$ are zero because sub matrix A_{12} and A_{21} both have more than a row of zeros. This means $\det(\boldsymbol{C}) = \det(A_{11}) \times \det(A_{22})$. Now we can take sub matrix A_{11} and divide it in four sub matrix $\frac{n}{4} \times \frac{n}{4}$ and do the same trick again. With this method calculations are made much faster.

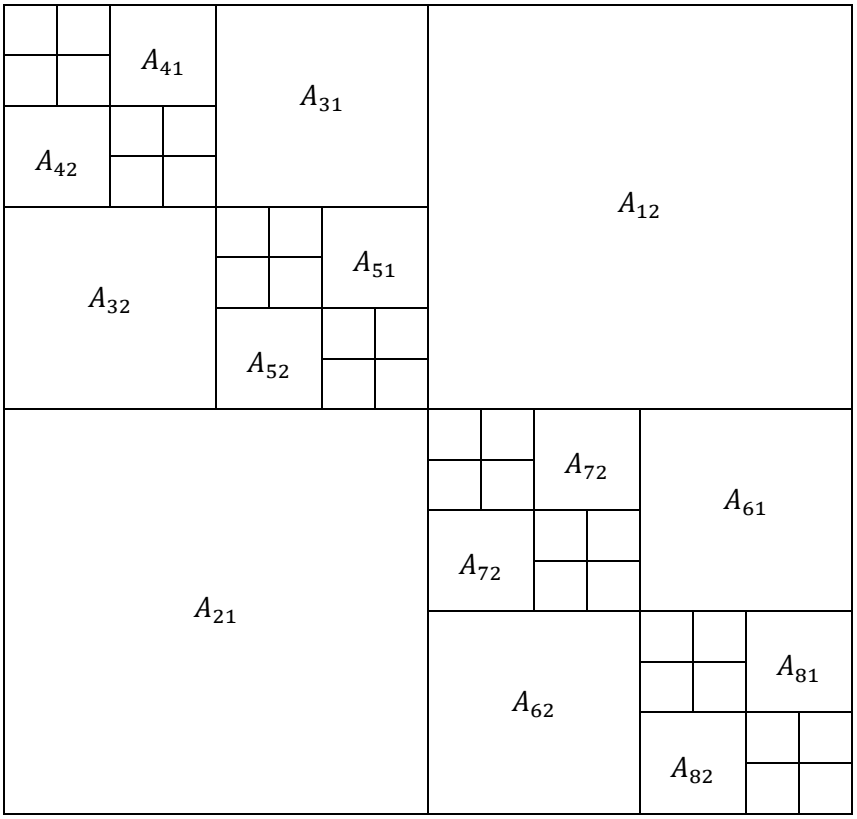

Tab.5: Block matrix

5.4 Validations

The strategy followed to verify the results can be summarized in three steps: first the results have been checked to be in agreement with the conservation of energy principle, second the program was run in a configuration for which the results could have been computed analytically and third the numerical solutions for a configuration not solvable analytically have been validated by measurements available in literature.

Verifying the conservation energy principle is an easy task once we recall the technique used to create the program. The fields, thanks to the Maxwell's equations linearity, are nothing but the superposition of the fields coming from every layer of our body, satisfying the boundary conditions given in chapter 4. $|E|^2$, incident on the first interface, represents the total electric energy entering the system. $\left|E_{r,1}\right|^2$ represents the total electric energy reflected by the system, and it's a superposition of the contributions coming from all the layers. $\left|E_{t,M+1}\right|^2$ is the electric energy in the last layer, and represents the total electric energy transmitted. The same can be said for magnetic energy. Thus to satisfy the energy conservation, considering conducting and magnetic media as well, the following equality must be verified:

$$|U|^2 \geq \sqrt{\left|U_{r,1}\right|^2 + \left|U_{t,M+1}\right|^2}$$

Where U is the total (magnetic and electric) energy incident on the first interface, $U_{r,1}$ is the total energy reflected at the first interface and $U_{t,M+1}$ is the total energy transmitted in the last layer.

In order to verify the results analytically I decided to collapse the multilayered structure in a monolayer and then apply Fresnel's coefficients to find the values of the fields. For perpendicular polarization Fresnel's coefficients are:

$$\frac{E_t}{E} = \frac{2\cos i \sin r}{\sin(r+i)} \qquad \frac{E_r}{E} = -\frac{\sin(i-r)}{\sin(i+r)}$$

While for parallel polarization are:

$$\frac{E_t}{E} = \frac{2\cos i \sin r}{\sin(i+r)\cos(i-r)} \qquad \frac{E_r}{E} = \frac{\tan(i-r)}{\tan(i+r)}$$

i and r represent, as in chapter 4, the angle of incidence and the angle of refraction, respectively. $E_t \; and \; E_r$ represent generic reflected and transmitted fields, while E is the field incident on the first interface.

Lastly, as expected from the law of interference, if a layer of a given homogeneous material of refractive index n_1 is put between two layers of another homogeneous material of refractive index n_2, we obtain a reflectivity which varies sinusoidally with thickness.

The maxima are in: $d = \frac{(2K+1)\lambda}{4}$ with $K = 0,1,2, \ldots$

The minima are in: $d = \frac{K\lambda}{2}$ with $K = 0,1,2, \ldots$

Where d is the thickness and λ the wavelength.

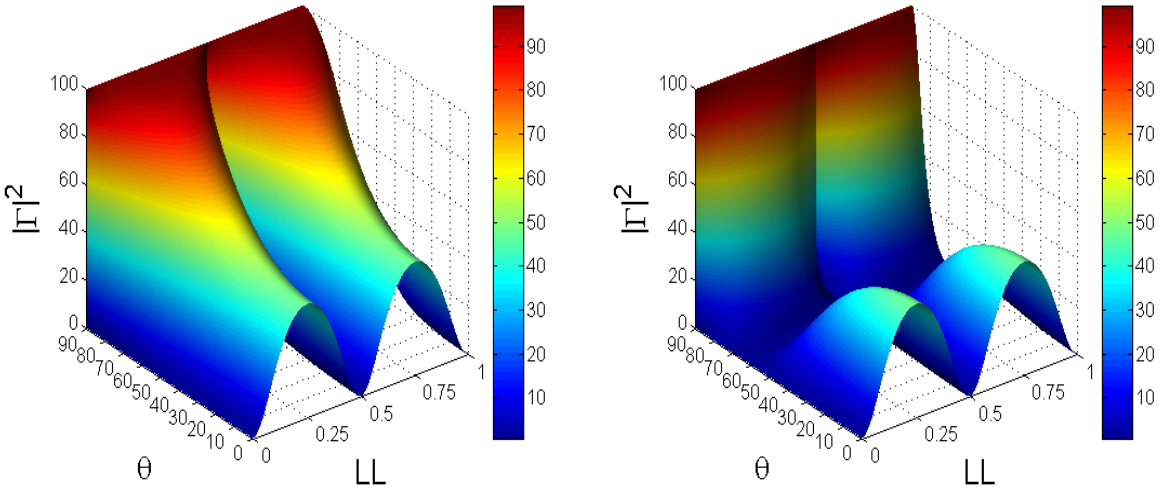

Figure 1.1 Reflectivity vs. thickness and angle of incidence for perpendicular (left) and parallel polarization. Notice the sinusoidal shape and the presence of Brewster's angle for parallel polarization, in accordance with theory. Both reflectivity goes to 100% for $\theta = 90°$, as expected. The material have refraction indices $n_1 = 1.5$ (corresponding to glass) and $n_2 = 1$ (corresponding to air)

Chapter 6

Designing an Omnidirectional mirror

In this chapter Matlab software for isotropic multilayer will be used to design a mirror able to reflect with efficiency close to 90% the light incoming from all angles and from both polarizations. Defects will then be added to the layers and the response analyzed for non-periodic configurations.

6.1 Omnidirectional mirrors

Until recently it was generally thought that it was impossible to have an omnidirectional dielectric mirror, that is a mirror which is perfectly reflecting at all angle of incidence and for parallel and perpendicular polarizations. Let's take a closer look to the prerequisite a multilayered structure must have to become an omnidirectional mirror.

A necessary but not sufficient condition for omnidirectional reflection requires the maximum angle of refraction $\theta_{H,max}$ inside the first layer to be less than the Brewster's angle θ_B at the second interface, so that the Brewster's angle can never be accessed. If this condition is not satisfied , a TM wave would not be reflected, thus transmitting through the structure. With reference to figure 1 of chapter 3:

$$\theta_{H,max} = \sin^{-1}\frac{n_a}{n_H} \quad \theta_B = \tan\frac{n_L}{n_H}$$

$$\theta_{H,max} < \theta_B \quad n_a < \frac{n_H n_L}{\sqrt{{n_H}^2 + {n_L}^2}}$$

Good omnidirectional mirror should have a broad range of wavelength over which they exibit perfect or almost perfect reflection for both polarizations and for every angle. We will see that as the angle and the wavelength grow, the bands of perfect reflection for the two polarization tend to shift away from each other. A careful choice of parameters as thickness, index contrast and number of layers is needed to guarantee a sufficiently broad band of omnidirectional reflection around the nominal wavelength.

6.2 Designing the mirror using Matlab programs

I decided to design a mirror made of non dispersive, non conducting and non magnetic media. This is due to the fact that I already have to deal with six variables, and the previous assumption allows me to drop three of them, even if the program, as mentioned before, can handle such a general case. Reflectance $|\Gamma|^2$ depends, in my approximation, upon:

- $LH - LL$ = difference of thicknesses of the layers
- $nH - nL$ = difference of refraction indices
- N = number of layers
- θ = angle of incidence
- λ = wavelength of incident light
- Polarization
- n_a refraction index of the outer medium
- n_b refraction index of the substrate

Thus $|\Gamma|^2 = f(LH - LL, nH - nL, N, \theta, \lambda, Pol, n_a, n_b)$. It's clear that looking for a global maximum in such a multidimensional space is a complex and time consuming procedure, that's why I decided to probe the space with cleverly chosen values until I reached a local maximum fit for the purpose.

$|\Gamma|^2 = f(LH - LL, nH - nL)$

First let's analyze the dependence of reflectance upon the difference of thicknesses for TE and TM polarizations. The other variables are set to:

$$N = 24, \theta = 45°,\ \lambda = 500\,nm\,, n_a = 1\,, n_b = 1.52, nH = 2.32, nL = 1.45$$

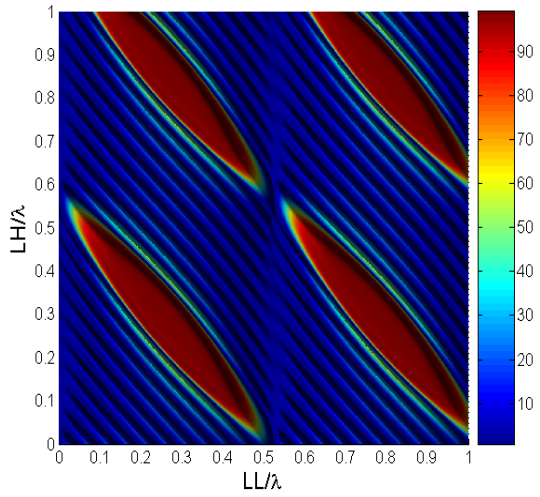

1.1 Reflectivity vs. Layer Thickness for TM pol.

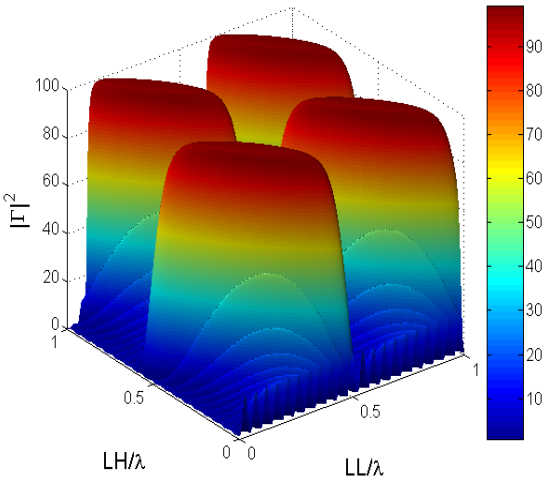

1.2 Reflectivity vs. Layer Thickness for TM pol. ,3D view

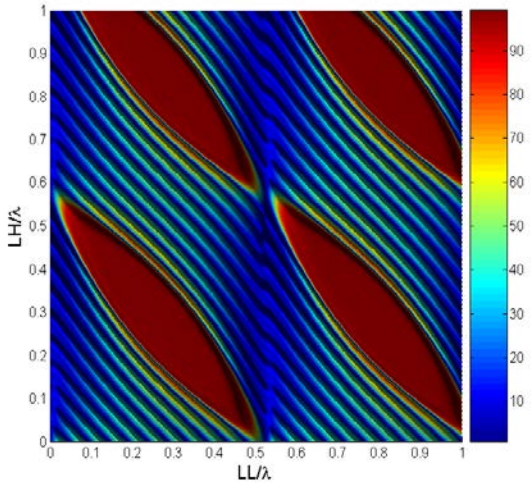

2.1 Reflectivity vs. Layer Thickness for TE pol.

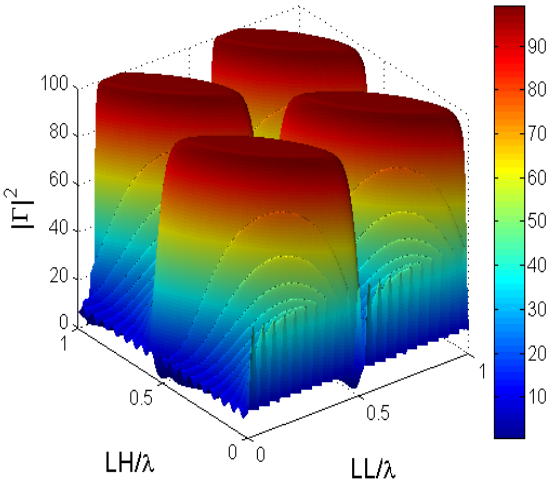

2.2 Reflectivity vs. Layer Thickness for TE pol.,3D view

From figure 1.1 and 2.1 we can see there is only one value of thickness equal for both layers which maximizes reflectance, and it's $\mathbf{0.25} \cdot \boldsymbol{\lambda}$. There's a physical resason for such a behaviour and lies in the fact that reflected waves are always in phase at the interface. On the other hand thickness value $\mathbf{0.5} \cdot \boldsymbol{\lambda}$ corresponds to waves which interfere negatively at the interface and it's easy to see from the graph we have a minimum. Thickness from now on will be set to $\mathbf{0.25} \cdot \boldsymbol{\lambda}$ for both layers. There is also a technological reason behind this choice: layer production is a complex matter which requires precision of order of fraction of wavelength, thus it's easier to work with a single thickness rather than two.

Reflectance depends upon refractive indices as follows:

$N = 24, \theta = 45°,\ \lambda = 500\,nm$, and $LH = LL = 0.25 \cdot \lambda, n_a = 1, n_b = 1.5$:

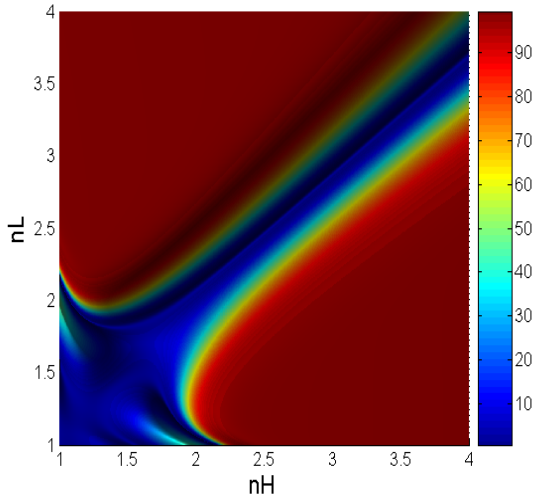

3.1 Reflectivity vs Refraction index for TM pol.

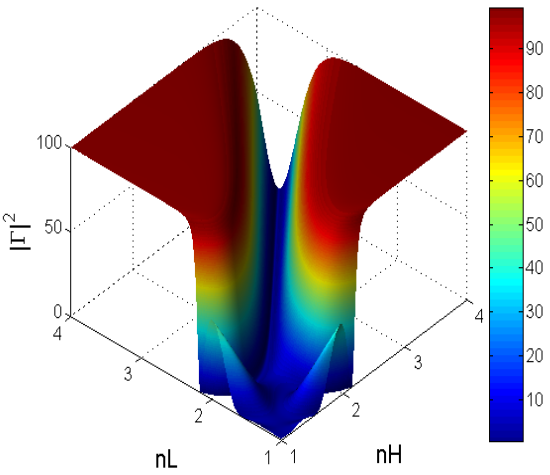

3.2 Reflectivity vs Refraction index for TM pol. 3D

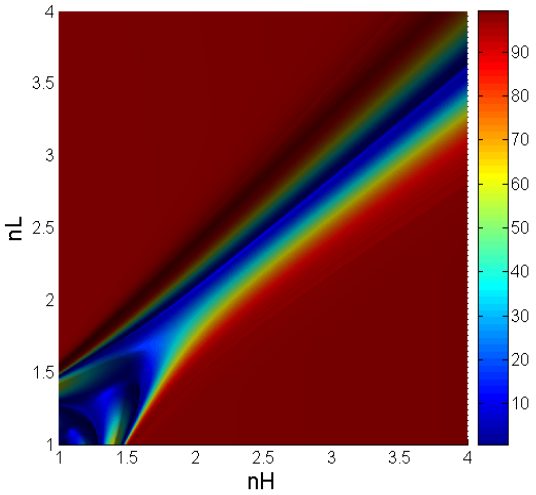

4.1 Reflectivity vs Refraction index for TE pol.

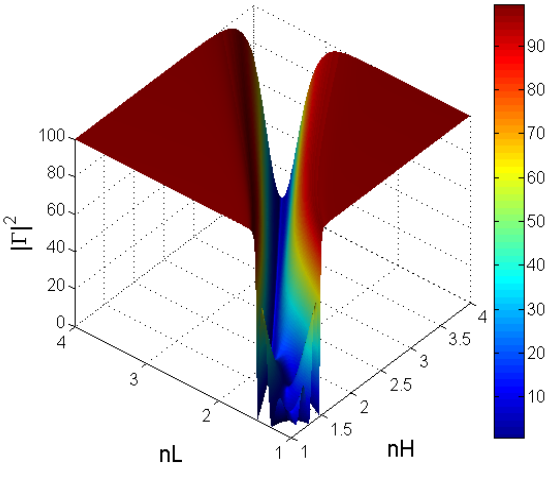

4.2 Reflectivity vs Refraction index for TE pol. 3D

The slight asymmetry in the figures is due to the presence of the outer medium of index n_a and the substrate of index n_b. Maximum reflectance it's achievable by choosing $nL = 1.5$ and $nH = 2.3$ thus justifying the values chosen for nL and nH in the simulation for the thickness. Anyway it's unlikely we can obtain a contrast of 0.8 on the indices with PLD and more careful investigation must be made, i.e by varying other parameters such as N , to obtain good values of reflectance with smaller index contrast.

$$|\boldsymbol{\Gamma}|^{\boldsymbol{2}} = \boldsymbol{f}(\boldsymbol{nL} - \boldsymbol{nH}, \boldsymbol{N}, \boldsymbol{\theta})$$

Let's take a closer look on the dependence of $|\Gamma|^2$ from $nL - nH, N$ and θ.

$LL = LH = 0.25 \cdot \lambda, \lambda = 500, n_a = 1, n_b = 1.52$ and N will be 10,24,104.

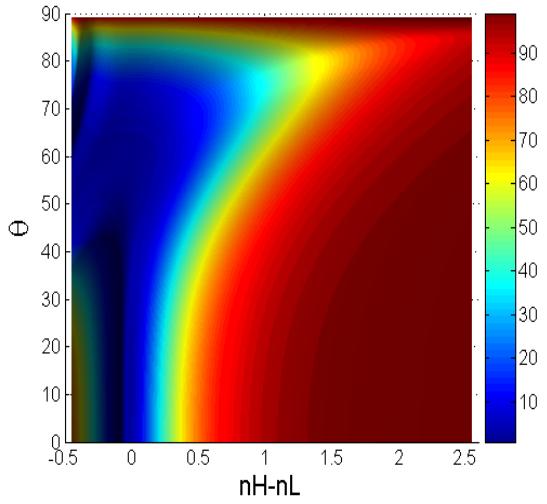

5.1 Reflectance dependence on $\boldsymbol{\theta}$ and $\boldsymbol{\Delta n}$, 10 layers, TM pol

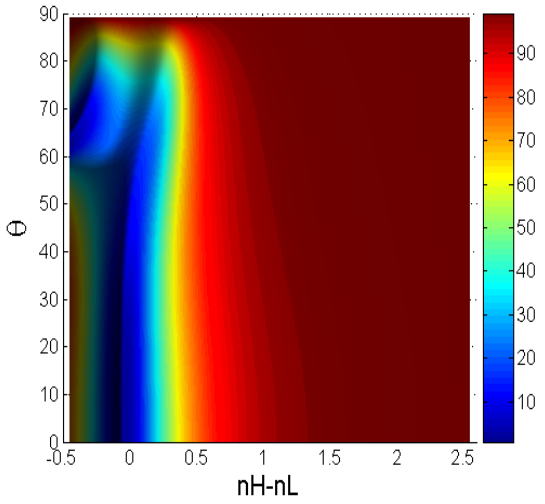

5.2 Reflectance dependence on $\boldsymbol{\theta}$ and $\boldsymbol{\Delta n}$, 10 layers, TE pol

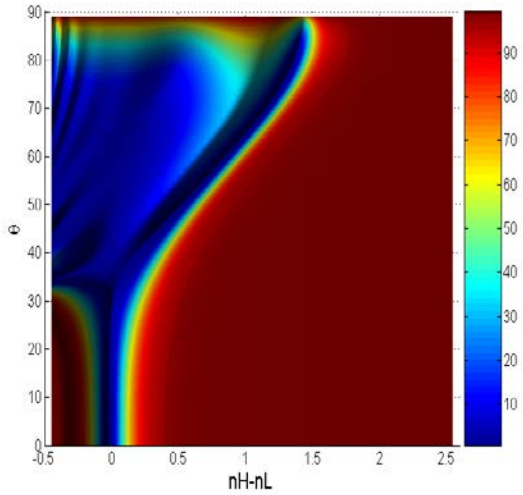

6.1 Reflectance dependence on $\boldsymbol{\theta}$ and $\boldsymbol{\Delta n}$, 24 layers, TM pol

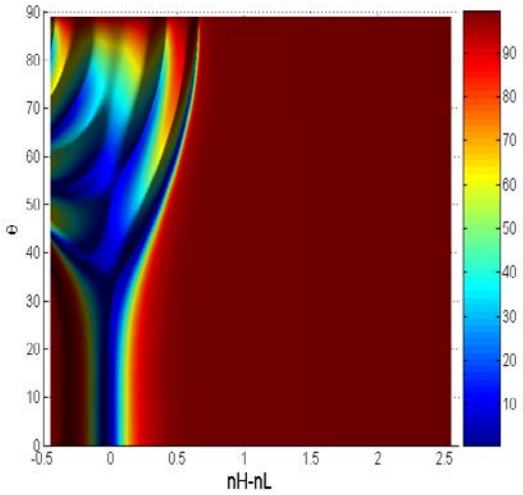

6.2 Reflectance dependence on $\boldsymbol{\theta}$ and $\boldsymbol{\Delta n}$, 24 layers, TE pol

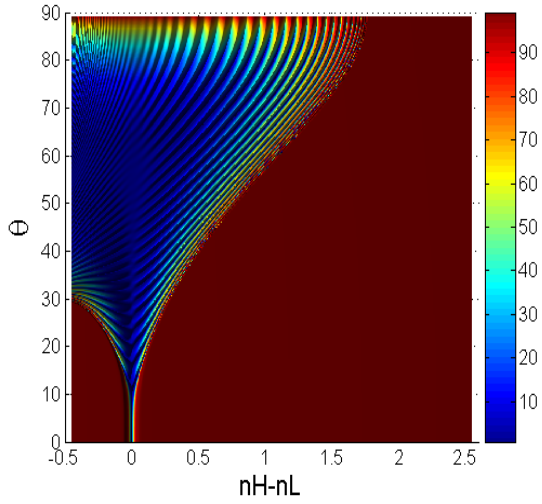

7.1 Reflectance dependence on $\boldsymbol{\theta}$ and $\boldsymbol{\Delta n}$, 104 layers, TM pol

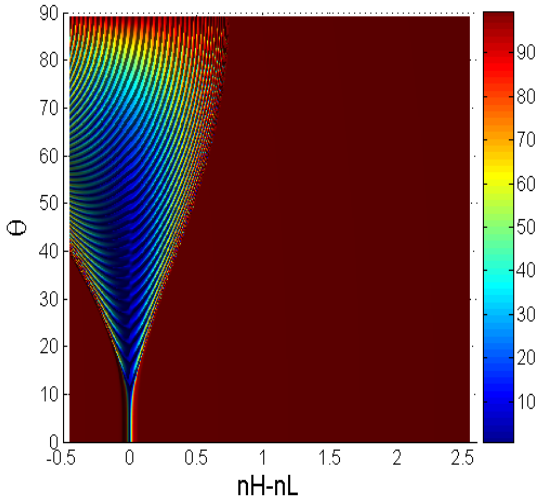

7.2 Reflectance dependence on $\boldsymbol{\theta}$ and $\boldsymbol{\Delta n}$, 104 layers, TE pol

By increasing the layers is possible to achieve maximum reflectance with **very little** index contrast for incidence angles between 0° and 50°. For angles greater than 50° index contrast **must be increased above 1 for any number of layers**. Reflectance for TM waves depends more than for TE waves on index contrast. For TE polarization it's possible to obtain maximum reflection with a contrast of 1 for any angle even with the 10 layers configuration. This is ultimately due to the presence of Brewster's angle for TM waves. Increasing the numbers of layers comes at a price of more complex and time consuming construction procedures and increases the probability to add a **defect** in the multilayered body which can negatively affect performances. Anyway can be the sole solution to maximize reflection if it's impossible to achieve good contrast between layers, if the angle of interest of incident waves lies between 0° and 50°. An in-depth study that relates costs, defect probability and reflection efficiency is recommended but beyond the scope of this presentation.

$$|\Gamma|^2 = f(\lambda, \theta)$$

Wavelength has been set in all previous calculations to be 500nm and values of thickness and refraction index have been found which maximizes reflectance for this wavelength.

$\lambda = 500\ nm$ represent the peak value of sun's emission spectrum. However It's important to probe the properties of our mirror for different wavelengths, specifically over the visible light, as it will presumably be used in photovoltaic cells. A mirror fit for such an utilization should have good reflectance for a broad range of wavelength.

Parameters are set to: $LL = LH = 0.25 \cdot \lambda,\ n_a = 1, n_b = 1.52\ N = 24, nH = 2.3, nL = 1.5.$

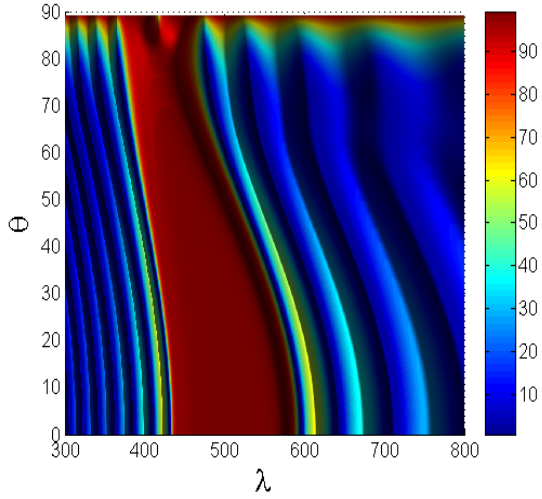

8.1 Reflectance dependence on $\boldsymbol{\theta}$ and $\boldsymbol{\lambda}$, 24 layers, TM pol

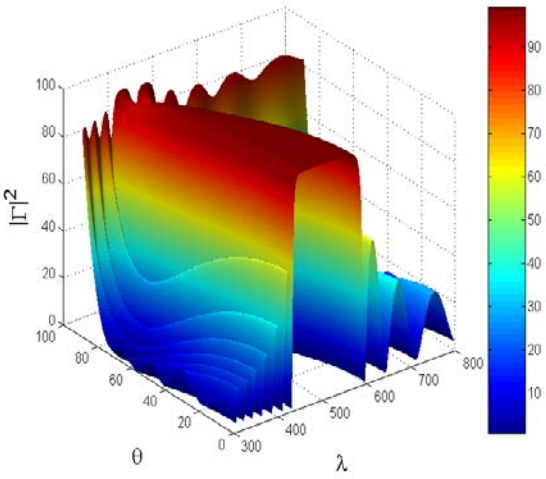

8.2 Reflectance dependence on $\boldsymbol{\theta}$ and $\boldsymbol{\lambda}$, 24 layers, TM pol, 3D

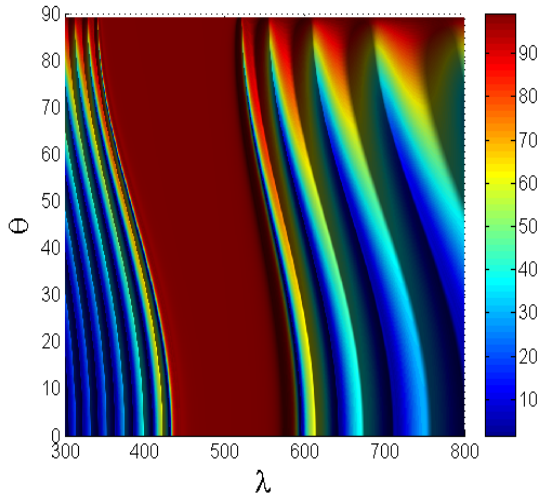

9.1 Reflectance dependence on $\boldsymbol{\theta}$ and $\boldsymbol{\lambda}$, 24 layers, TE pol

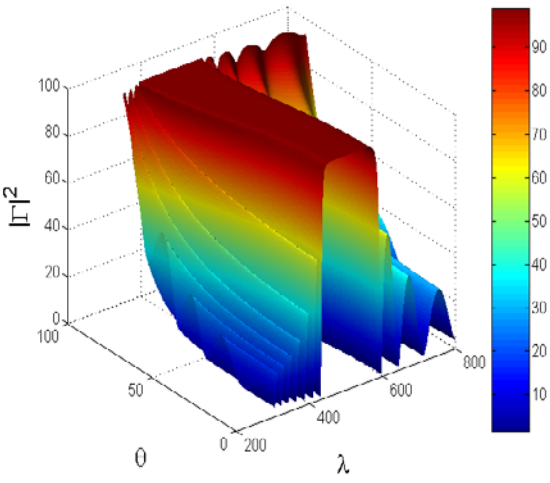

9.2 Reflectance dependence on $\boldsymbol{\theta}$ and $\boldsymbol{\lambda}$, 24 layers, TE pol, 3D

From the graph it's evident that reflectance is maximized for a range between 400nm and 600nm. For TE polarization the range where we have maximum reflectance increases as the angle increases. On the contrary for TM polarization the range shrinks and shift towards lower wavelengths as the angle increases, and reflection itself become lower and lower. Anyway since the mirror it's designed to be used for photovoltaic cells it's important to maximize reflectance for angles between 0° and 60°, the angles from where the light is most likely to come. Chosen configuration perfectly meets this requirement. It's possible to improve reflectance at high angles by increasing the number of layers. By doubling the layers (N=48) the response is as follows:

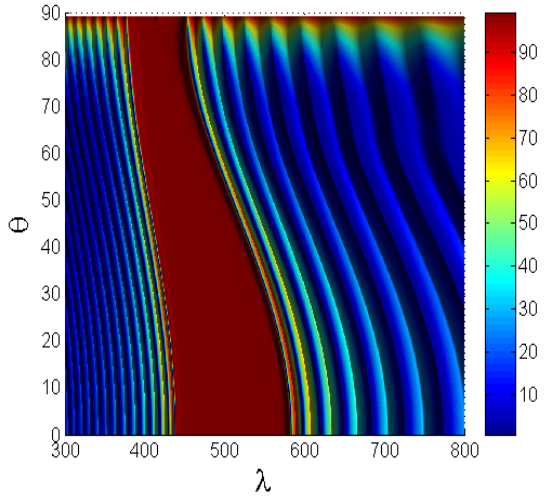

10.1 Reflectance dependence on $\boldsymbol{\theta}$ and $\boldsymbol{\lambda}$, 48 layers, TM pol

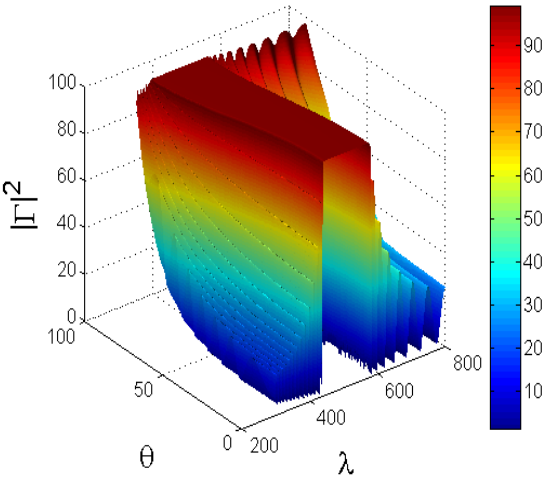

10.2 Reflectance dependence on $\boldsymbol{\theta}$ and $\boldsymbol{\lambda}$, 48 layers, TM pol, 3D

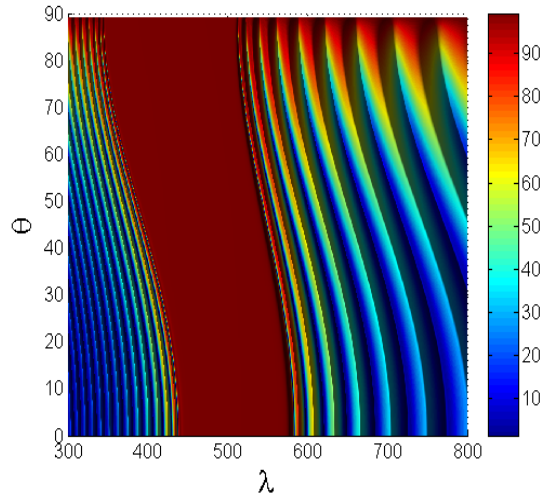

11.1 Reflectance dependence on $\boldsymbol{\theta}$ and $\boldsymbol{\lambda}$, 48 layers, TE pol

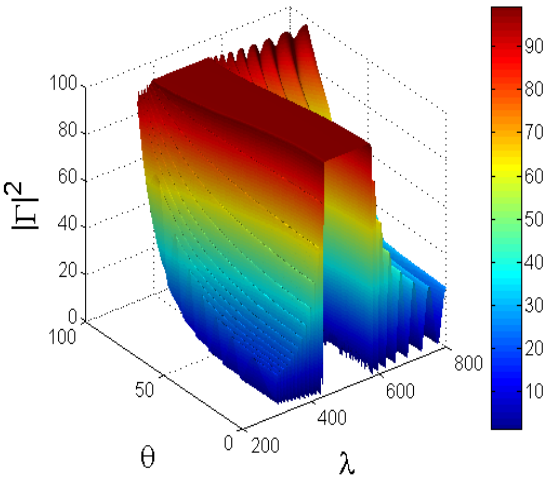

11.2 Reflectance dependence on $\boldsymbol{\theta}$ and $\boldsymbol{\lambda}$, 24 layers, TE pol, 3D

By increasing the difference between the indices it's possible to broaden the bandwidth of perfect reflection. Although it's desirable, we have already seen it is difficult to obtain.

The graphs that follow are calculated using $N = 48, LH = LL = 0.25\lambda, NH = 3.3, nL = 1.5, n_a = 1, n_b = 1.52$.

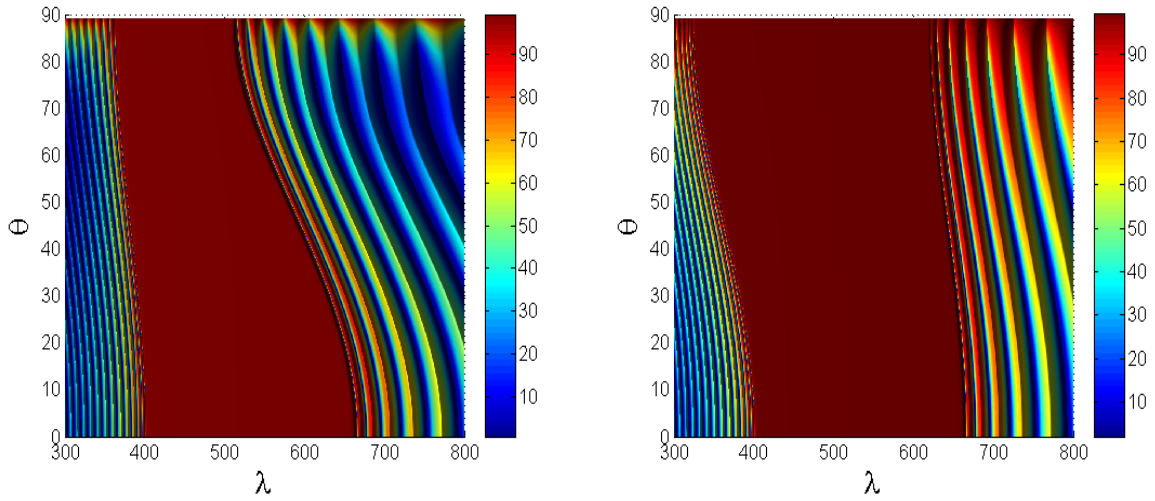

12 Reflectance dependence on $\boldsymbol{\theta}$ and $\boldsymbol{\lambda}$, 48 layers, $\boldsymbol{\Delta n = 1.3}$, TM polarization is on the left

6.3 Localized Defects

It's time to take a look on how localized defects in periodicity can affect the performance of our mirror. This is an important question because it's related directly with the feasibility of such a device. An in-depth analysis of how defects affects performance however requires to probe, once again, a multidimensional space. Number of defects, thickness, contrast, position, ratio of layers and defects, all dependences should be considered for a good optimization. I will consider only the influence of one defect for a low index layer and one defect for a high index layer at different position. Even in its simplicity, this analysis gives important information. Let's see how a single low index defect can affect reflectance for different position in the layer.

Parameters are set to: $N = 24, \theta = 45°, \lambda = 500nm, LH = LL = 0.25\lambda, nH = 2.3, nL = 1.5, n_a = 1, n_b = 1.52$.

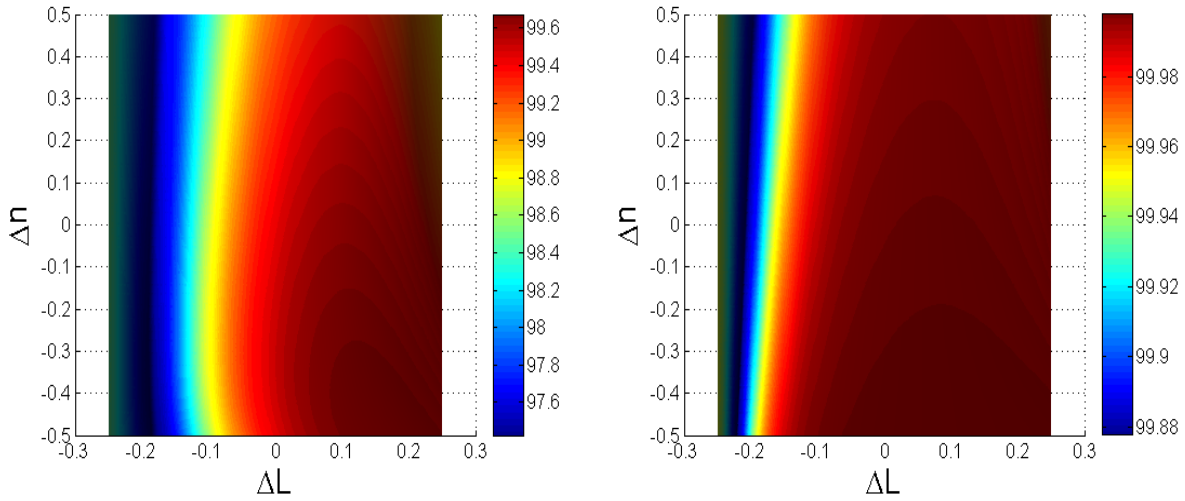

13 Reflectance as a function of $\boldsymbol{\Delta L, \Delta n}$ for a low index defect localized in position 2, TM polarization is on the left.

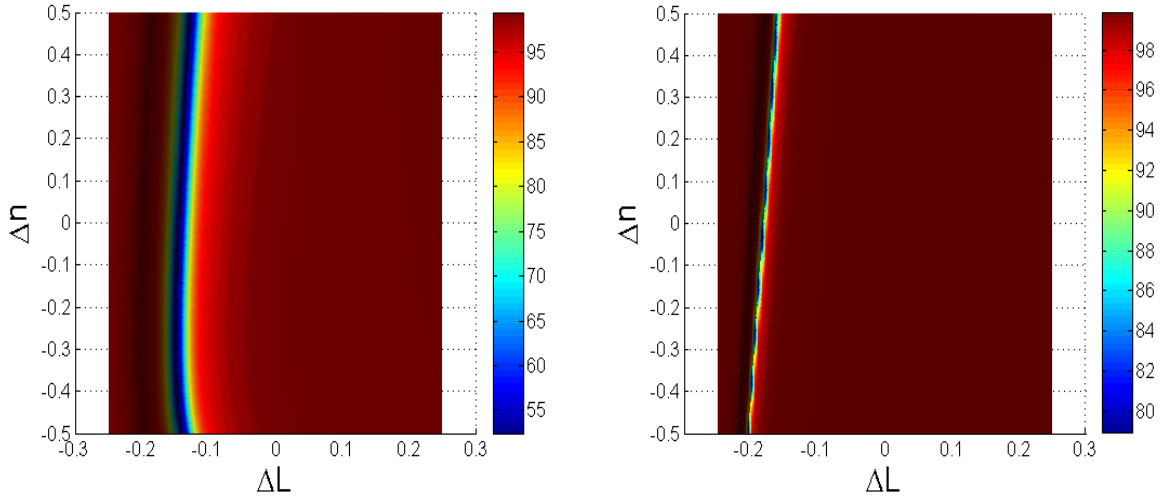

14 Reflectance as a function of $\boldsymbol{\Delta L}, \boldsymbol{\Delta n}$ for a low index defect localized in position 8, TM polarization is on the left.

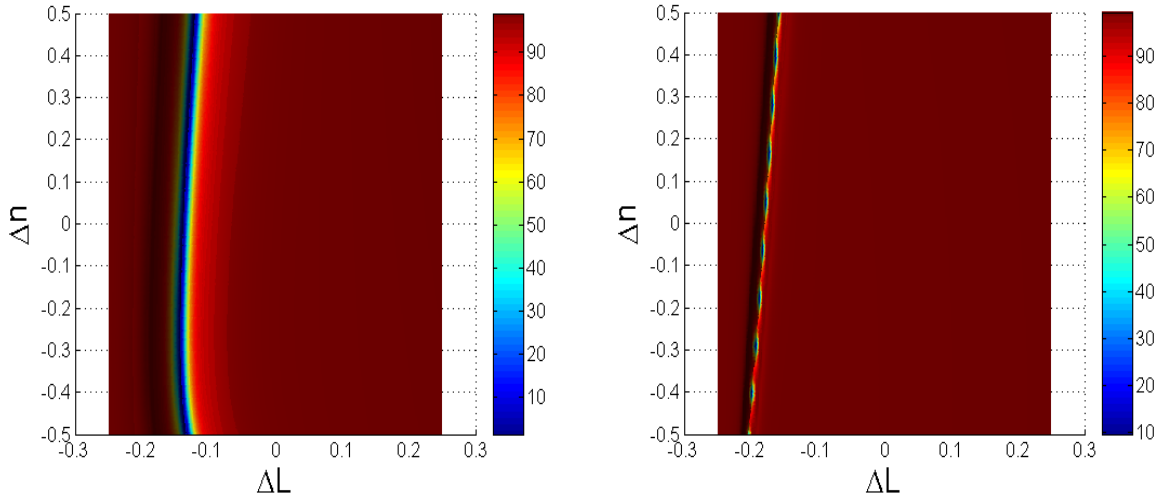

15 Reflectance as a function of $\boldsymbol{\Delta L}, \boldsymbol{\Delta n}$ for a low index defect localized in position 12, TMpolarization is on the left.

The behavior repeats symmetrically as the defect move from layer 12 to layer 24. This means the worst position for a single defect is position 12. Reflectance is a very sensitive function of defect thickness and defect position, while depends weakly on defect index. The thickness of the band where reflectance experiences a drop becomes narrower as the defect move toward position 12, but the drop in reflectance increases from an acceptable 3% to a stunning 90%. Although precision is required to avoid those dangerous gaps, the mirror have a sufficiently broad "safe" zone to be build in.

If the defect is localized in a high index layer, reflectance depends on position in a very similar way, but the drop in reflectance is higher. Thus even more precision is needed when making high index layers.

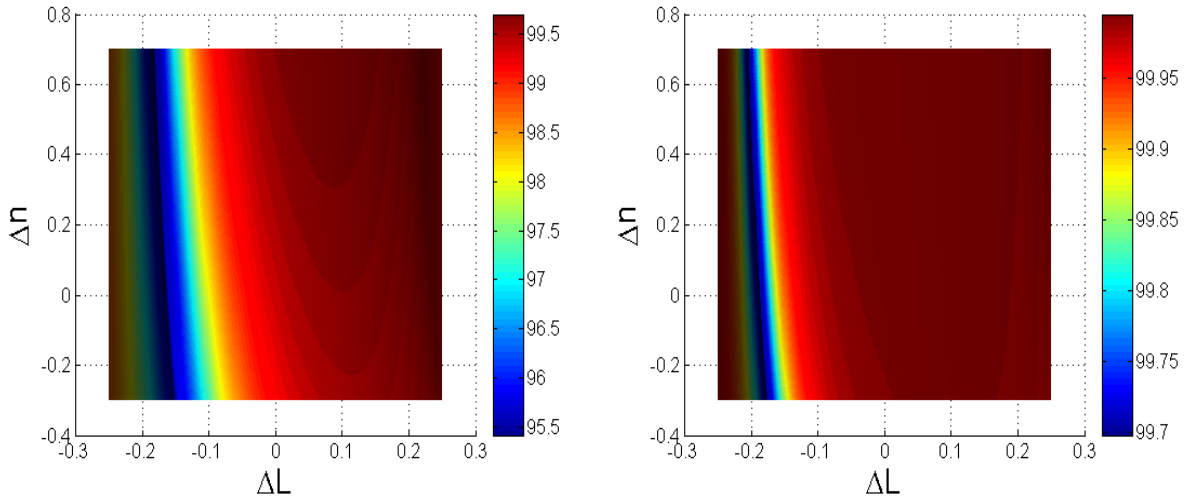

16 Reflectance as a function of $\boldsymbol{\Delta L}, \boldsymbol{\Delta n}$ for a high index defect localized in position 3, TM is on the left.

The simulation also shows that once again the issue come from the TM polarization, while the TE is relatively untouched by defects.

Let's take a look on how defects act on light incident at different wavelength. By Using the same parameters as previous simulations, and by setting a high index defect in position 11, with $n_d = 2.3$ (since reflectance varies slightly with the index it's more meaningful to vary the thickness), these are the results:

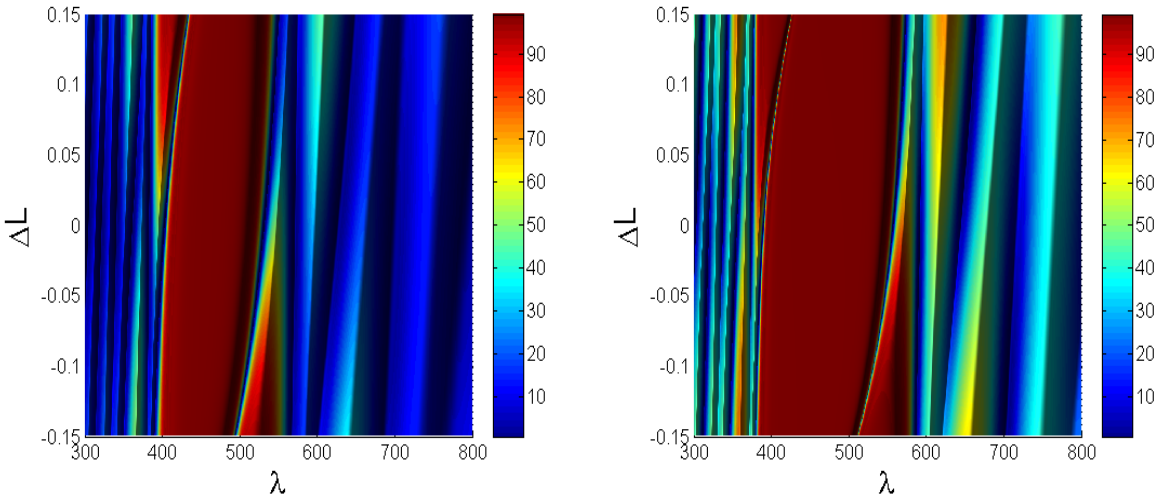

17 Reflectance as a function of defect thickness and wavelength, with defect in position 11, TM polarization is on the left

The bandwidth of maximum reflectance becomes narrower as the thickness of the defect grows, although a band of lower reflectance rise, shifted upward in wavelength, after a critical thickness of 0.05λ.

6.4 Non-periodic mirror

It's very interesting to see what happen if two mirror of different periodicity are put one on top of the other. We'll consider the specific case of two mirrors with same index contrast but different thicknesses. The upper one has 12 layers of thickness 0.25λ, while the lower has 12 layers of variable thickness. This configuration can be used to investigate how to improve maximum reflectance bandwidth of our previously designed mirror without changing the contrast between indices. Physically we have an upper mirror with a thickness designed to reflect with high efficiency some wavelengths, and transmit the others. Under this mirror we have another mirror made of layers of different thickness with respect to the upper one, which is able to reflect the wavelengths transmitted by the first. There's no reason to restrict the number of mirrors to two, as long as the response gets improved. Anyway for the purpose of this presentation only the case with two mirrors will be displayed.

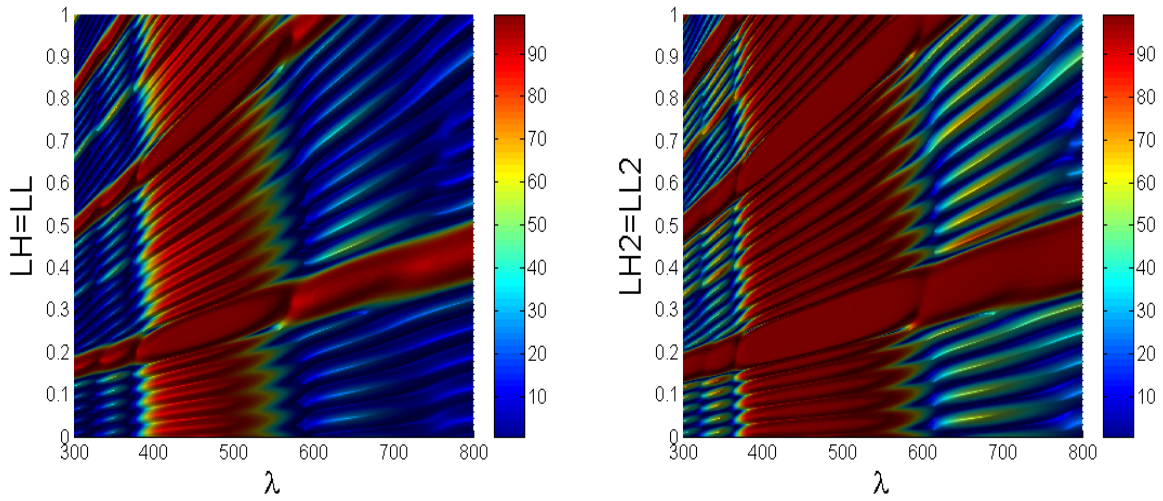

28 Reflectance as a function of wavelength and layer thickness of the lower mirror, both layers have the same thickness

As we can see from the graph, a 24 layers 0.25λ doesn't maximize bandwidth. A 0.25λ 12 layers mirror followed by a 12 layers 0.3λ mirror offer high reflectance over a broader range of wavelengths, without changing index contrast.

.

Chapter 7

The anisotropic program

This chapter dwells on the mathematical and physical description of propagation of electromagnetic waves in anisotropic media.

7.1 In-depth analyses of anisotropic media

In this chapter I will explain the underlying structure of the program which solves the anisotropic case. The program uses a different approach than the one used for the isotropic media discussed in previous chapters, yet similar in some aspects.

First of all let's set a xyz coordinate system which coincide with the principal dielectric axes (so that the permittivity tensor is diagonal), the x-y plane is the interface plane, the x-z is the plane of incidence and let's take the wave vector **k** to lie in the x-z plane at an angle θ from the z-axis. Although this case is still not the most general one with a completely arbitrary direction for **k**, it does contain most of the essential features of propagation in birefringent media.

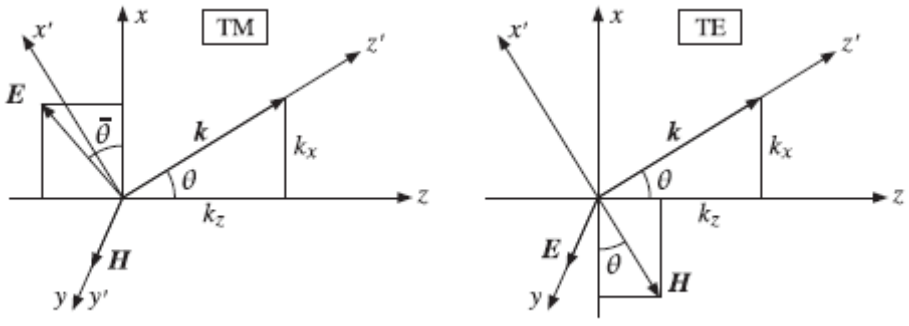

Figure 1 Uniform plane waves in a birefringent medium

The constitutive relations are assumed to be $\boldsymbol{B} = \mu 0 \boldsymbol{H}$ and a diagonal permittivity tensor for **D**. Let $\epsilon_1, \epsilon_2, \epsilon_3$ be the permittivity values along the three principal axes and define the corresponding refractive indices $n_i = \sqrt{\epsilon_i \epsilon_0},\ i = 1,2,3$, the **D-E** relation become:

$$\begin{bmatrix} D_x \\ D_y \\ D_z \end{bmatrix} = \epsilon_0 \begin{bmatrix} {n_1}^2 & 0 & 0 \\ 0 & {n_2}^2 & 0 \\ 0 & 0 & {n_3}^2 \end{bmatrix} \begin{bmatrix} E_x \\ E_y \\ E_z \end{bmatrix}$$

For a biaxial medium the three n_i are all different, while for a uniaxial we take the xy axis to be ordinary, with $n_1 = n_2 = n_o$ and the z-axis to be extraordinary with $n_3 = n_e$. The wave vector **k** can be resolved along the z and x directions as follows:

$$\boldsymbol{k} = k\hat{\boldsymbol{k}} = k(\hat{\boldsymbol{x}}\cos\theta + \hat{\boldsymbol{z}}\sin\theta) = \hat{\boldsymbol{x}}k_x + \hat{\boldsymbol{z}}k_z$$

By analogy with the isotropic case we may define an ***effective refractive index*** N such that:

$$k = Nk_0 = N\frac{\omega}{c}$$

In order to find N we should once again solve the Maxwell's equations. To do this let's consider incident waves of the form:

$$\boldsymbol{E}(\boldsymbol{r}) = \boldsymbol{E}e^{-i\boldsymbol{k}\cdot\boldsymbol{r}} \quad \boldsymbol{H}(r) = \boldsymbol{H}e^{-i\boldsymbol{k}\cdot\boldsymbol{r}}$$

Replacing the gradient operator ∇ by $-i\boldsymbol{k}$ and with a little algebra Maxwell's equations become:

$$\boldsymbol{k}\times\boldsymbol{E} = \omega\mu_0\boldsymbol{H} \quad \boldsymbol{k}\times\boldsymbol{H} = -\omega\boldsymbol{D}$$
$$\boldsymbol{k}\cdot\boldsymbol{D} = 0 \quad \boldsymbol{k}\cdot\boldsymbol{H} = 0$$

Replacing $\boldsymbol{k}$ with $N\frac{\omega}{c}\hat{\boldsymbol{k}}$ as seen before we have:

$$\boldsymbol{H} = \frac{N}{c\mu_0}\hat{\boldsymbol{k}}\times\boldsymbol{E} \quad \boldsymbol{D} = -\frac{1}{\omega}N\frac{\omega}{c}\hat{\boldsymbol{k}}\times H$$

The equation for **D** can be further elaborated to give:

$$\hat{\boldsymbol{k}}\times(\boldsymbol{E}\times\hat{\boldsymbol{k}}) = \frac{1}{\epsilon_0 N^2}\boldsymbol{D}$$

With $c^2\mu_0 = \frac{1}{\epsilon_0}$. The $\hat{\boldsymbol{k}}\times(\boldsymbol{E}\times\hat{\boldsymbol{k}})$ represent the component of **E** that is transverse to the propagation unit vector $\hat{\boldsymbol{k}}$. Using the identity $\hat{\boldsymbol{k}}\times\left(\boldsymbol{E}\times\hat{\boldsymbol{k}}\right) = \boldsymbol{E} - \hat{\boldsymbol{k}}(\hat{\boldsymbol{k}}\cdot\boldsymbol{E})$ we obtain:

$$\boldsymbol{E} - \frac{1}{\epsilon_0 N^2}\boldsymbol{D} = \hat{\boldsymbol{k}}(\hat{\boldsymbol{k}}\cdot\boldsymbol{E}) \qquad \textbf{(1)}$$

Because **D** is linear in **E,** the equation above is a homogeneous linear equation. In order to have a nonzero solution its determinant must be zero. This provides a condition from which N can be determined. To obtain both the TM and TE solution first we suppose **E** has all three components and rewrite equation **(1)** component-wise:

$$\left(1-\frac{{n_1}^2}{N^2}\right)E_x = (E_x\sin\theta + E_z\cos\theta)\sin\theta$$

$$\left(1-\frac{{n_2}^2}{N^2}\right)E_y = 0$$

$$\left(1-\frac{{n_3}^2}{N^2}\right)E_z = (E_x\sin\theta + E_z\cos\theta)\cos\theta$$

The TE case has $E_y \neq 0$ and $E_x = E_z = 0$, whereas the TM case has $E_x \neq$, $E_z \neq 0$ and $E_y = 0$. In the TE case $N = n_2$, straightforwardly from the equations above and the fields are:

$$\boldsymbol{E}(\boldsymbol{r}) = E_y\hat{\boldsymbol{y}}e^{-ik_0xn_2\sin\theta - ik_0zn_2\cos\theta}$$

$$\boldsymbol{H}(\boldsymbol{r}) = \frac{E_y}{\mu_0 c}n_2(-\hat{\boldsymbol{x}}\cos\theta + \hat{\boldsymbol{z}}\sin\theta)e^{-ik_0xn_2\sin\theta - ik_0zn_2\cos\theta}$$

For the TM case we must solve the system:

$$\left(1-\frac{{n_1}^2}{N^2}\right)E_x = (E_x\sin\theta + E_z\cos\theta)\sin\theta$$

$$\left(1-\frac{{n_3}^2}{N^2}\right)E_z = (E_x\sin\theta + E_z\cos\theta)\cos\theta$$

By setting the determinant to zero we obtain the expression for N in the TM case:

$$N = \frac{n_1n_2}{\sqrt{{n_1}^2(\sin\theta)^2 + {n_3}^2(\cos\theta)^2}}$$

The field are therefore:

$$\boldsymbol{E}(\boldsymbol{r}) = E_x(\hat{\boldsymbol{x}} - \hat{\boldsymbol{z}}\frac{{n_1}^2}{{n_3}^2}\tan\theta)e^{-ik_0x\frac{n_1n_2}{\sqrt{{n_1}^2(\sin\theta)^2+{n_3}^2(\cos\theta)^2}}\sin\theta - ik_0z\frac{n_1n_2}{\sqrt{{n_1}^2(\sin\theta)^2+{n_3}^2(\cos\theta)^2}}\cos\theta}$$

$$\boldsymbol{H}(\boldsymbol{r}) = \frac{E_x}{c\mu_0}\frac{{n_1}^2}{\cos\theta}\hat{y}e^{-ik_0x\frac{n_1n_2}{\sqrt{{n_1}^2(\sin\theta)^2+{n_3}^2(\cos\theta)^2}}\sin\theta - ik_0z\frac{n_1n_2}{\sqrt{{n_1}^2(\sin\theta)^2+{n_3}^2(\cos\theta)^2}}\cos\theta}$$

Now we know the fields for every polarization in an anisotropic material, what we need is the reflectivity of the multilayered structure. As explained in chapter 2 and 3 the tangential

component of electric field must be conserved at the interface (the component E_x for TM, and E_y for TE polarization).The presence of an interface between two different media implies further considerations; if the interface connects two anisotropic media we must assume the principal axes have the same orientation for both, i.e the materials have the same crystalline structure. Then we can write:

$$e^{-ik_+x} = e^{-ik_-x} = e^{-ik_+'x} = e^{-ik_-'x}$$

Again, as seen before, at the interface only the exponential part relative to propagation along the z-axis survives. Reflectivity is obtained through a propagation matrix of the form:

$$\begin{bmatrix} E_{Ti+} \\ E_{Ti-} \end{bmatrix} = \frac{1}{\tau_{Ti}} \begin{bmatrix} e^{i\delta_i} & \rho_{Ti}E^{-i\delta_i} \\ \rho_{Ti}E^{i\delta_i} & e^{-i\delta_i} \end{bmatrix} \begin{bmatrix} E_{T,i+1,+} \\ E_{T,i+1,-} \end{bmatrix}$$

With respect to the following picture:

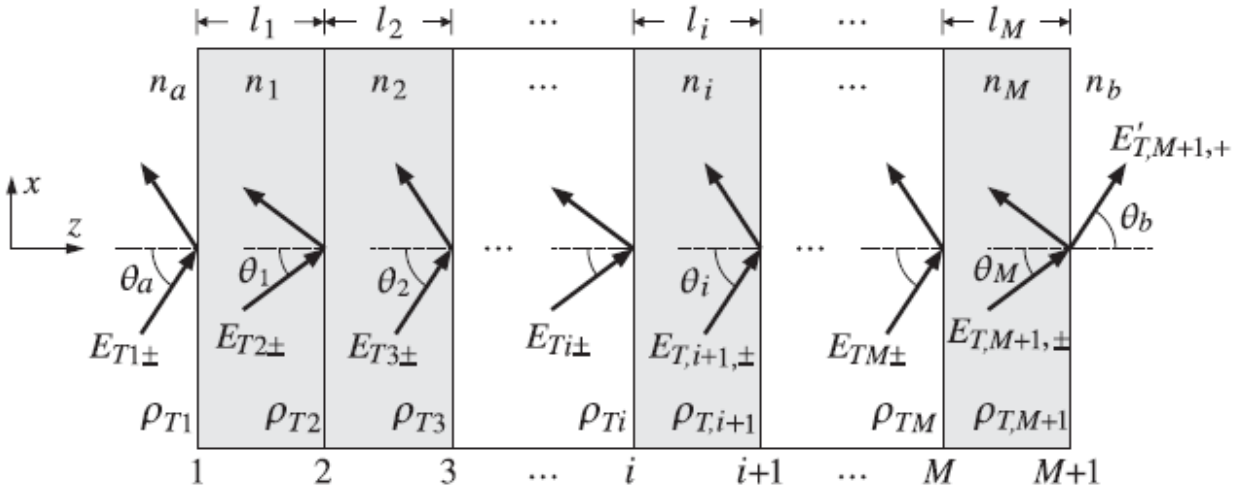

Figure 2: oblique incidence on multilayer dielectric structure

- E_{Ti+}, E_{Ti-} are the electric field incident and reflected left of interface i
- $E_{T,i+1,+}, E_{T,i+1,-}$ are the electric fields incident and reflected right of interface i
- $\rho_{Ti} = \frac{n_{2,i-1}\cos\theta_{i-1} - n_{2,i}\cos\theta_i}{n_{2,i-1}\cos\theta_{i-1} + n_{2,i}\cos\theta_i}$ where N is the effective index of refraction for Te
- $\rho_{Ti} = \frac{\frac{{n_{1,i-1}}^2}{N_{i-1}\cos\theta_{i-1}} - \frac{{n_{1,i}}^2}{N_i\cos\theta_i}}{\frac{{n_{1,i-1}}^2}{N_{i-1}\cos\theta_{i-1}} + \frac{{n_{1,i}}^2}{N_i\cos\theta_i}}$ where N is the effective index of refraction for TM

- $\delta_i = Nk_0 l_i \cos\theta$ where l_i is the thickness of the layer

- $\tau_{Ti} = \frac{2n_{2,i-1}\cos\theta_{i-1}}{n_{2,i-1}\cos\theta_{i-1}+n_{2,i}\cos\theta_i}$ for TE polarization

- $\tau_{Ti} = \frac{2\frac{{n_{1,i-1}}^2}{N_{i-1}\cos\theta_{i-1}}}{\frac{{n_{1,i-1}}^2}{N_{i-1}\cos\theta_{i-1}}+\frac{{n_{1,i}}^2}{N_i\cos\theta_i}}$ for TM polarization

The reflection response Γ_i , which is defined as $\frac{E_{Ti-}}{E_{Ti+}}$,will therefore satisfy the recursion :

$$\Gamma_{Ti} = \frac{\rho_{Ti} + \Gamma_{T,i+1}e^{-2\delta_i}}{1 + \rho_{Ti}\Gamma_{T,i+1}e^{-2\delta_i}}$$

initialized at $\Gamma_{T,M+1}$, the last interface, where there is only a wave propagating in medium M+1 and no reflected wave, simplifying the conditions.

The main difference between isotropic and anisotropic programs lies in the fact that, while the isotropic problem calculate transmitted and reflected fields for every layer at the same time, the anisotropic program handle the problem in a recursive way, calculating step by step the reflection response. It's not possible, if someone is interested in reflection response at, let's say interface 3, to have information about reflection of the body at interface 1 without running the program again. Anyhow that's the price to pay to account for anisotropy, which greatly complicates the description of phenomena and the length of calculations.

6.2 Anisotropic mirrors

It's possible to investigate the properties of an anisotropic multilayered structure with an approach similar to that used in chapter 6 for omnidirectional mirrors. Anyway the sheer number of variables involved would require a more rigorous approach which is beyond the scope of this work. In order to point out the differences between isotropic and anisotropic media I will give the results obtained for a particularly interesting configuration. This configuration has been chosen to have biaxial high/low layers refractive indices mismatched only in the x or the y direction, so that one can design a mirror structure that reflects only the TM or only the TE polarization, assumed x-z as the plane of incidence.
Parameters are as follow:

$N = 20, n_a = [1;1;1], n_b[1;1;1],\ nH = [1.86;1.57;1.57],\ \ nL = [1.57;1.57;1.57],\ \ \theta = 0°,$
$LH = LL = 0.25\lambda$

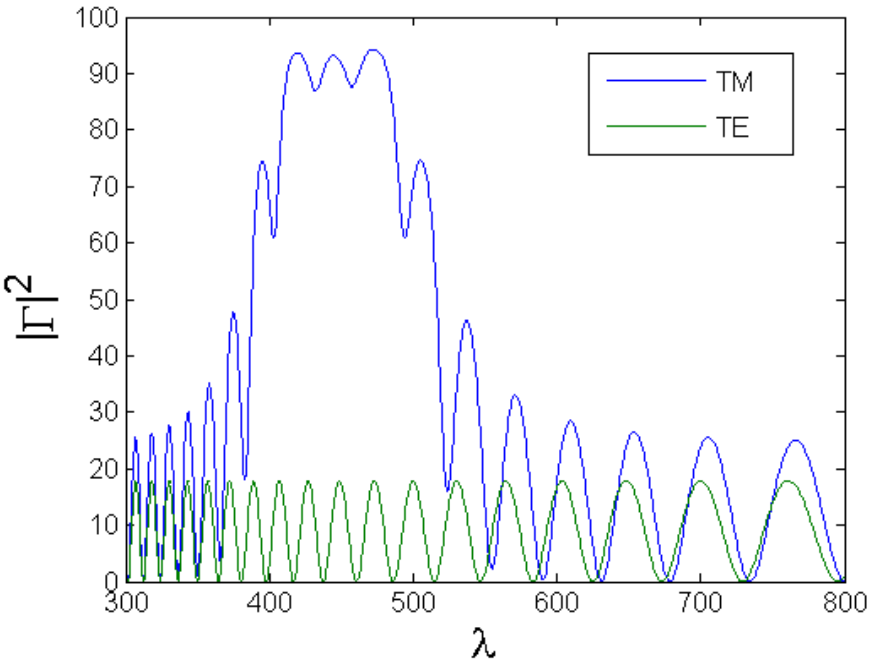

Figure 3: Reflectance vs. wavelength for an anisotropic mirror. The plane of incidence is the XZ plane. A 25% thickness gradient (the layer thicknesses LH, LL decrease linearly from quarter-wavelength to 25% less than that at the end.) This increases the effective bandwidth of the reflecting bands, as shown in the last paragraph of chapter 6.

Chapter 8

Photonic bands in multilayered dielectric structures

Computing the photonic bands is a widespread method used to characterize the properties of photonic crystals with periodicities in two and three dimensions, but sometimes is used also for monodimensional crystals. In this chapter the theory needed to understand and calculate the band structure has been explained, and the core for a two-dimensional eigensolver software has been hinted.

8.1 The Master Equation

Electromagnetic waves propagation in a photonic crystal is ruled by **Macroscopic Maxwell's equations**, which in SI are:

$$\nabla \cdot B = 0 \qquad \nabla \times E + \frac{\partial B}{\partial t} = 0$$

$$\nabla \cdot D = \rho \qquad \nabla \times H - \frac{\partial D}{\partial t} = J$$

If ρ e J are equal to zero, i.e there are no electromagnetic radiation source inside the material, equations become:

$$\nabla \cdot B = 0 \qquad \nabla \times E + \frac{\partial B}{\partial t} = 0$$

$$\nabla \cdot D = 0 \qquad \nabla \times H - \frac{\partial D}{\partial t} = 0$$

We can link displacement field D with electric field E by:

$$\frac{D_i}{\varepsilon_0} = \sum_j \varepsilon_{ij} E_j + \sum_{j,k} \chi_{ijk} E_j E_k + O(E^3)$$

This relation accounts for anisotropy in the material by means of tensor ε_{ij}, and for deviation from linearity expressed by the second summation. If we assume fields are sufficiently weak to meet the linearity condition, we can neglect second order terms and write:

$$\frac{D_i}{\varepsilon_0} = \sum_j \varepsilon_{ij} E_j$$

Which becomes $\boldsymbol{D}(r) = \varepsilon_0 \varepsilon(\boldsymbol{r})\boldsymbol{E}(\boldsymbol{r})$ in the isotropic case. Similarily $\boldsymbol{B}(r) = \mu_0 \mu(\boldsymbol{r})\boldsymbol{H}(\boldsymbol{r})$.

Maxwell's equations become:

$$\nabla \times H(r,t) - \varepsilon_0 \varepsilon(r) \frac{\partial E(r,t)}{\partial t} = 0 \quad \nabla \times E(r,t) + \mu_0 \mu(r) \frac{\partial H(r,t)}{\partial t} = 0 \qquad (1.1)$$

$$\nabla \cdot \varepsilon(r) E(r,t) = 0 \qquad \nabla \cdot H(r,t) = 0 \qquad (1.2)$$

We can further elaborate these equations by separate the spatial component of the fields from the time dependent component with Fourier. Separation is possible because Maxwell's equations are linear:

$$E(r,t) = E(r)e^{-i\omega t} \qquad (1.3)$$

$$H(r,t) = H(r)e^{-i\omega t}$$

Substituing (1.3) in (1.1) we obtain:

$$\nabla \times \left(\frac{1}{\varepsilon(r)} \nabla \times H(r) \right) = \left(\frac{\omega}{c} \right)^2 H(r) \qquad (1.4)$$

From now on this will be regarded as the **Master Equation** for photonic band computations.

8.2 Stokes-Helmoltz decomposition and Coulomb's Gauge

Equations $\nabla \cdot \varepsilon(r)E(r) = 0$, $\nabla \cdot H(r) = 0$ implies the lack of magnetic or electric sources in the medium. Equivalently we can say, if we consider the fields as plane waves of equation $H(r) = ae^{ikr}$, that the waves are transverse, i.e they satisfy the condition $a \cdot k = 0$.

We can write the generic vectorial field by using the Stokes-Helmoltz decomposition:

$$u = \nabla\phi + \nabla \times A$$

Where ϕ e A are the scalar and vectorial potentials, respectively. The preceding relation links vector u= (u_1, u_2, u_3) to (ϕ, A_1, A_2, A_3); We need one more relation to identify uniquely the quantities because there are three equations and for unknowns. We therefore use the Coulomb's gauge:

$$\nabla \cdot A = 0$$

The scalar potential corresponds to the Coulomb's potential due to charge density ρ; hence ther name Coulomb's gauge:

$$\phi = \int \frac{\rho(x', t)}{|x - x'|} d^3x'$$

Coulomb's gauge isn't the only possible. For example Lorentz's Gauge exists and is defined as:

$$\nabla \cdot A + \frac{1}{c}\frac{\partial \phi}{\partial t} = 0$$

However Coulomb's gauge is often used in problems where there are no sources, while Lorentz's gauge is used, because of the independence on the reference system, when special relatività is taken into account.

Using Coulomb's gauge we get the well known homogeneous wave equations:

$$\nabla^2\phi + \frac{1}{c^2}\frac{\partial^2 \phi}{\partial t^2} = 0$$

$$\nabla^2 A + \frac{1}{c^2}\frac{\partial^2 A}{\partial t^2} = 0$$

Which are solved by:

$$\phi(x, t) = \phi\big(k \cdot x - c_p t\big)$$

$$A(x, t) = A(k \cdot x - c_s t)$$

That represents two waves travelling in direction k with speed $c_p e\ c_s$.

8.3 Electromagnetic Energy and Variational Principle

Let's consider the Master equation (1.4):

$$\nabla \times \left(\frac{1}{\varepsilon(r)} \nabla \times H(r)\right) = \left(\frac{\omega}{c}\right)^2 H(r)$$

Let's characterize operator $\widehat{\Phi}$ as:

$$\widehat{\Phi}H(r) \triangleq \nabla \times \left(\frac{1}{\varepsilon(r)}\nabla \times H(r)\right)$$

$\widehat{\Phi}$ is a linear and Hermitian operator. Hermitian means it's valid the following relation:

$$(F, \widehat{\Phi}G) = (\widehat{\Phi}F, G).$$

In order for an operator to be Hermitian there must be no difference between applying it to one of the two function F or G before taking the inner product, the result will be the same.

In dielectrics the energy is concentrated mainly in regions of high dielectric constant . We can see this by means of an analogous version for electromagnetic waves of the variational principle from quantum mechanics: the lowest eigenvalue of the master equation (1.4) corresponds to the lowest frequency mode, and thus corresponds to the field pattern which minimizes the functional defined by:

$$U_f(H) \triangleq \frac{(H, \widehat{\Phi}H)}{(H, H)}$$

We can rewrite the functional $U_f(H)$ using the electric field and we can verify that:

$$U_f(H) \triangleq \frac{(\nabla \times E, \nabla \times E)}{(E, \varepsilon(r)E)}$$

And the inner products is:

$$U_f(H) = \frac{\int d^3r |\nabla \times E(r)|^2}{\int d^3r\, \varepsilon(r)|E(r)|^2}$$

We can see the functional is minimized for higher values of $\varepsilon(r)$. What happens in dielectrics has a marked analogy to what happens in quantum mechanics with the wave function, which concentrates itself in low potential zones at the same time minimizing kinetic energy.

Energy functional is a different concept from physical Energy stored within the fields. Physical energy, both magnetical and electrical, is proportional to the square of the strength of the field as described by the following relations:

$$U_m = \frac{\mu_0}{4}\int d^3r \mu(r)|H(r)|^2$$

$$U_e = \frac{\varepsilon_0}{4}\int d^3r \varepsilon(r)|E(r)|^2$$

Functional U_f on the other hand is independent from fields strength because it has fields on both the numerator and the denominator. Thus multiplying the fields for a constant affects the physical energy, but not on the energy functional that can therefore act on normalized vibrational mode and return information about the profiles of the modes themselves but not about the amplitudes.

8.4 Magnetic vs. Electric fields

Why in previous paragraphs Maxwell's equations have been formulated as an eigenvalue problem for magnetic instead of electric fields?

The answer is simple: let's consider the eigenvalue problem for the electric field:

$$\nabla \times \nabla \times \mathrm{E}(\mathrm{r}) = \left(\frac{\omega}{c}\right)^2 \varepsilon(r)\, E(r) \qquad 1.5$$

This is a generalized eigenproblem of the form $Ax = \omega^2 Bx$. This means there are operators on both sides of the equation. We can convert it in an ordinary eigenproblem by dividing (1.5) for $\varepsilon(r)$ but we will have a non-Hermitian operator.

However we could stick to the generalized eigenproblem both the operators , $\nabla \times \nabla \times \mathrm{e}\ \varepsilon(r)$, are Hermitian, but now we would have a transversailty constraint $\nabla \cdot \varepsilon E = 0$ dependent on ε, which as negative effects on numerical .

8.5 Scaling properties of Maxwell's equations

One interesting feature of electromagnetism in dielectric is that there is no fundamental length scale other then the assumption the system is macroscopic, as briefly introduced in chapter 1. The thickness of every layer cannot be pushed to the limit of a single atom for two reasons: first the media would lose the planarity of interfaces and second we couldn't use macroscopic Maxwell's equations anymore. Once pointed out this important aspect, we nevertheless can probe the behavior of system that have similar physical properties but differ in their overall spatial scale. The solution of the problem at one length scale determines the solutions at all other length scales. This simple fact is of considerable practical importance. For example, the micro fabrication of complex micron-scale photonic crystals can be quite difficult. But models can be easily made and tested in the microwave regime, at the much larger length scale of centimeters, if materials can be found that have nearly the same dielectric constant. The considerations in this section guarantee that the model will have the same electromagnetic properties. Scale-invariance can easily be demonstrated from the Master equation given in paragraph 7.1. Such a property doesn't exist in, for example, atomic physics, where Schrödinger equation has a fundamental length scale, the Bohr radius.

8.6 Photonic Crystal spectra

The **spectrum** of a photonic crystal is the totality of all of the eigenvalues ω. Does this spectrum look like a continuous range of values, or the frequencies form a discrete sequence $\omega 0, \omega 1, \ldots$?

The answer depends on the *spatial domain* of the mode profiles **H**(**r**) (or **E**). If the fields are spatially bounded, either because they are localized around a particular point or because they are periodic in all three dimensions (and therefore represent a bounded profile repeated indefinitely), then the frequencies ω form a discrete set. Otherwise they can form a single continuous range, a set of continuous ranges, or a combination of continuous ranges and discrete sets (for a combination of localized and extended modes).

This property is quite general for many Hermitian eigenproblems, it follows from the orthogonality of the modes. This result, applied to photonic crystals, leads to the concepts of discrete frequency bands and of localized modes near crystal defects.

8.7 Symmetries and Bloch Theorem

If a dielectric structure has a certain symmetry, then the symmetry offers a convenient way to categorize the electromagnetic modes of that system. Symmetries of a system allow one to make general statements about that system's behavior. Photonic crystals, like traditional crystals of atoms or molecules, have discrete translational symmetry. That is, they are not invariant under translations of any distance, but rather, only distances that are a multiple of some fixed step length. The simplest example of such a system is a structure that is repetitive in one direction, like the configuration in figure 1.

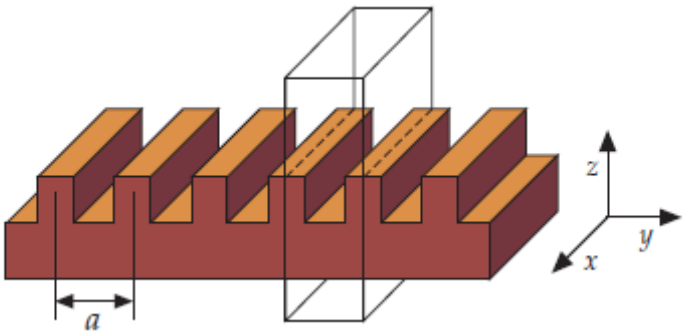

Figure 1. A dielectric configuration with discrete translational symmetry. If we imagine that the system continues forever in the *y* direction, then shifting the system by an integral multiple of *a* in the *y* direction leaves it unchanged.

For this system we have continuous translational symmetry in the *x* direction, but now we have discrete translational symmetry in the *y* direction.

The basic step length is the **lattice constant** *a*, and the basic step vector is called the **primitive lattice vector**, which in this case is $\boldsymbol{a} = a\,\hat{\boldsymbol{y}}$. Because of this discrete symmetry, $\varepsilon(\boldsymbol{r}) = \varepsilon(\boldsymbol{r} \pm \boldsymbol{a})$. By repeating this translation, we see that $\varepsilon(\boldsymbol{r}) = \varepsilon(\boldsymbol{r} + \boldsymbol{R})$ for any **R** that is an integral multiple of **a**; that is, $\boldsymbol{R} = l\boldsymbol{a}$, where l is an integer.

Because of the translational symmetries, $\hat{\boldsymbol{\Phi}}$ must commute with *all* of the translation operators in the *x* direction, as well as the translation operators for lattice vectors $\boldsymbol{R} = la\,\hat{\boldsymbol{y}}$ in the *y* direction. With this knowledge, we can identify the modes of $\hat{\Phi}$ as simultaneous eigenfunctions of both translation operators. These eigenfunctions are plane waves:

$$\hat{T}_{\hat{\boldsymbol{x}}} e^{ik_x x} = e^{-ik_x d} e^{ik_x x}$$

$$\hat{T}_R e^{ik_y y} = e^{-ik_y la} e^{ik_y y}$$

Where d is an arbitrary constant and $\hat{\boldsymbol{T}}_{\hat{\boldsymbol{x}}}, \hat{\boldsymbol{T}}_{\hat{\boldsymbol{y}}}$ are the translational operators for, respectively, continuus and descrete symmetry. We can begin to classify the modes by specifying *kx* and *ky*. However, not all values of *ky* yield different eigenvalues. Consider two modes, one with wave vector *ky* and the other with wave vector $ky + \frac{2\pi}{a}$. Inserting in previous equations shows they have the same eigenvalues. In fact, all of the modes with wave vectors of the form $ky + m\frac{2\pi}{a}$, where *m* is an integer, form a degenerate set; they all have the same $\hat{T}_R$ eigenvalue of $e^{-ik_y la}$. Augmenting *ky* by an integral multiple of $b = \frac{2\pi}{a}$ leaves the state unchanged. We call $\boldsymbol{b} = b\,\hat{\boldsymbol{y}}$ the primitive **reciprocal lattice vector**. Since any linear combination of these degenerate eigenfunctions is itself an eigenfunction with the same eigenvalue, we can take linear combinations of our modes to put them in the form:

$$H_{k_x,k_y}(r) = e^{ik_x x} \cdot e^{ik_y y} \cdot \boldsymbol{u}_{\boldsymbol{k_y}}(y,z)$$

u(*y*, *z*) is a periodic function in *y*: we can verify that $\boldsymbol{u}(y + la, z) = \boldsymbol{u}(y, z)$. The discrete periodicity in the *y* direction leads to a *y* dependence for **H** that is simply the product of a plane wave with a *y*-periodic function. We can think of it as a plane wave, as it would be in free space, but modulated by a periodic function because of the periodic lattice:

$$\boldsymbol{H}(\ldots, y, \ldots) \propto \cdot e^{ik_y y} \cdot \boldsymbol{u}_{\boldsymbol{k_y}}(y, \ldots)$$

This result is commonly known as **Bloch's theorem**. One key fact about Bloch states is that the Bloch state with wave vector ky and the Bloch state with wave vector $ky + mb$ are identical. The ky's that differ by integral multiples of $b = \frac{2\pi}{a}$ are not different from a physical point of view. Thus, the mode frequencies must also be periodic in ky: $\omega(ky) = \omega(ky + mb)$. In fact, we

need only consider *ky* to exist in the range $-\frac{\pi}{a} < ky \leq \frac{\pi}{a}$. This region of important, nonredundant values of *ky* is called the **Brillouin zone**.

8.8 Brillouin zone

The wave vector **k** serves to specify the phase relationship between the various cells that are described by **u,** following the representation with Bloch's theorem we encountered in the previous paragraph. If **k** is incremented by a **reciprocal lattice vector G**, then the phase between cells is incremented by $\boldsymbol{G} \cdot \boldsymbol{R}$ ($\boldsymbol{R}$ is a primitive lattice vector) which we know is $2\pi N$ and not really a phase difference at all. So incrementing **k** by **G** results in the same physical mode.

This means that there is a lot of redundancy in the label **k**. We can restrict our attention to a finite zone in reciprocal space in which you *cannot* get from one part of the volume to another by adding any **G**. All values of **k** that lie outside of this zone, by definition, can be reached from within the zone by adding **G**, and are therefore redundant labels. There are actually many such zones, but we focus on the region that is closest to **k** = 0

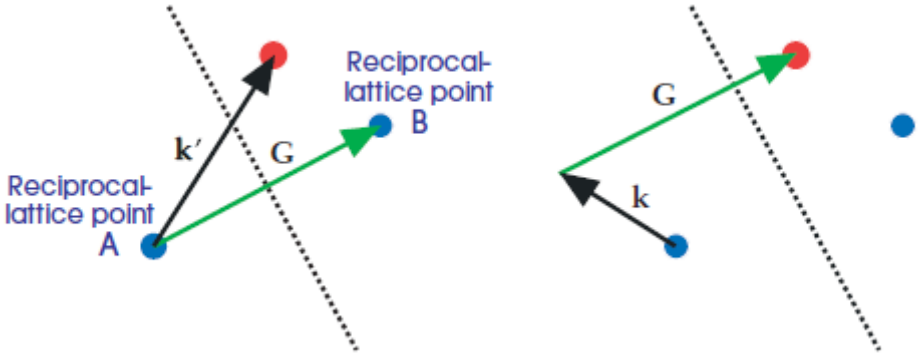

Figure 2: Characterization of the Brillouin zone. any lattice vector (such as $\mathbf{k}'$) that reaches an arbitrary point on the other side (red) can be expressed as the sum of a same-side vector (such as $\mathbf{k}$) plus a reciprocal lattice vector $\mathbf{G}$.

This zone is the (first) **Brillouin zone**. A more visual way to characterize it is the following: around any lattice point in reciprocal space, highlight the volume that is closer to *that* lattice point than to *any other* lattice point. If we call the original lattice point the origin, then the highlighted region is the Brillouin zone. Here are some two dimensional examples:

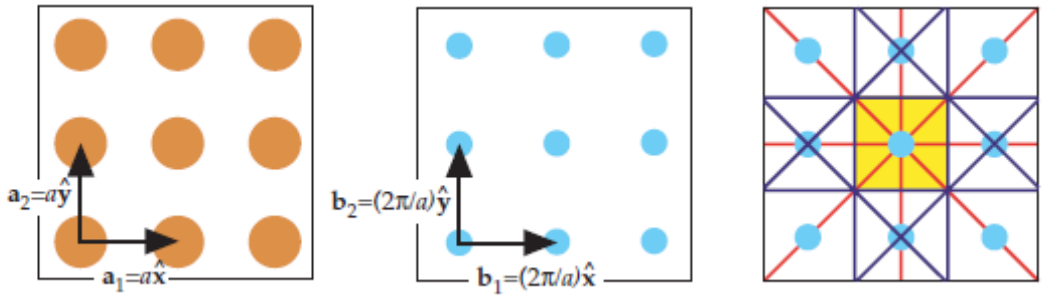

Figure 3: Brillouin zone for square lattice

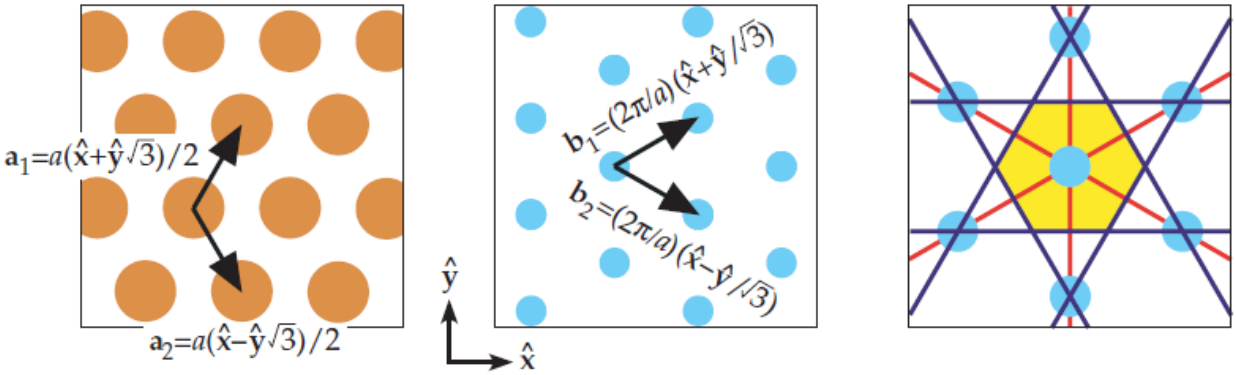

Figure 4: Brillouin zone for triangular lattice

For three dimensional lattice the Brillouin zone can have very complex shape and won't be considered in this discussion. If we focus our attention on the Brillouin zone for the square lattice (but the same holds for the triangular lattice) we can see that even inside the Brillouin zone itself has some redundancy. In fact we can highlight a triangular subzone, which is $\frac{1}{8}$ of the entire zone, and realize the Brillouin zone is nothing but a repetition of this subzone, called ***irreducible Brillouin zone.***

8.9 The Physical Origin of Photonic Band Gaps

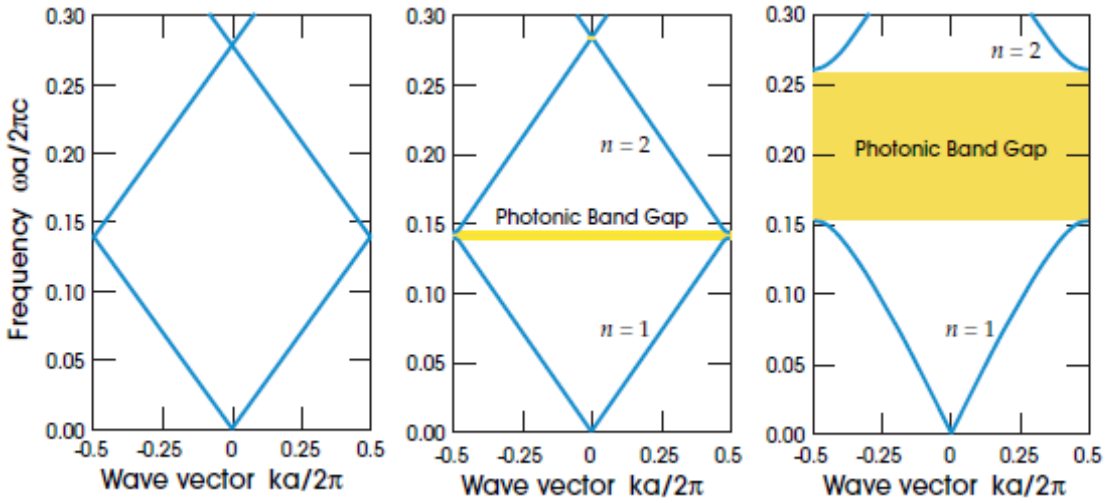

Figure 5: The photonic band structures for three different multilayer films. In all three cases, each layer has a width 0.5*a*. *Left:* every layer has the same dielectric constant $\varepsilon = 13$. *Center:* layers alternate between ε of 13 and 12. *Right:* layers alternate between ε of 13 and 1.

In figure 5, we plot $\omega_n(k)$ for three different multilayer films. The left-hand plot is for a system in which all of the layers have the same dielectric constant; the medium is actually uniform in all three directions. The center plot is for a structure with alternating dielectric constants of 13 and 12, and the right-hand plot is for a structure with a much higher dielectric contrast of 13 to 1.

The left-hand plot is for a homogeneous dielectric medium for which we have arbitrarily assigned a periodicity of *a*. But we already know that in a homogeneous medium, the speed of light is reduced by the index of refraction. The modes lie along the *light line*, given by $\omega(k) = \frac{ck}{\sqrt{\varepsilon}}$ because we have insisted that *k* repeat itself outside the Brillouin zone, the light line folds back into the zone when it reaches an edge. One can regard this as simply a way of relabeling the solutions, in which $k + \frac{2\pi}{a}$ is replaced by *k*. The center plot, which is for a *nearly*-homogeneous medium, looks like the homogeneous case with one important difference: there is a gap in frequency between the upper and lower branches of the lines. There is no allowed mode in the crystal that has a frequency within this gap, regardless of *k*. We call such a gap a **photonic band gap**. The right-hand plot shows that the gap widens considerably as the dielectric contrast is increased. A crystal with a band gap might make a very good narrow-band filter, by rejecting all (and only) frequencies in the gap. A resonant cavity, carved out of a photonic crystal, would have perfectly reflecting walls for frequencies in the gap. We can understand the gap's physical origin by considering the electric field mode profiles for the states immediately *above* and *below* the gap. The gap between bands *n* = 1 and *n* = 2 occurs at the edge of the Brillouin zone, at $k = \frac{\pi}{a}$. For $k = \frac{\pi}{a}$, the modes have a

wavelength of 2a, twice the crystal's spatial period (or *lattice constant*). There are two ways to center a mode of this type. We can position the nodes in each $low - \varepsilon$ layer, as in figure 3(a), or in each $high - \varepsilon$ layer, as in figure 3(b). Any other position would violate the symmetry of the unit cell about its center.

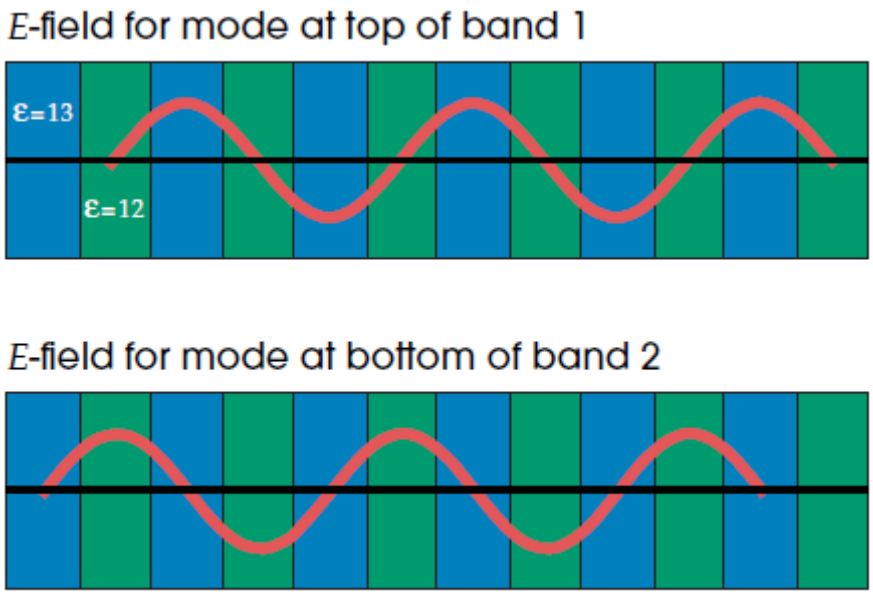

Figure 6: Electric fields of band 1 and 2 for the central configuration of figure 5

Using the electromagnetic variational theorem, we found that the low frequency modes concentrate their energy in the $high - \varepsilon$ regions, and the high frequency modes have a larger fraction of their energy (although not necessarily a majority) in the $low - \varepsilon$ regions. With this in mind, it is understandable why there is a frequency difference between the two cases. The mode just *under* the gap has more of its energy concentrated in the $\varepsilon = 13$ regions as shown in figure 7, giving it a lower frequency than the next band, most of whose energy is in the $\varepsilon = 12$ regions.

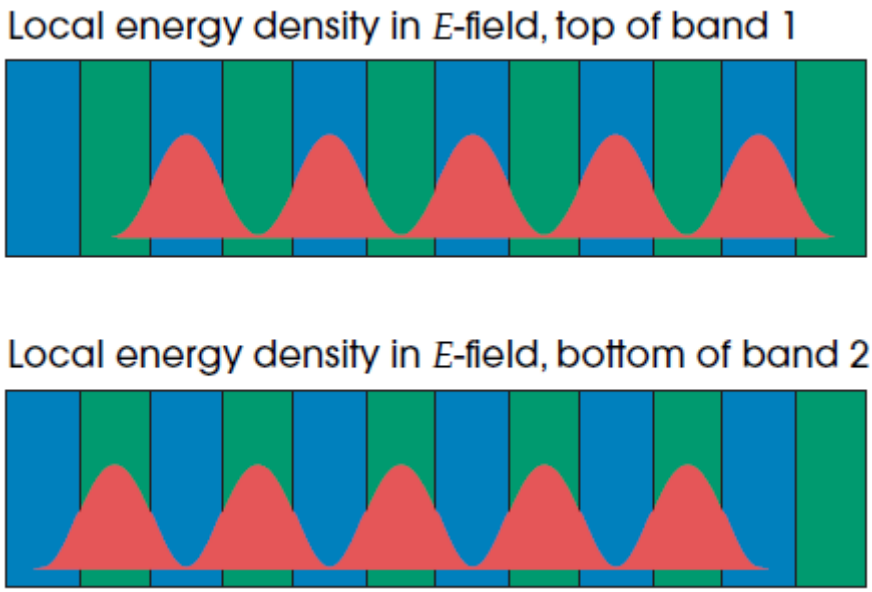

Figure 7: Energy density of band 1 and 2 for the central configuration of figure 5

The bands above and below the gap can be distinguished by where the energy of their modes is concentrated: in the $high - \varepsilon$ regions, or in the $low - \varepsilon$ regions. The situation is analogous to the electronic band structure of semiconductors, in which the *conduction band* and the *valence band* bracket the fundamental gap.

Let's describe the configuration with a large dielectric contrast. In this case, we find that the field energy for *both* bands is primarily concentrated in the $high - \varepsilon$ layers, but in different ways, the first band being more concentrated than the second. These fields are shown in figure 8, corresponding to the right panel of figure 5. The gap arises from this difference in field energy location.

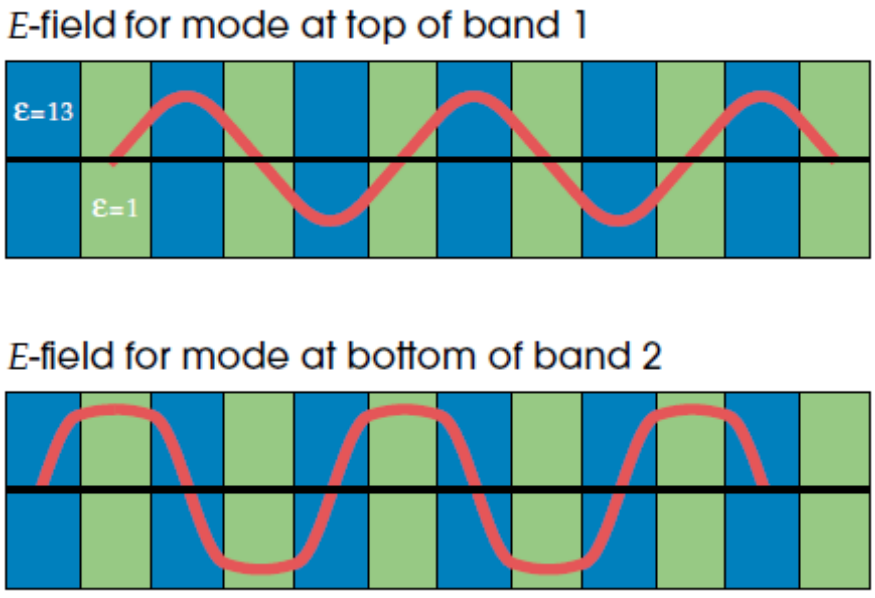

Figure 8: Electric fields of band 1 and 2 for the configuration on the right of figure 5.

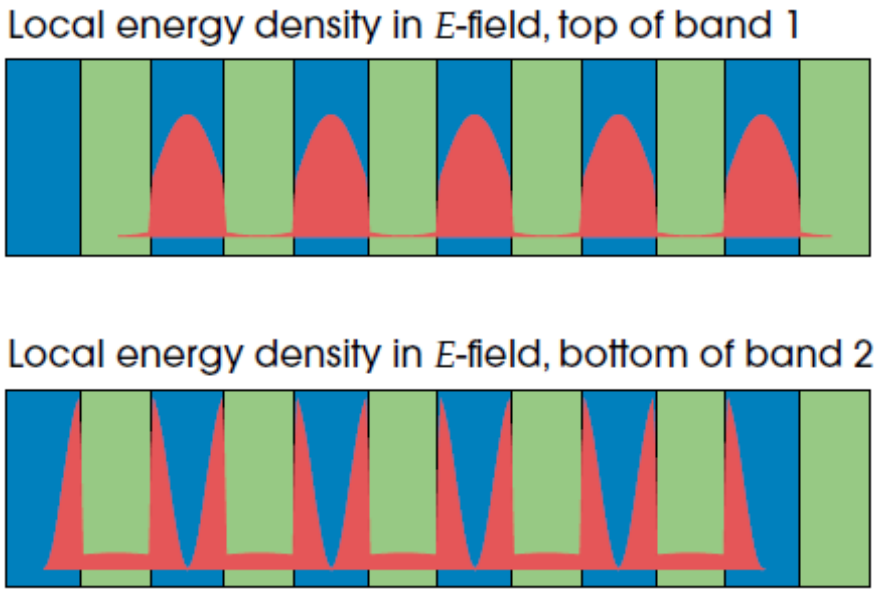

Figure 9: Energy density of band 1 and 2 for the configuration on the right of figure 5

We conclude this section with the observation that in one dimension, a gap usually occurs between *every* set of bands, at either the Brillouin zone's edge or its center. Finally, we emphasize that band gaps always appear in a one-dimensional photonic crystal for *any* dielectric contrast. The smaller the contrast, the smaller the gaps, but the gaps open up as soon as $\frac{\varepsilon_1}{\varepsilon_2} \neq 1$[1].

8.10 Evanescent Modes in Photonic Band Gaps

The periodicity of the crystal induced a gap in its band structure. No electromagnetic modes are allowed to have frequencies in the gap. But what happens when we send a light wave (with a frequency in the photonic band gap) onto the face of the crystal from outside? No purely real wave vector exists for any mode at that frequency. Instead, the wave vector is complex. The wave amplitude decays exponentially into the crystal. When I say that there are no states in the photonic band gap, I mean that there are no *extended* states. Instead, the modes are **evanescent**, decaying exponentially:

$$\boldsymbol{H}(\boldsymbol{r}) = e^{ik\boldsymbol{r}}\boldsymbol{u}(\boldsymbol{r})e^{-\kappa\boldsymbol{r}}$$

They are just like the Bloch modes, but with a complex wave vector $k + i\kappa$. The imaginary component of the wave vector causes the decay on a length scale of $\frac{1}{\kappa}$.

[1] There is a special exception for the *quarter-wave stack* described in the next section. In that case, while there is always a gap at the edge of the Brillouin zone, there is no gap at the center, because every successive pair of bands is degenerate at $k = 0$

It's possible to see where the complex wave vector originates. For frequencies slightly higher than the top of the gap, $\Delta\omega > 0$. In this case, Δk is purely real, and we are within band 2. However, for $\Delta\omega < 0$, when we are within the gap, Δk is purely imaginary. The states decay exponentially since $\Delta k = i\kappa$. As we traverse the gap, the decay constant κ grows as the frequency reaches the gap's center, then disappears again at the lower gap edge. Larger gaps usually result in a larger κ at midgap, and thus less penetration of light into the crystal. Although evanescent modes are solutions of the eigenvalue problem, they diverge as ***r*** goes to $\pm\infty$ .Consequently, there is no physical way to excite them within a crystal. However, a defect or an edge in an otherwise perfect crystal can terminate this exponential growth and thereby sustain an evanescent mode. If one or more evanescent modes is compatible with the structure and symmetry of a given crystal defect, we can then excite a *localized* mode within the photonic band gap. It's possible to localize states near the middle of the gap much more tightly than states near the gap's edge.

8.11 Planewave Eigensolver

Bloch's Theorem and Photonic bands represent a powerful tool to be exploited to design a program able to solve two and three dimensional problems. The programs I designed offer high flexibility but suffer a strong limitation: They can be used only for one dimensional photonic crystals. I will therefore present in this section a sketch on how to design a multidimensional electromagnetic eigensolver, using the concepts expressed above[2].

The program employs a spectral method with a planewave basis. In one dimension it corresponds to the familiar **Fourier series**. In particular, we are solving

$$[(i\boldsymbol{k}+\nabla)\times\frac{1}{\varepsilon(\boldsymbol{r})}(i\boldsymbol{k}+\nabla)\times\boldsymbol{u_k}(\boldsymbol{r})] = \hat{\Theta}_{\boldsymbol{k}}\boldsymbol{u_k}(\boldsymbol{r}) = \frac{\omega(\mathbf{k})^2}{c^2}\mathbf{u_k}(\mathbf{r})$$

for a periodic function $u_k(x) = u_k(x + a)$ with period a.

Any reasonable periodic function can be represented by an infinite sum of sines and cosines, or, in terms of complex exponentials:

$$u_k(x) = \sum_{n=-\infty}^{+\infty} c_n(k)e^{\frac{i2\pi n}{a}x}$$

For complex Fourier-series coefficients $c_n(k) = \frac{1}{a}\int_0^a dx e^{\frac{i2\pi n}{a}x}\, u_k(x)$. Each term in the sum is a periodic function with period a. To use this representation on a computer, we need to truncate the sum to have a finite number (N) of terms. This is feasible because the coefficients c_n are

[2] Further reading can be found in [15].

decaying with $|n|$, even though the rate of convergence depends on the smoothness of $u_k(x)$; if $u_k(x)$ is $l - times$ differentiable, then $|c_n|$ decreases faster than $\frac{1}{|n|^l}$. Thus, we use the *N* lowest$-|n|$ terms (say, $-\frac{N}{2}$ to $\frac{N}{2} - 1$). We have transformed the problem from finding $u_k(x)$ to solving a set of linear equations for the *N* unknowns c_n. We can generalize the Fourier series to several dimensions by recognizing that the $\frac{2\pi n}{a}$ in the complex exponential is none other than a reciprocal lattice vector of the one-dimensional lattice with period a. By analogy, the multidimensional Fourier series is:

$$\boldsymbol{u_k(r)} = \sum_{\boldsymbol{G}} \boldsymbol{c_G(k)} e^{i\boldsymbol{G}\cdot\boldsymbol{r}}$$

where the sum is over all of the reciprocal lattice vectors **G**, and:

$$\boldsymbol{c_G} = \frac{1}{V} \int d^3\boldsymbol{r}\, e^{-i\boldsymbol{G}\cdot\boldsymbol{r}} \boldsymbol{u_k(r)}$$

where *V* is the unit-cell volume. By construction, each term in the sum is periodic in **r** with respect to the lattice vectors **R**, since **G**· **R** is a multiple of 2π by definition. Note that, since $\boldsymbol{u_k}$ is a vector field, our Fourier-series coefficients $\boldsymbol{c_G}$ are now vectors as well. If we apply the transversality constraint to equation $\boldsymbol{u_k(r)} = \sum_{\boldsymbol{G}} \boldsymbol{c_G(k)} e^{i\boldsymbol{G}\cdot\boldsymbol{r}}$ we obtain a simple constraint on the coefficients:

$$(\boldsymbol{k} + \boldsymbol{G}) \cdot \boldsymbol{c_G} = 0$$

It's clear transversality is automatically obeyed if we build the field $\boldsymbol{H} = \boldsymbol{u_k^{}} e^{i\boldsymbol{k}\cdot\boldsymbol{r}}$ out of plane waves that are themselves transverse. Therefore, for each **G** it's possible to choose two perpendicular unit vectors $\hat{\boldsymbol{e}}_{\boldsymbol{G}}^{(1)}$ and $\hat{\boldsymbol{e}}_{\boldsymbol{G}}^{2}$ orthogonal to $\boldsymbol{k} + \boldsymbol{G}$, and write:

$$\boldsymbol{c_G} = c_{\boldsymbol{G}}^{(1)} \hat{\boldsymbol{e}}_{\boldsymbol{G}}^{(1)} + c_{\boldsymbol{G}}^{(2)} \hat{\boldsymbol{e}}_{\boldsymbol{G}}^{(2)} .$$

We have thus reduced the problem to two unknowns $c_{\boldsymbol{G}}^{(1)}$ and $c_{\boldsymbol{G}}^{(2)}$ per **G**, and we need not worry about transversality any more. Given the transverse Fourier-series representation, it's time to derive a set of equations to determine the coefficients $\boldsymbol{c_G}$ by substitution into the master equation. By Fourier transforming both sides of the master equation we obtain:

$$\sum \left[-\varepsilon_{\boldsymbol{G}'-\boldsymbol{G}}^{-1} \cdot (\boldsymbol{k} + \boldsymbol{G}') \times (\boldsymbol{k} + \boldsymbol{G}) \times\right] \boldsymbol{c_G} = \frac{\omega^2}{c^2} \boldsymbol{c_{G'}}$$

in terms of the Fourier transform (series coefficients) $\varepsilon_{\boldsymbol{G}}^{-\mathbf{1}}\, of\, \varepsilon^{-1}(\boldsymbol{r})$.

Previous Equation is an *infinite* set of linear equations for the infinite set of unknowns represented by $\boldsymbol{c_G}$. We can truncate this infinite set of equations using the **discrete Fourier transform** (DFT). The DFT essentially replaces the Fourier transform by a discrete sum. Once we have truncated to a finite set of **G** values, we obtain a *finite* matrix eigenequation of the form $Ax = \omega^2 x$, where *x* is the column-vector of our unknown $c_{\boldsymbol{G}}^{l}$ and *A* is the matrix of the coefficients on the left-hand side.

The reason why we don't get a generalized eigenproblem $Ax = \omega^2 Bx$, or rather why *B* here is the identity, is that the planewave basis functions are orthogonal to one another.

The coefficients $\varepsilon^{-1}_{\mathbf{G}'-\mathbf{G}}$ are generally nonzero for all $\boldsymbol{G}'$ and **G**, matrix *A* is *dense* (mostly nonzero), and multiplying *Ax* takes $O(N^2)$ time. **Fast Fourier transform** (FFT) algorithms can compute the multidimensional DFT over *N* points in $O(N \log N)$ time. This means we can multiply $c_{\boldsymbol{G}}$ by the operator on the left-hand side of the equation via a three-step process. First, we take the crossproduct $(\boldsymbol{k} + \boldsymbol{G}) \times \boldsymbol{c_G}$, which takes $O(N)$ time. Then, we compute the (inverse) FFT to transform into position (**r**) space, where we can multiply by $\varepsilon^{-1}(\boldsymbol{r})$ in $O(N)$ time. Finally, we FFT back to **G** coordinates to perform the final cross-product $(\boldsymbol{k} + \boldsymbol{G}') \times$. In all, this process takes $O(N \log N)$ time and requires $O(N)$ storage, which is fast enough for iterative methods to be efficient.

Another important technical advantage of the planewave representation for iterative eigensolvers are **preconditioners**. A preconditioner, in an iterative method, is essentially an approximate solution to the equation that is used to accelerate each step of the iteration. A good preconditioner can speed up the solution by *orders of magnitude*, from thousands of iterations to tens, but the development of such a preconditioner is a difficult and problem-dependent task. For the planewave method, however, efficient preconditioning is simple: one can precondition by considering only the diagonal entries of *A*, which are just $|\boldsymbol{k} + \boldsymbol{G}|^2$, since these entries dominate the problem for large $|\mathbf{G}|$.

Summary and conclusion

The software developed in this work has been used as a design tool for multilayered structures and the results have been verified and found to be in agreement with measurements. Designers and experimenters now have a highly flexible and very general tool which can simulate on a computer the behavior of monodimensional multilayered structure such as mirrors, filter, cavities, widely used in industrial or research applications. Whether you decide to buy on the market the device which best fit for your purpose or to build such device by yourself, a few run of the software package will answer every question and give every parameter needed. The implementation of non periodic structure can be used to simulate the presence of production defect and to estimate the impact of said defects on overall performances. This can lead to process optimization studies which aim at minimize the onset of defects. Exotic and unusual behaviors can be studied using the anisotropic program in tandem with the complete non periodicity.

The software is efficient, requiring a few minutes at maximum to give solutions and it's portable thanks to the user friendly interface implemented via C++. It's also possible for users familiar with Matlab to edit the routines or the functions themselves in order to solve unpredicted or unimplemented problems . In the last chapter I gave some hints to what I consider the next step in developing the software, 2D and 3D lattice analyses. Photonic crystal have been mainly manufactured as monodimensional multilayer, but in the last few years researchers have started to focus their attention on bidimensional crystal, which exhibit interesting properties thanks to particular configuration of their band-gaps. 3D crystals are still a mostly unexplored field, but they probably harbor the potential for major breakthrough in photonics and opto-electronics thanks to their complete band-gaps.

Appendix

Isotropic Media, TM polarization

```
% Risolutore multistrato

function [Gamma]=
multidieI(n,L,lambda,theta,Strati,muRel,sigma,Defect,position_Defect,sigma_defec
t,N_defect,x_Defect,mu_Defect)

if nargin<8,
Defect=1,position_Defect=0,sigma_defect=0,N_defect=0,x_Defect=0,mu_Defect=0;end
if nargin<7, sigma=[0,0,0,0];end
if nargin<6, muRel=[1,1,1]; end

C_luce= 299.792458*10^6   % m/s
%lambda= lambda                  % m
%nu= C_luce/lambda
omega=2*pi*(C_luce/lambda);             % cicli/sec

mu_vuoto= 4*pi*10^(-7)                % H/m
mu_matAria= mu_vuoto
muRel_matA= muRel(1)
muRel_matB= muRel(2)
mu_matA= mu_vuoto*muRel_matA
mu_matB=  mu_vuoto*muRel_matB
muRel_FinalMat= muRel(3)
mu_FinalMat= mu_vuoto*muRel_FinalMat

epsilon_vuoto= 8.8541*10^(-12)                    % F/m
epsilonRel_aria= 1.00059
epsilon_matAria= epsilon_vuoto*epsilonRel_aria

N_Aria= sqrt((mu_matAria*epsilon_matAria)/(mu_vuoto*epsilon_vuoto))
N_matA= n(1)
N_matB= n(2)
N_FinalMat= n(3)


epsilon_matA = (((N_matA)^2*mu_vuoto)/mu_matA)*epsilon_vuoto
epsilon_matB = (((N_matB)^2*mu_vuoto)/mu_matB)*epsilon_vuoto
epsilon_FinalMat = (((N_FinalMat)^2*mu_vuoto)/mu_FinalMat)*epsilon_vuoto

sigma_matAria= sigma(1)
sigma_matA=    sigma(2)
sigma_matB=     sigma(3) %conduttivita' S/m
sigma_FinalMat= sigma(4)
```

```
d_1= L(1)*lambda      % spessore dielettrico A in m

d_2= L(2)*lambda  % spessore dielettrico B
x_3 = d_1 + d_2  % spessori totali

E_11p=  1   % ampiezza campo elettrico incidente polarizzato perpendicolarmente
teta_11= theta*pi/180  % angolo di incidenza campo elettrico
x_1=  L(1)*lambda;      % spessore strato d' aria

%Strati=    load('C:\Dev-Cpp\Layers.dat')  % numero degli strati acquisito con
C++
%Defect =   load('C:\Dev-Cpp\Difetti.dat') % Numero Strati "Difetto" acquisito
via C++
%position_Defect = load('C:\Dev-Cpp\posizione_difetti.dat'); % posizione degli
strati "difetto" acquisita via C++
%sigma_defect = load('C:\Dev-Cpp\sigma_difetti.dat')
%N_defect = load('C:\Dev-Cpp\N_difetti.dat')
%x_Defect = load('C:\Dev-Cpp\x_difetti.dat').*10^-9;
%mu_Defect = load('C:\Dev-Cpp\mu_difetti.dat').*mu_vuoto

disp('fine caricamento')

r = 2*Strati+2   % numero di righe e di colonne
c = 2*Strati+2

if (Defect-1) == 0
    epsilon_defect=0
else
for w = 1:Defect,  % permittività dei difetti

    epsilon_defect(w)=(((N_defect(w))^2*mu_vuoto)/mu_Defect(w))*epsilon_vuoto
end
end
if (Defect-1) == 0
    K_defect=0
else
for w = 1:Defect,  % Vettori d' onda per i difetti

    Kr_defect(w)=
omega*sqrt((epsilon_defect(w).*mu_Defect(w))./2).*sqrt(sqrt(1+(sigma_defect(w)./
(epsilon_defect(w)*omega)).^2)+1);
    Ki_defect(w) =
omega*sqrt((epsilon_defect(w).*mu_Defect(w))./2).*sqrt(sqrt(1+(sigma_defect(w)./
(epsilon_defect(w)*omega)).^2)-1);
    K_defect(w) = Kr_defect(w)+i.*Ki_defect(w);
end
end

Kr_Aria =
omega*sqrt((epsilon_matAria*mu_matAria)/2)*sqrt(sqrt(1+(sigma_matAria/(epsilon_m
atAria*omega))^2)+1)   % Vettori d' onda per gli strati
Ki_Aria =
omega*sqrt((epsilon_matAria*mu_matAria)/2)*sqrt(sqrt(1+(sigma_matAria/(epsilon_m
atAria*omega))^2)-1)
Kr_matA =
omega*sqrt((epsilon_matA*mu_matA)./2)*sqrt(sqrt(1+(sigma_matA/(epsilon_matA*omeg
a))^2)+1)
Ki_matA =
omega*sqrt((epsilon_matA*mu_matA)./2)*sqrt(sqrt(1+(sigma_matA/(epsilon_matA*omeg
a))^2)-1)
```

```
Kr_matB =
omega*sqrt((epsilon_matB*mu_matB)./2)*sqrt(sqrt(1+(sigma_matB/(epsilon_matB*omeg
a))^2)+1)
Ki_matB =
omega*sqrt((epsilon_matB*mu_matB)./2)*sqrt(sqrt(1+(sigma_matB/(epsilon_matB*omeg
a))^2)-1)
Kr_FinalMat =
omega*sqrt((epsilon_FinalMat*mu_FinalMat)/2)*sqrt(sqrt(1+(sigma_FinalMat/(epsilo
n_FinalMat*omega))^2)+1)
Ki_FinalMat =
omega*sqrt((epsilon_FinalMat*mu_FinalMat)/2)*sqrt(sqrt(1+(sigma_FinalMat/(epsilo
n_FinalMat*omega))^2)-1)


K_Aria = Kr_Aria+i.*Ki_Aria
K_matA = Kr_matA+i.*Ki_matA
K_matB = Kr_matB+i.*Ki_matB
K_FinalMat = Kr_FinalMat+i.*Ki_FinalMat

%disp('fine caricamento K')
%N_Aria
%teta_11
sin11= N_Aria*sin(teta_11);   % angoli di rifrazione

teta(1)= teta_11; %   Aria
    disp('pre for w')
for w = 2:(2*Strati)+1
%for w = 2:(4)

    %w% strati A e B piu' difetti
  for cont_pos = 1:(Defect)

%w_cont_pos=[w,cont_pos]
    if  w == 2*position_Defect(cont_pos) || w == 2*position_Defect(cont_pos)+1,

        teta(w) = asin(sin11/N_defect(cont_pos));

    else

       for cont = 0:(2*Strati+1),

           if w == (4*cont+2) || w == (4*cont+3),

              teta(w) = asin(sin11/N_matA);

           elseif w == (4*cont) || w == (4*cont+1)

                teta(w) = asin(sin11/N_matB);


           end
       end
    end
 end
 end
teta
pause
 % strato finale di materiale
```

```
 teta(2*Strati+2)= asin(sin11/N_FinalMat);

 % Colonne : w --> K

         % strato 1 (Aria)
        epsilon_matAria
         k(1)= K_Aria
        CM(1)= sqrt(epsilon_matAria/mu_matAria)


         % coppie di materiali A e B ed eventuale difetto
          disp('pre  2 for w')
         for w=2:(2*Strati)+1,
             for cont_pos=1:Defect,

             if w == (2*position_Defect(cont_pos)) || w ==
(2*position_Defect(cont_pos))+1,

                 k(w)= K_defect(cont_pos);
                 CM(w) = sqrt(epsilon_defect(cont_pos)/mu_Defect(cont_pos));

             else

             for cont=0:(2*Strati+1),

                 if w==(4*cont+2) || w==(4*cont+3),

                     k(w)= K_matA;
                     CM(w)= sqrt(epsilon_matA/mu_matA);

                 elseif w==(4*cont) || w==(4*cont+1)

                     k(w)= K_matB;
                     CM(w)= sqrt(epsilon_matB/mu_matB);


                 end
             end
             end
             end
         end

        % strato finale di materiale

         k(2*Strati+2)= K_FinalMat
         CM(2*Strati+2)= sqrt(epsilon_FinalMat/mu_FinalMat)

         % Righe : v -- x

         % strato1 (aria)

         x(1) = x_1;
         x(2) = x_1;

         % coppie di materiali A e B ed eventuale difetto
          disp('pre 3 for w')
         for v = 2:2:(2*Strati),
             for cont_pos = 1:(Defect),
```

```
                if v == 2*position_Defect(cont_pos),

                    x(v+1) = x(v) + x_Defect(cont_pos);
                    x(v+2) = x(v) + x_Defect(cont_pos);

                elseif mod((v+2)/2,2)==0,

                    x(v+1) = x(v) + d_1;
                    x(v+2) = x(v) + d_1;

                else
                        x(v+1) = x(v) + d_2;
                        x(v+2) = x(v) + d_2;

                end
            end
        end


        x=x(1:r)
        pause
        disp('pre 4 for w')
        for w=2:2:r,
            for v=1:c,
              %  w_cont_pos=[w,v]
                phi(w,v)= CM(v);
            end
        end

        for w=1:2:r,
            for v=1:c,
                phi(w,v)=1;
            end
        end
        phi
        % polarizzato perpendicolarmente

        for w=2:2:r,
        for v=1:c,

          Angolo(w,v)= cos(teta(v));
        end
        end

        for w=1:2:r,
            for v=1:c,
                Angolo(w,v) = 1;

            end
        end

        Angolo
        for w = 1:r,
            for v= 1:c,

                gamma(w,v) = i*x(w)*k(v) ;
                alpha(w,v) = ((-1)^(w+1))*delta(w,v) + ((-
1)^(w+1))*delta(w,v+1) + ((-1)^(w))*delta(w+1,v) - ((1-(-1)^(w))/2)*delta(w+2,v)
+ ((1-(-1)^(w-1))/2)*delta(w,v+2) ;
```

```
                beta(w,v) = ((-1)^(w))*(delta(w,v)) + ((-1)^(w+1))*delta(w,v+1)
+ ((-1)^(w+1))*(delta(w+1,v)) - ((1-(-1)^(w))/2)*delta(w+2,v) + ((1-(-1)^(w-
1))/2)*delta(w,v+2) ;

                ap(w,v) = phi(w,v)*Angolo(w,v)*alpha(w,v);
                bg(w,v)=beta(w,v)*gamma(w,v);
                ebg=exp(bg);
                C(w,v)=ap(w,v)*ebg(w,v);
            end
        end
        gamma
        alpha
        beta
        ap
        bg
        ebg
        C
        T(1)=-E_11p*exp(i*x_1*K_Aria);
        T(2)=-
E_11p*sqrt(epsilon_matAria/mu_matAria)*cos(teta_11)*exp(i*x_1*K_Aria);

        for v=3:c,
              T(v)=0;
        end
        T
        A=inv(C)*T.';
        A
       for es=1:c
           Mod_A(es)=abs(A(es));
       end
       Mod_A
       Summ=Mod_A(1)+Mod_A(c)

        for es=1:c
            Int_A(es)=(Mod_A(es))^2;
        end
         Int_A(1)
        Gamma=Int_A(1)
        clear A T C
```

Isotropic Media, TE polarization

```
% Risolutore multistrato

function [Gamma]=
multidieI(n,L,lambda,theta,Strati,muRel,sigma,Defect,position_Defect,sigma_defec
t,N_defect,x_Defect,mu_Defect)

if nargin<8,
Defect=1,position_Defect=0,sigma_defect=0,N_defect=0,x_Defect=0,mu_Defect=0;end
if nargin<7, sigma=[0,0,0,0];end
if nargin<6, muRel=[1,1,1]; end

C_luce= 299.792458*10^6   % m/s
%lambda= lambda                  % m
%nu= C_luce/lambda
omega=2*pi*(C_luce/lambda);             % cicli/sec

mu_vuoto= 4*pi*10^(-7)               % H/m
mu_matAria= mu_vuoto
muRel_matA= muRel(1)
muRel_matB= muRel(2)
mu_matA= mu_vuoto*muRel_matA
mu_matB=  mu_vuoto*muRel_matB
muRel_FinalMat= muRel(3)
mu_FinalMat= mu_vuoto*muRel_FinalMat

epsilon_vuoto= 8.8541*10^(-12)                    % F/m
epsilonRel_aria= 1.00059
epsilon_matAria= epsilon_vuoto*epsilonRel_aria

N_Aria= sqrt((mu_matAria*epsilon_matAria)/(mu_vuoto*epsilon_vuoto))
N_matA= n(1)
N_matB= n(2)
N_FinalMat= n(3)


epsilon_matA = (((N_matA)^2*mu_vuoto)/mu_matA)*epsilon_vuoto
epsilon_matB = (((N_matB)^2*mu_vuoto)/mu_matB)*epsilon_vuoto
epsilon_FinalMat = (((N_FinalMat)^2*mu_vuoto)/mu_FinalMat)*epsilon_vuoto

sigma_matAria= sigma(1)
sigma_matA=    sigma(2)
sigma_matB=     sigma(3) %conduttivita' S/m
sigma_FinalMat= sigma(4)

d_1= L(1)*lambda      % spessore dielettrico A in m

d_2= L(2)*lambda  % spessore dielettrico B
x_3 = d_1 + d_2  % spessori totali

E_11p=  1   % ampiezza campo elettrico incidente polarizzato perpendicolarmente
teta_11= theta*pi/180  % angolo di incidenza campo elettrico
x_1=  L(1)*lambda;      % spessore strato d' aria
```

```
%Strati=    load('C:\Dev-Cpp\Layers.dat')  % numero degli strati acquisito con
C++
%Defect =   load('C:\Dev-Cpp\Difetti.dat') % Numero Strati "Difetto" acquisito
via C++
%position_Defect = load('C:\Dev-Cpp\posizione_difetti.dat'); % posizione degli
strati "difetto" acquisita via C++
%sigma_defect = load('C:\Dev-Cpp\sigma_difetti.dat')
%N_defect = load('C:\Dev-Cpp\N_difetti.dat')
%x_Defect = load('C:\Dev-Cpp\x_difetti.dat').*10^-9;
%mu_Defect = load('C:\Dev-Cpp\mu_difetti.dat').*mu_vuoto

disp('fine caricamento')

r = 2*Strati+2   % numero di righe e di colonne
c = 2*Strati+2

if (Defect-1) == 0
    epsilon_defect=0
else
for w = 1:Defect,  % permittività dei difetti

    epsilon_defect(w)=(((N_defect(w))^2*mu_vuoto)/mu_Defect(w))*epsilon_vuoto
end
end
if (Defect-1) == 0
    K_defect=0
else
for w = 1:Defect,  % Vettori d' onda per i difetti

    Kr_defect(w)=
omega*sqrt((epsilon_defect(w).*mu_Defect(w))./2).*sqrt(sqrt(1+(sigma_defect(w)./
(epsilon_defect(w)*omega)).^2)+1);
    Ki_defect(w) =
omega*sqrt((epsilon_defect(w).*mu_Defect(w))./2).*sqrt(sqrt(1+(sigma_defect(w)./
(epsilon_defect(w)*omega)).^2)-1);
    K_defect(w) = Kr_defect(w)+i.*Ki_defect(w);
end
end

Kr_Aria =
omega*sqrt((epsilon_matAria*mu_matAria)/2)*sqrt(sqrt(1+(sigma_matAria/(epsilon_m
atAria*omega))^2)+1)   % Vettori d' onda per gli strati
Ki_Aria =
omega*sqrt((epsilon_matAria*mu_matAria)/2)*sqrt(sqrt(1+(sigma_matAria/(epsilon_m
atAria*omega))^2)-1)
Kr_matA =
omega*sqrt((epsilon_matA*mu_matA)./2)*sqrt(sqrt(1+(sigma_matA/(epsilon_matA*omeg
a))^2)+1)
Ki_matA =
omega*sqrt((epsilon_matA*mu_matA)./2)*sqrt(sqrt(1+(sigma_matA/(epsilon_matA*omeg
a))^2)-1)
Kr_matB =
omega*sqrt((epsilon_matB*mu_matB)./2)*sqrt(sqrt(1+(sigma_matB/(epsilon_matB*omeg
a))^2)+1)
Ki_matB =
omega*sqrt((epsilon_matB*mu_matB)./2)*sqrt(sqrt(1+(sigma_matB/(epsilon_matB*omeg
a))^2)-1)
Kr_FinalMat =
omega*sqrt((epsilon_FinalMat*mu_FinalMat)/2)*sqrt(sqrt(1+(sigma_FinalMat/(epsilo
n_FinalMat*omega))^2)+1)
```

```
Ki_FinalMat =
omega*sqrt((epsilon_FinalMat*mu_FinalMat)/2)*sqrt(sqrt(1+(sigma_FinalMat/(epsilo
n_FinalMat*omega))^2)-1)


K_Aria = Kr_Aria+i.*Ki_Aria
K_matA = Kr_matA+i.*Ki_matA
K_matB = Kr_matB+i.*Ki_matB
K_FinalMat = Kr_FinalMat+i.*Ki_FinalMat

%disp('fine caricamento K')
%N_Aria
%teta_11
sin11= N_Aria*sin(teta_11);   % angoli di rifrazione

teta(1)= teta_11; %   Aria
    disp('pre for w')
for w = 2:(2*Strati)+1
%for w = 2:(4)

    %w% strati A e B piu' difetti
  for cont_pos = 1:(Defect)

%w_cont_pos=[w,cont_pos]
    if  w == 2*position_Defect(cont_pos) || w == 2*position_Defect(cont_pos)+1,

        teta(w) = asin(sin11/N_defect(cont_pos));

    else

       for cont = 0:(2*Strati+1),

           if w == (4*cont+2) || w == (4*cont+3),

              teta(w) = asin(sin11/N_matA);

           elseif w == (4*cont) || w == (4*cont+1)

                teta(w) = asin(sin11/N_matB);


           end
       end
    end
 end
 end
teta
pause
 % strato finale di materiale

 teta(2*Strati+2)= asin(sin11/N_FinalMat);

 % Colonne : w --> K

         % strato 1 (Aria)
        epsilon_matAria
         k(1)= K_Aria
        CM(1)= sqrt(epsilon_matAria/mu_matAria)
```

```
          % coppie di materiali A e B ed eventuale difetto
           disp('pre  2 for w')
          for w=2:(2*Strati)+1,
              for cont_pos=1:Defect,

              if w == (2*position_Defect(cont_pos)) || w ==
(2*position_Defect(cont_pos))+1,

                  k(w)= K_defect(cont_pos);
                  CM(w) = sqrt(epsilon_defect(cont_pos)/mu_Defect(cont_pos));

              else

              for cont=0:(2*Strati+1),

                  if w==(4*cont+2) || w==(4*cont+3),

                      k(w)= K_matA;
                      CM(w)= sqrt(epsilon_matA/mu_matA);

                  elseif w==(4*cont) || w==(4*cont+1)

                      k(w)= K_matB;
                      CM(w)= sqrt(epsilon_matB/mu_matB);


                  end
              end
              end
              end
          end

         % strato finale di materiale

          k(2*Strati+2)= K_FinalMat
          CM(2*Strati+2)= sqrt(epsilon_FinalMat/mu_FinalMat)

          % Righe : v -- x

          % strato1 (aria)

          x(1) = x_1;
          x(2) = x_1;

          % coppie di materiali A e B ed eventuale difetto
           disp('pre 3 for w')
          for v = 2:2:(2*Strati),
              for cont_pos = 1:(Defect),

                  if v == 2*position_Defect(cont_pos),

                      x(v+1) = x(v) + x_Defect(cont_pos);
                      x(v+2) = x(v) + x_Defect(cont_pos);

                  elseif mod((v+2)/2,2)==0,

                      x(v+1) = x(v) + d_1;
```

```
                    x(v+2) = x(v) + d_1;

                else
                        x(v+1) = x(v) + d_2;
                        x(v+2) = x(v) + d_2;

                end
            end
        end


        x=x(1:r)
        pause
        disp('pre 4 for w')
        for w=1:2:r,
            for v=1:c,
              %  w_cont_pos=[w,v]
                phi(w,v)= CM(v);
            end
        end

        for w=2:2:r,
            for v=1:c,
                phi(w,v)=1;
            end
        end
        phi
        % polarizzato perpendicolarmente

        for w=1:2:r,
        for v=1:c,

          Angolo(w,v)= cos(teta(v));
        end
        end

        for w=2:2:r,
            for v=1:c,
                Angolo(w,v) = 1;

            end
        end

        Angolo
        for w = 1:r,
            for v= 1:c,

                gamma(w,v) = i*x(w)*k(v) ;
                alpha(w,v) = ((-1)^(w+1))*delta(w,v) + ((-
1)^(w+1))*delta(w,v+1) + ((-1)^(w))*delta(w+1,v) - ((1-(-1)^(w))/2)*delta(w+2,v)
+ ((1-(-1)^(w-1))/2)*delta(w,v+2) ;
                beta(w,v) = ((-1)^(w))*(delta(w,v)) + ((-1)^(w+1))*delta(w,v+1)
+ ((-1)^(w+1))*(delta(w+1,v)) - ((1-(-1)^(w))/2)*delta(w+2,v) + ((1-(-1)^(w-
1))/2)*delta(w,v+2) ;

                ap(w,v) = phi(w,v)*Angolo(w,v)*alpha(w,v);
                bg(w,v)=beta(w,v)*gamma(w,v);
                ebg=exp(bg);
                C(w,v)=ap(w,v)*ebg(w,v);
            end
```

```
 end
 gamma
 alpha
 beta
 ap
 bg
 ebg
 C
 T(1)=-E_11p*exp(i*x_1*K_Aria) )*cos(teta_11);
 T(2)=-E_11p*sqrt(epsilon_matAria/mu_matAria)*exp(i*x_1*K_Aria);

 for v=3:c,
       T(v)=0;
 end
 T
 A=inv(C)*T.';
 A
for es=1:c
    Mod_A(es)=abs(A(es));
end
Mod_A
Summ=Mod_A(1)+Mod_A(c)

 for es=1:c
     Int_A(es)=(Mod_A(es))^2;
 end
  Int_A(1)
 Gamma=Int_A(1)
 clear A T C
```

Anisotropic media, both polarizations

```
function [Gamma,Z] = anisotropo(n,L,lambda,theta,pol)


if nargin<=4, pol='te'; end
if nargin==3, theta=0; end

if size(n,2)==1, n = n'; end

K = size(n,1);
M = size(n,2)-2;

if K==1, n = [n; n; n]; end
if K==2, n = [n(1,:); n]; end

if M==0, L = []; end

theta = theta * pi/180;

if pol=='te',
    Nsin2 = (n(2,1)*sin(theta))^2;
    c = sqrt(1 - Nsin2 ./ n(2,:).^2);
    nT = n(2,:) .* c;
    r = n2r(nT);
else
    Nsin2 = (n(1,1)*n(3,1)*sin(theta))^2 / (n(3,1)^2*cos(theta)^2 +
n(1,1)^2*sin(theta)^2);
    c = sqrt(1 - Nsin2 ./ n(3,:).^2);
    nTinv = c ./ n(1,:);
    r = -n2r(nTinv);
end

if M>0,
    L = L .* c(2:M+1);
end

Gamma = r(M+1) * ones(1,length(lambda));

for i = M:-1:1,
    delta = 2*pi*L(i)./lambda;
    z = exp(-2*j*delta);
    Gamma = (r(i) + Gamma.*z) ./ (1 + r(i)*Gamma.*z);
end

Z = (1 + Gamma) ./ (1 - Gamma);
```

Routines for computations

This routine computes reflectance dependence on angle and frequency and plots a corresponding 3D graphic.

```
na = 1; nb = 1.52; nH = 2.42; nL = 1.45;
LH = 0.25; LL = 0.25 ;
la0 = 500;
la = linspace(300,800,500);
th = linspace(0,89,199);
N = 5;
for j=1:length(la)
    for i=1:length(th)
n = [na, nH, repmat([nL,nH], 1, N), nb];
L = [LH, repmat([LL,LH], 1, N)];
Ge(j,i) = 100*abs(multidiel(n,L,la(j)/la0, th(i), 'te')).^2;
Gm(j,i) = 100*abs(multidiel(n,L,la(j)/la0, th(i), 'tm')).^2;
G0(j,i) = 100*abs(multidiel(n,L,la(j)/la0)).^2;
    end
end

figure;surf(th,la,Ge,'edgecolor','none')
shading interp
camlight right;
lighting phong;
figure;surf(th,la,Gm,'edgecolor','none')
shading interp
camlight right;
lighting phong;
figure;surf(LH,la,G0,'edgecolor','none')
shading interp
camlight right;
lighting phong;
xlabel 'L / \lambda';
ylabel '\lambda (\num)';
zlabel '|\Gamma|^2';
```

This routines computes the reflectance for non-periodic mirrors and plots a 3D graphic.

```
clear all

na=1;
nb=1.52;
nH=2.32;
nL= 1.45;
LH1=0.25
LL1=0.25
LH=linspace(0,1,1000);
LL=linspace(0,1,1000);
la0=500;

M=5
N =5;

th=45;

la=linspace(300,800,1000);

for i=1:length(la)
for j=1:length(LL)
n = [na, nH, repmat([nL,nH], 1, N),repmat([nL,nH], 1, M), nb];
L = [LH(j), repmat([LL(j),LH(j)], 1, N),repmat([LL1,LH1], 1, M)];
Ga(j,i) = 100*abs(multidiel(n, L, la(i)/la0, th, 'tm')).^2;
Gm(j,i) = 100*abs(multidiel(n, L, la(i)/la0, th, 'te')).^2;
end
end
%plot(LH,Ga,LH,Gm);
figure;surf(la,LL,Ga,'edgecolor','none')
shading interp
camlight left;
lighting phong;
material dull;
ylabel 'LH';
xlabel 'LL';
zlabel '|\Gamma|^2';
figure;surf(la,LL,Gm,'edgecolor','none')
shading interp
camlight left;
material dull;
lighting phong;
ylabel 'LH';
xlabel 'LL';
zlabel '|\Gamma|^2';
```

Additional software

Software for Brewster's angles computations for isotropic and anisotropic media:

```
function [thb,thcTE,thcTM] = brewster(na,nb)


   na = na(:); nb = nb(:);                                    % Trasformo in
                                                               vettori colonna
if length(na)==1, na=[na; na; na]; end                      % isotropico
if length(na)==2, na=[na(1); na(1); na(2)]; end             % uniassiale
if length(nb)==1, nb=[nb; nb; nb]; end
if length(nb)==2, nb=[nb(1); nb(1); nb(2)]; end

if na(3)==nb(3),
    thb = [];                    % l' angolo di Brewster non esiste
else
    thb = atan(na(3) * nb(3) * sqrt((na(1)^2-nb(1)^2)/(na(3)^2-nb(3)^2)) /
na(1)^2) * 180/pi;
end

if na(3)>nb(3),
    thcTM = asin(na(3)*nb(3)/sqrt(na(3)^2*nb(3)^2 + na(1)^2*(na(3)^2-nb(3)^2)))
* 180/pi;
else
    thcTM = asin(na(3)*nb(3)/sqrt(na(3)^2*nb(3)^2 + nb(1)^2*(nb(3)^2-na(3)^2)))
* 180/pi;
end

if na(2)>nb(2),
    thcTE = asin(nb(2)/na(2)) * 180/pi;
else
    thcTE = asin(na(2)/nb(2)) * 180/pi;
end
```

Software for Fresnel's coefficients computation for isotropic and anisotropic media:

```
function [rte,rtm] = fresnel(na,nb,theta)

na = na(:); nb = nb(:);                                  % trasformo in vettori
colonna
if length(na)==1, na=[na; na; na]; end                   % isotropo
if length(na)==2, na=[na(1); na(1); na(2)]; end          % uniassiale
if length(nb)==1, nb=[nb; nb; nb]; end
if length(nb)==2, nb=[nb(1); nb(1); nb(2)]; end

theta = pi*theta/180;

Na = 1./sqrt(cos(theta).^2/na(1)^2 + sin(theta).^2/na(3)^2);

xe = (na(2)*sin(theta)).^2;                                        % caso
polarizzazione TE
xm = (Na.*sin(theta)).^2;                                          % caso
polarizzazione TM

rte = (na(2)*cos(theta) - sqrt(nb(2)^2 - xe)) ./ ...
      (na(2)*cos(theta) + sqrt(nb(2)^2 - xe));

if na(3)==nb(3),
    rtm = (na(1) - nb(1)) / (na(1) + nb(1)) * ones(1,length(theta));
else
    rtm = (na(1)*na(3) * sqrt(nb(3)^2 - xm) - nb(1)*nb(3) * sqrt(na(3)^2 - xm))
./ ...
          (na(1)*na(3) * sqrt(nb(3)^2 - xm) + nb(1)*nb(3) * sqrt(na(3)^2 - xm));
end
```

Software for computation of refraction angles in isotropic or anisotropic media:

```
function thb = snell(na,nb,tha,pol)

na = na(:); nb = nb(:);

if length(na)==1, na=[na; na; na]; end                  % isotropo
if length(na)==2, na=[na(1);na(1); na(2)]; end          % uniassiale
if length(nb)==1, nb=[nb; nb; nb]; end
if length(nb)==2, nb=[nb(1); nb(1); nb(2)]; end

tha = tha * pi/180;

if pol STRCMP 'tm',
    A = nb(1)^2 * nb(3)^2 * (na(1)^2 - na(3)^2) - na(1)^2 * na(3)^2 * (nb(1)^2 -
nb(3)^2);
    B = nb(1)^2 * nb(3)^2 * na(3)^2;
    thb = asin(na(1)*na(3)*nb(3)*sin(tha)./sqrt(A*sin(tha).^2 + B));
else
    thb = asin(na(2)*sin(tha)/nb(2));
end

thb = thb * 180/pi;
```

Bibliography

[1] Johnson, Steven G., M. L. Povinelli, M. Solja˘ci´c, A. Karalis, S. Jacobs, and J. D. Joannopoulos. 2005. "*Roughness losses and volume-current methods in photonic crystal waveguides.*" *Appl. Phys. B* 81:283–293.

[2] Taflove, Allen, and Susan C. Hagness. 2000. *Computational Electrodynamics: The Finite-Difference Time-Domain Method*. Norwood, MA: Artech.

[3] Chew,Weng Cho, Jian-Ming Jin, Eric Michielssen, and Jiming Song, eds. 2001. *Fast and Efficient Algorithms in Computational Electromagnetics*. Norwood, MA: Artech.

[4] John D Joannopoulos, Johnson SG, Winn JN & Meade RD (2008), *Photonic Crystals: Molding the Flow of Light* (2nd ed.), Princeton NJ: Princeton University Press.

[5] Douglas B. Chrisey and Graham K. Hubler ,*Pulsed Laser Deposition of Thin Films*, John Wiley & Sons, 1994.

[6] Griffiths, David Jeffrey, *Introduction to electrodynamics*, Prentice-Hall, 1999.

[7] Jackson, John David, *Classical electrodynamics*, John Wiley & Sons, 1989.

[8] Ashby, Neil, *American Journal of Physic*s, Vol.43, 553, 1975.

[9] Ohanian, H.C, *American Journal of Physics, Vol.51, 1024, 1983.*

[10] Brillouin, Léon (1960), *Wave Propagation and Group Velocity*, New York: Academic Press Inc.

[11] Landau and Lifschitz, *Electrodynamics of continuous media*, Pergamon Press, 1984.

[12] Born M. and Wolf E. , *Principles of Optics*, Pergamon Press, 1980.

[13] M. F. Weber, C. A. Stover, L. R. Gilbert, T. J. Nevitt, and A. J. Ouderkirk, "*Giant Birefringent Optics in Multilayer Polymer Mirrors*", Science, 287, 2451 (2000).

[14] Kittel, Charles, *Introduction to Solid State Physics*. John Wiley and Sons, 7th edition, 1996.

[15] Sakoda, Kazuaki, Optical properties of Photonic Crystals, Springer, 1st edition, 2001.